PHASE EXTRACTION OF OPTICAL INTERFEROMETRIC SIGNALS BASED ON IMPROVED TIME-FREQUENCY METHOD WITH APPLICATION TO HIGH STRAIN RATE MEASUREMENT

By
AMIT SUR
ENGG01201204004

Bhabha Atomic Research Center, Mumbai

A thesis submitted to the

Board of Studies in Engineering Sciences

In partial fulfillment of requirements

for the Degree of

DOCTOR OF PHILOSOPHY

of

HOMI BHABHA NATIONAL INSTITUTE

April, 2021

Homi Bhabha National Institute

Recommendations of the Viva Voce Committee

As members of the Viva Voce Committee, we certify that we have read the dissertation prepared by Amit Sur entitled "Phase extraction of optical interferometric signals based on improved time-frequency method with application to high strain rate measurement" and recommend that it may be accepted as fulfilling the thesis requirement for the award of Degree of Doctor of Philosophy.

Chairman - Dr. A. P. Tiwari | Date: 24/4/21

Guide / Convener - Dr. Archana Sharma | Date: 24.04.2021

Co-guide - Dr. T. C. Kaushik | Date:

Examiner – Prof. Vikram M. Gadre | Date: 24 April 2021

Member 1- Dr. A. K. Bhattacharjee | Date: 24/04/21

Member 2- Dr. V.H. Patankar | Date: 24.04.2021

Member 3- Dr. S. Kar | Date: 24.04.2021

Final approval and acceptance of this thesis is contingent upon the candidate's submission of the final copies of the thesis to HBNI.

We hereby certify that We have read this thesis prepared under our direction and recommend that it may be accepted as fulfilling the thesis requirement.

Date:

Place:

Dr. T. C. Kaushik
Co-guide

Dr. Archana Sharma
Guide

STATEMENT BY AUTHOR

This dissertation has been submitted in partial fulfillment of requirements for an advanced degree at Homi Bhabha National Institute (HBNI) and is deposited in the Library to be made available to borrowers under rules of the HBNI.

Brief quotations from this dissertation are allowable without special permission, provided that accurate acknowledgement of source is made. Requests for permission for extended quotation from or reproduction of this manuscript in whole or in part may be granted by the Competent Authority of HBNI when in his or her judgment the proposed use of the material is in the interests of scholarship. In all other instances, however, permission must be obtained from the author.

Amit Sur

(Amit Sur)

DECLARATION

I, hereby declare that the investigation presented in the thesis has been carried out by me. The work is original and has not been submitted earlier as a whole or in part for a degree / diploma at this or any other Institution / University.

Amit Sur

(Amit Sur)

List of Publications arising from the thesis

Journal

1. **Amit Sur**, K D Joshi, Archana Sharma and T C Kaushik, "VISAR signal analysis with emphasis on ellipse fitting" *Review of Scientific Instruments, Vol.88*, 125002, December **2017**.

2. **Amit Sur**, K D Joshi, Archana Sharma and T C Kaushik, "Optical phase extraction based on reassigned continuous wavelet transform with application to simultaneous displacement and velocity measurement" *Review of Scientific Instruments, Vol.91*, 015001, January **2020**.

3. **Amit Sur**, K D Joshi, Archana Sharma and T C Kaushik, "Instantaneous frequency extraction of highly non-stationary optical interferometric signal using Reassigned Smoothed Pseudo Wigner-Ville Distribution", *Optik-International Journal for Light and Electron Optics*, Vol. *231*,166436, January **2021**.

Conferences

1. **Amit Sur**, Amit S Rav, Gaurav Pandey, K D Joshi and S. C. Gupta, "Analysis of velocimetry signal based on continuous wavelet transform: application to shock wave physics experiments" *IEEE Conference Proceedings,* ICAES, Pilani, India, September **2013**.

2. **Amit Sur**, Amit S Rav, K D Joshi, S. C. Gupta and Kallol Roy, "Fringe analysis software: application to velocity measurement in dynamic compression experiment" *IEEE Conference Proceedings INDICON*, Pune, India, December **2014**.

3. **Amit Sur**, Amit S Rav, K D Joshi, S. Mukhopadhyay, T C Kaushik and S. C. Gupta, "Wavelet Transform based Phase Extraction for Interferometer Signal Analysis" *IEEE Conference Proceedings INDICON*, New Delhi, India, December **2015**.

(Amit Sur)

Dedicated to my Grandmother

ACKNOWLEDGEMENTS

I would like to thank my guide Dr. Archana Sharma and co-guide Dr. T C Kaushik for supervising, inspiring and most untiring help at all stages of my journey. I am very much thankful to my immediate superior Dr. K D Joshi for sharing his knowledge pertaining to this subject and everyday guidance, which helped me to complete this work in a present form. I am grateful to Dr. Kallol Roy for motivating me to carry out the study and supervising me at initial stage of the course. I am also thankful to Dr. S Mukhophadhyay for fruitful discussion and guidance at different stages of my journey. I am extremely thankful to Dr. Satish C Gupta and Dr. R K Sinha for allowing me to pursue this study. I also extend my sincere thanks to Chairman, Doctoral committee and other members for their help and logical suggestions. I am very much thankful to Shri Amit S Rav, Shri Gaurav Pandey, Shri S V Ingale and Shri S P Nayak for various technical discussion and useful suggestions. I am also thankful to Shri Bhaskar Sharma, Shri Sharad Borade, Shri P C Das and Shri Kulbhushan Singh for technical assistance.

Finally, I would like to extend my sincere gratitude to my wife Sanhita for sharing pain and joy and standing by me throughout the project. I would like to take this opportunity to thank my son Aarohan whose smiling face as new born baby made me happy that helped me to complete course work at IITB. I am thankful to my parents and other family members for their love, affection and unconditional support throughout the project. I would have been happier if my father could see that my journey is finally completed.

CONTENTS

LIST OF FIGURES

LIST OF TABLES

CHAPTER 7 Conclusion

The current research explored some novel techniques for optical phase extraction algorithm with aim to velocity measurement in high strain rate experiments by interferometric technique. The developed technique alleviates the existing methods and provides more accurate results. Phases as well as frequency of the fringe signals were explored from single fringe as well as multi fringe signals.

Chapter 3 introduced the concept of phase shifting method of various configuration i.e. two fringe, four fringe based techniques. Phase unwrapping technique was developed and demonstrated and ellipse fitting technique was introduced for correcting various measurement imperfections.

Chapter 4 presented the concept of Continuous Wavelet Transform technique for phase extraction. Two different techniques namely phase estimation method and frequency estimation was explored. Importance of ridge extraction was highlighted and modification of mother wavelet (complex Morlet) in conjunction with reassignment technique was proposed to extract the phase using direct maxima search algorithm for ridge detection.

Reassigned smoothed pseudo Wigner Ville distribution (RSPWVD) based technique was introduced in chapter 5 and provided an elegant approach of phase extraction from single fringe based cubic phase signal. Simulation and experimental investigation showed an improved accuracy of the extracted IF and phase of the signal.

Chapter 6 presented an elaborate study of some of the proposed phase extraction algorithms with the application to free surface velocity measurement in high strain rate experiments. Novel ellipse fitting technique was introduced to correct the measurement imperfections like phase angle and amplitude. Comparative studies of different ellipse fitting technique were carried out and Gauss Newton algorithm with initial condition from Bookstein method was proposed. Simulation and experimental results justified the proposed method. This chapter also discussed the possible application of IF extraction of fringe signals for measuring free surface velocity profile using heterodyne laser interferomerty. Simulated heterodyne type fringe signals were generated from measured VISAR velocity profiles and Reassigned CWT based technique was proposed for accurate extraction of velocity profile.

For future work, ridge detection technique with less computational burden could be investigated for proper representation of instantaneous frequency of the signal which has enormous applications in practical. Generalization of CWT in time frequency analysis is also an interesting problem. Polynomial Wigner Ville Distribution could be studied for multi-component polynomial phase signal. Complex time distribution (CTD) could be explored for polynomial signal. Ellipse fitting based on extended Kalman filter (EKF) method may provide the better result for fractional fringe signal with poor SNR value.

Abstract

Optical interferometry-based non-contact type measurements play a key role in determination of free surface velocity of target material under high strain rate experiments. Michelson interferometer in velocity as well as displacement mode configuration is widely used. As the information of velocity is hidden in phase or instantaneous frequency (IF), it is important to extract the phase or IF of the fringe signal. In time domain approach, multiple fringes are required to extract phase and numerical differentiation which is noise sensitive required to get the IF. Although computationally less expensive, the accuracy of this method may get affected significantly by various measurement imperfections like, nonlinearity, amplitude and phase angle error. On the other hand, in frequency domain approach single fringe may be sufficient to extract IF and numerical differentiation could be avoided. In this thesis, phase extraction based on quadrature phase shifting method, reassigned Continuous Wavelet Transform (CWT) method and Smoothed Pseudo Wigner-Ville Distribution (SPWVD) method have been described and developed. In phase shifting method amplitude and phase angle error have been corrected by efficient ellipse fitting method by combing algebraic as well as geometric technique. In CWT, time-bandwidth product of Morlet wavelet is optimised and simultaneous reassignment technique is applied for accurate IF extraction. SPWVD method is proposed for extracting IF of highly non-stationary polynomial frequency modulated fringe signal. Cohen class signal representation is followed and time and frequency resolutions are independently optimized using Gaussian separable kernel. Reassignment technique is further applied for sharpening of the spectrogram with these optimized kernels that improves accuracy in IF significantly. Finally, some of these developed phase extraction algorithms are applied to free surface velocity measurement under high strain rate experiments and different dynamic mechanical properties of AL2024T4 target material are derived from extracted velocity profile.

CHAPTER 1 Introduction

1.1 Phase Extraction Fundamental

The phase extraction of optical interferometric signals play important role in analyzing the opto-electrical signals generated while measuring the physical parameters such as displacement, strain, velocity, surface profile etc. employing non-contact methods such as interferometery [1-3]. Necessity of such measurements arises during non-destructive testing, profilometry and dynamic failure under shock wave loading etc. For example, free surface velocity history of target material under high strain rate experiment carries useful information on material behavior [4-8] for determination of yield strength and fracture strength at high strain rates (commonly known as dynamic yield strength and spall strength, respectively), and phase transitions. The displacement interferometer and velocity interferometers are commonly used techniques for measurement of free surface velocity. In these techniques the information of these physical quantities are stored in phase or instantaneous frequency (IF) of the recorded interference fringe signal [3]. Therefore, the extraction of phase or IF of the fringe signal using different signal processing algorithms becomes an important problem.

Mathematical form of typical interferometric fringe signal can be expressed as-

$$I(t) = a(t) + b(t)\cos(\phi(t)) \tag{1.1}$$

$$\phi(t) = 2\pi f(t)t \tag{1.2}$$

where $I(t)$ is the measured intensity, $a(t)$ is the background intensity, $b(t)$ is the fringe amplitude, $\varphi(t)$ and $f(t)$ are phase and frequency of the signal respectively. The aim of the analysis is to extract phase $\varphi(t)$ and or frequency $f(t)$ of the signal based on the different interferometer configuration.

Various methods of phase extraction algorithms are available in literature, which are broadly categorized as-(1) time domain approach by using phase shifting algorithm (2) frequency domain approach. In time domain approach multiple fringe signals are required to extract the phase. But in frequency domain approach single fringe is capable of producing phase of the signal. Moreover, in this technique phase and frequency can be simultaneously obtained which is often requirement. For example, displacement and velocity of a target material under impact experiment carry important information which can be obtained by measuring phase and frequency of the fringe signal simultaneously. In this approach we can avoid the numerical differentiation which is sensitive to error prone for getting the velocity (frequency) from measured only displacement (phase) of the signal. However, both the approach has merits and demerits.

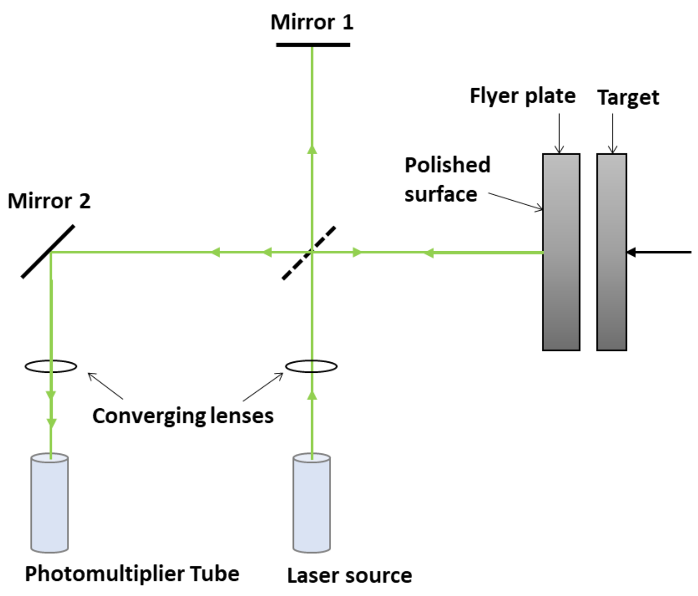

Fig. 1.1 Displacement mode Michelson interferometer

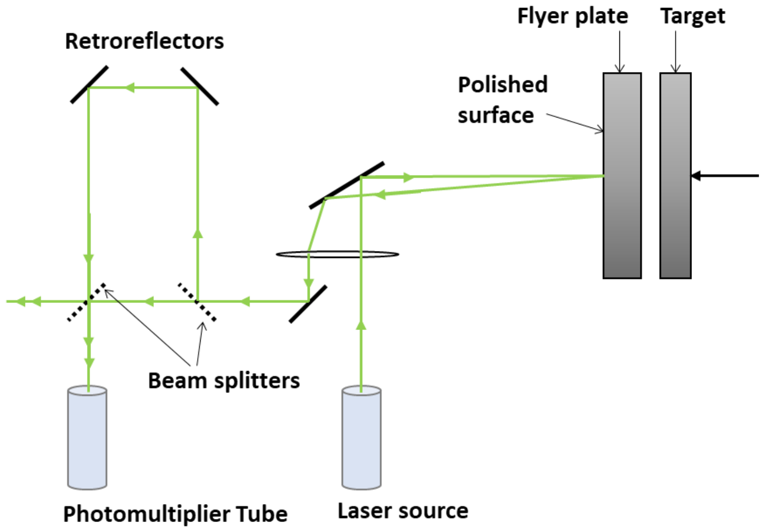

Fig. 1.2 Velocity mode Michelson interferometer

1.2 Interferometers Based on Michelson Interferometery

For use in high strain rate impact experiments, Michelson and Fabry-Perrot based interferometers are used [7]. However, Michelson interferometers in two categories according to their implementation are quite popular [4,7]. The two categories are displacement interferometers and velocity interferometers. Difference between these two types of interferometers and their working principles are discussed below.

1.2.1 Displacement Interferometer

A typical setup of displacement type Michelson-interferometer is depicted in Fig 1.1. In this configuration, surface of the target plate is polished to form one of the legs of the interferometer. Other leg of the interferometer is a stationary mirror M1. A laser beam is split in to two parts using a beam-splitter and these two beams incident on the polished target surface and the mirror M1. The laser beam reflected from the target surface and the mirror M1 are superimposed and a stationary interference fringe pattern is generated. Interaction with the shock wave causes the free surface of the target to move. This movement of free surface of target results in time dependent changes in the path difference between the beams from the two legs thereby generating shift in fringes. This shift in fringes is then used to infer the velocity of free surface as a function of time by applying following expression:

$$v(t) = \frac{\lambda}{2} f_i(t) \tag{1.3}$$

Where, $v(t)$ is velocity of the free surface in time t, $f_i(t)$ is instantaneous frequency of fringe in time t, and λ_0 is wavelength of the original laser beam. The fringe shift of optical signal is converted to an electrical signal using photomultiplier tube and recorded in oscilloscopes. However if phase of the fringe signal is extracted then displacement history of the free surface of target can be directly plotted.

The instrument is very sensitive and has excellent distance resolution. This interferometer can generate one complete fringe shift for a small free surface displacement of $\lambda_0/2$ only. Though, the extreme sensitivity has advantage of very fine resolution, it imposes a limitation on the maximum velocity that can be measured using this instrument. This problem arises due to frequency response limitation of the electronic equipment such as photomultiplier tube, amplifier, oscilloscopes used in the system. Moreover, shock wave has tendency to destroy the mirror finish of the free surface of target that often fails to maintain specular characteristic of interference pattern.

1.2.2 Velocity Interferometer

In contrast to the measurement of velocity as a function of time in displacement interferometer, the velocity interferometer employ measurement of differential Doppler shift of the light reflected off the moving target surface. In this configuration, interference pattern is generated by interaction of two laser beams reflected from the free surface at two different instants of time. The delay in between reflection of the two beams is created either by increasing the path length known as Specular Velocity Interferometer (SVI) or, by placing a solid etalon bar known as Velocity Interferometer System for Any Reflector (VISAR) in one of the legs of the interferometer [4,7]. This allows inferring velocity history of the free surface with very few numbers of fringes and also overcomes the fringe frequency limitations of displacement type interferometer. The velocity history of the target free surface is encoded in the phase of the fringe signals.

1.3 Research Objective

The aim of the present research activities is to develop novel analysis technique of phase and frequency extraction using both time and frequency domain approaches by addressing the existing shortcomings of the different techniques with application to velocity measurement in high strain rate experiments.

1.4 Contribution

The outline of the present studies is as follows:

Chapter 2 presents literature survey of existing phase extraction techniques of both temporal and frequency domain approaches.

Chapter 3 introduces phase shifting method of phase extraction algorithm and highlights the shortcomings of existing technique and presents possible solution.

Chapter 4 presents frequency domain approach of phase extraction by using Continuous Wavelet Transform (CWT).

Chapter 5 proposes Reassigned Smoothed Pseudo Wigner Ville Distribution method for cubic phase signal.

Chapter 6 highlights the application of some of the proposed methods in free surface velocity measurement in high strain rate experiments.

Chapter 7 summarizes the contribution of work and presents scope of possible future work.

CHAPTER 2 Literature Survey

Phase extraction algorithms are available in literature in the context of fringe analysis with major applications to metrology by using digital holographic interferometry, fringe projection interferometry and digital speckle pattern interferometry etc. [1-3]. In all these applications, optical fringe signals are directly captured by CCD camera and image analysis based phase extraction is applied. In some interferometric configuration, optical fringe signals are converted to voltage signals by using PMT or other photo detector and stored in digital storage oscilloscopes and analysis is carried out with this voltage signal to extract the phase of the signal [4]. Various methods of phase extraction are developed- broadly categorized as time domain approach and frequency domain approach [3].

In time domain approach multiple fringe signals are required to extract the phase known as phase shifting method. Different algorithms are proposed in this technique- N-bucket algorithm, least square approach, Carre's algorithm etc. N-bucket algorithm with four frames based technique is quite popular [9,10]. Accuracy of phase measurement depends upon the correctness of the phase shifting technique, which is often affected by various nonlinearities, hysteresis and other imperfections. To address this issue, various error compensating techniques have been proposed in literature [11,12]. Stochastic search, state space model and maximum likelihood estimation based approach have also been explored [13,14]. Further, in many cases amplitude and phase angle error between two quadrature fringe signals is unavoidable. However, this can be corrected by ellipse fitting technique [15-17] as quadratre fringe signals represent family of ellipse in Lissajous pattern. In certain applications, measured fringe signals do not complete the angular 2π rotation in Lissajous pattern and ellipse becomes incomplete or fractional. Despite so much of research activity already have been carried out in ellipse fitting, search for proper fitting algorithm to analyze the fractional fringe signal is still an active research topic.

In frequency domain approach, single fringe is capable of producing phase of the signal. Moreover in this technique, phase and frequency can be simultaneously obtained which are often required. For example, determination of material displacement and material velocity of a target subject to impact loading need information on both phase and frequency of the fringe signal simultaneously. In this approach noise sensitive numerical differentiation can be avoided for getting the velocity (frequency) from measured only displacement (phase) of the signal. Fourier transform based technique is most popular choice of frequency domain approach of phase extraction [18]. But when the fringe signals become non stationary, windowed Fourier transform [19] and wavelet transforms based techniques are applied [20-23]. Continuous Wavelet Transform (CWT) is more suitable as it makes use of adaptive time window that overcomes the fixed resolution problem in windowed Fourier transform. Morlet wavelet as mother wavelet is widely applied as it utilizes modulated sinusoidal signal in Gaussian window which is qualitatively similar to fringe signal [20]. Recently, generalised Morse wavelet as a superfamily of analytic wavelet is introduced with an added parameter that can change the shape of mother wavelet with the fixed time duration or bandwidth [24,25]. Comparative studies with other mother wavelet like Mexican hat, Paul, Morse, DOG etc. are also available in literature but Morlet is quite popular [21]. The product of central frequency and time variance of Gaussian window (f_0t) of Morlet wavelet determines the capability of extracting low and high frequency signal component simultaneously with a reasonable accuracy. Modification of Morlet wavelet parameters was explored by Abid et al [26] who suggested that time variance of 0.5 is optimum for fringe analysis. Later Rueda et al [27] investigated it in the context of power system low frequency electromechanical oscillation identification and proposed several criteria for selecting central frequency and time variance parameters. However, modifying only Morlet wavelet parameters do not always provide the best possible result, increasing time-frequency energy density may be required for preserving good localisation properties. The modulus of maximum of wavelet coefficients form a path known as wavelet ridge [28-31]. Ideally ridge can be extracted from the time-frequency (T-F) energy density using the maximum modulus of complex array. However, due to various imperfections, maxima search algorithm fails to detect the exact ridge points. To address this problem, in 1997 R. A. Carmona et al [28] proposed various algorithms of ridge detection like cost function minimization, snake penalisation, phase map algorithm, simulated annealing and later in 1999 proposed crazy climber algorithm [29]. All these algorithms use complex dynamic optimization techniques. Later, only cost function minimization and phase map algorithms have been applied for optical phase extraction application by many researchers [21,30,31]. Avoiding these complex ridge detection algorithms and effective use of direct maxima search algorithm with possible modification of time-frequency energy density is still an open area for research.

Phase unwrapping is an important steps in phase extraction algorithm in both phase shifting method and frequency domain method. Many applications required to have robust phase unwrapping algorithms and literature in this direction is available in abandon [32,33].

Wigner Ville Distribution (WVD) method is recently introduced for direct phase as well as frequency estimation of fringe signal [34,36]. In this method complex phase unwrapping can be avoided. Though WVD has many good properties and provides best possible resolution among all of the time-frequency (TF) techniques, undesirable cross-term interference effect is its main drawbacks [37-39]. WVD is also highly non local and to make it local windowing operation is introduced popularly known as Pseudo Wigner-Ville Distribution (PWVD) [38]. One of the immediate consequences of windowing is suppression of cross-terms effect to some extent for multi-component signal. However, these benefits are achieved at the cost of blurring of the auto-terms of the signal and a loss of many desirable theoretical properties. The unsatisfactory result leads to the development of general form of quadratic representations by introducing 2-D kernel function proposed by Cohen [37]. By examining this kernel function various properties of bilinear TF distribution can be ascertained. Therefore, the smoothing in the ambiguity function domain combined with the kernel function allows both the suppression of the cross-terms and the preservation of the auto-ambiguity terms of the analyzed signal. When the kernel function is separable, an independent and progressive control can be applied to the WVD in both time and frequency directions known as Smoothed Pseudo Wigner-Ville Distribution (SPWVD) [37,38]. WVD has an optimum *t-f* representation for linear FM or quadratic phase signal. For nonlinear FM signal this optimality is lost and smeared spectral representation obtained. To address this problem to analyze the polynomial phase signal, polynomial Wigner-Ville distribution has been introduced [40,41]. However, when signal comes with polynomial phase along with nearly discontinuous IF, no investigation is yet carried out.

In the context of high strain rate application for the measurement of free surface velocity, Michelson interferometer in velocity and displacement mode is used [4,7]. VISAR [4] is popularly used as a velocity mode configuration. In this technique phase of the fringe signal carries the desired information. Many interesting material properties such as Hugonoit Elastic Limit (HEL), dynamic yield strength and spall strength can be inferred from the measured free surface velocity history of target material [7]. These material properties find immense applications in defense, geophysics, aerospace, automobile etc. VISAR is basically a modified version of wide angle Michelson interferometer in which two Doppler shifted lights reflected from target free surface at two different instants of time interfere each other to form fringe pattern [4]. Therefore, it works in the velocity mode or differential displacement mode configuration. Phase shifting method is used to analyze the fringe signal and quadrature coded interference fringes are utilized for differentiating between the acceleration and deceleration of target free surface. In displacement configuration heterodyne technique popularly known as Photonic Doppler Velocimetry (PDV) has come into use to overcome the challenges involved in the VISAR measurements. Comparative study of VISAR and PDV in terms of accuracy and precession is an active topic of research at present [42]. However, VISAR is still widely used and preferred technique in dynamic compression experiments where many issues related to signal analysis yet remain to be investigated. Gourdin explained the analysis technique in presence of large intensity changes [43]. Hemsing also pointed out various measurement imperfections like input light intensity variations, uncompensated dc offset voltages, nonlinearities in the photo detectors, unequal amplitudes of the detector signal etc [6] and corresponding corrective measures before carrying out experiments. Dolan [15] gave an elaborate study of VISAR signal analysis technique including velocity corrections, fringe ambiguity and uncertainty, amplitude and phase angle correction, dynamic contrast loss etc. Majority of these imperfections can be controlled by arranging good experimental set up. Though amplitude and phase angle error between two quadrature signals is unavoidable but it can be corrected by employing proper ellipse fitting technique. Dolan also discussed different ellipse fitting technique suitable for VSIAR signal. However comparative assessment of existing ellipse fitting techniques and their applicability to VISAR signal remains to be addressed properly.

As mentioned earlier in displacement mode heterodyne technique is applied and instantaneous frequency of the fringe signal carries the information of the free surface velocity. Fringe signal is also highly non stationary and STFT, CWT are used for extracting the IF [44,45]. Limited literatures are available for improving the analysis of varied class of signals.

CHAPTER 3 Phase Extraction by Quadrature Phase Shifting Method

3.1 Introduction

Phase shifting method is widely used and quite popular in phase measurement [1-4]. It is computationally simple and can handle nearly discontinuous phase variation. In this technique multiple fringes are required to extract the phase of the signal. There are many variations of phase shifting algorithms available such as two, three and four fringes based technique. However, most common phase shifting method is four fringe based technique. As mentioned earlier mathematical form of typical interferometric fringe signal can be expressed as-

$$I(t) = a(t) + b(t)\cos(\phi(t)) \tag{3.1}$$

where $I(t)$ is the measured intensity, $a(t)$ is the background intensity, $b(t)$ is the fringe amplitude, $\varphi(t)$ is phase of the signal. In the above equation three unknown exists: $a(t)$, $b(t)$ and $\varphi(t)$. $\varphi(t)$ carries the information of interest and other two variables need to be eliminated. To address this issue four fringes are needed with mutual phase shift of $\pi/2$ radians between them. Four fringes are now can be expressed as-

$$I_1(t) = a(t) + b(t)\cos(\phi(t)) \tag{3.2}$$

$$I_2(t) = a(t) + b(t)\cos\left(\phi(t) + \frac{\pi}{2}\right) \tag{3.3}$$

$$I_3(t) = a(t) + b(t)\cos(\phi(t) + \pi) \tag{3.4}$$

$$I_4(t) = a(t) + b(t)\cos\left(\phi(t) + \frac{3\pi}{2}\right) \tag{3.5}$$

Now subtracting (3.4) from (3.2) gives;

$$I_1(t) - I_3(t) = 2b(t)\cos(\phi(t)) \tag{3.6}$$

Further subtracting (3.3) from (3.5) gives;

$$I_4(t) - I_2(t) = 2b(t)\sin(\phi(t)) \tag{3.7}$$

Thus required phase information can be determined by dividing (3.7) by (3.6) which gives;

$$\phi(t) = \arctan\left(\frac{I_4 - I_2}{I_1 - I_3}\right) \tag{3.8}$$

The resultant phase is wrapped between –π to π or 0 to 2π due to inherent property of the mathematical *arctan* function and phase unwrapping algorithm is required to remove this 2π phase jump.

Although, this four fringe based technique ideally possess efficient usage of light, improves signal to noise ration, it also suffers from non ideal measurement effects (unequal amplitude and phase angle error) due to presence of polarizing beam splitter and other optical components. Thus equations (3.2) to (3.7) are re-written as-

$$I_1(t) = a_1(t) + b_1(t)\cos(\phi(t)) \tag{3.9}$$

$$I_2(t) = a_2(t) + b_2(t)\cos\left(\phi(t) + \frac{\pi}{2} - \varepsilon\right) \tag{3.10}$$

$$I_3(t) = a_3(t) + b_3(t)\cos(\phi(t) + \pi) \tag{3.11}$$

$$I_4(t) = a_4(t) + b_4(t)\cos\left(\phi(t) + \frac{3\pi}{2} - \varepsilon\right) \tag{3.12}$$

Now subtracting (3.11) from (3.9) gives;

$$I_1(t) - I_3(t) = a_3(t) - a_1(t) + (b_3(t) + b_1(t))\cos(\phi(t)) \tag{3.13}$$

Equation (3.13) can expressed as-

$$I_x(t) = a_x(t) + b_x(t)\cos(\phi(t)) \tag{3.14}$$

Similarly subtracting (3.10) from (3.12) gives;

$$I_4(t) - I_2(t) = a_4(t) - a_2(t) + (b_2(t) + b_4(t))\cos(\phi(t) - \varepsilon) \tag{3.15}$$

Equation (3.15) can be expressed as-

$$I_y(t) = a_y(t) + b_y(t)\cos(\phi(t) - \varepsilon) \tag{3.16}$$

Here ε is the phase angle error. In general background intensity of equation (3.14) and (3.16) are made zero by increasing or decreasing the gain of a particular detector or by adjusting numerically. Therefore equation (3.14) and (3.16) can be expressed as-

$$I_x(t) = b_x(t)\cos(\phi(t)) \tag{3.17}$$

$$I_y(t) = b_y(t)\cos(\phi(t) - \varepsilon) \tag{3.18}$$

By using above two equations phase can be expressed as-

$$\phi(t) = \arctan\left(\frac{I_y(t)}{I_x(t)}\frac{b_x(t)}{b_y(t)}\sec\varepsilon + \tan\varepsilon\right) \tag{3.19}$$

Equation (3.17) and (3.18) form an ellipse equation whose centre is at origin and major axis, minor axis and angle of rotation are b_x, b_y and ε respectively. Although phase expression seems to be very simple at first glance it also needs more work for non ideal measurement by proper ellipse fitting to get the required phase.

Therefore, it is emphasised on development of two fringe shift based phase shifting algorithm as it needs less number of components and easy to handle. Mathematical expression is quite similar to four fringe shift algorithm.

In case of two fringe shift based phase shifting algorithm, two non ideal equations can be written as

$$I_1(t) = a_1(t) + b_1(t)\cos(\phi(t)) \tag{3.20}$$

$$I_2(t) = a_2(t) + b_2(t)\cos\left(\phi(t) + \frac{\pi}{2} - \varepsilon\right) \tag{3.21}$$

$$I_2(t) = a_2(t) + b_2(t)\sin(\phi(t) - \varepsilon) \tag{3.22}$$

By using equation (3.20) and (3.22) phase can be expressed as-

$$\phi(t) = \arctan\left(\frac{I_2(t) - a_2(t) b_1(t)}{I_1(t) - a_1(t) b_2(t)} \sec\varepsilon + \tan\varepsilon \right) \tag{3.23}$$

Equation (3.19) and (3.21) form an ellipse equation whose centre is at (a_1,a_2) and major axis, minor axis and angle of rotation are b_1, b_2 and ε respectively. These five unknown parameters are obtained proper ellipse fitting method.

3.2 Ellipse Fitting

Ellipse fitting or any general conic fitting is an important problem in many fields such as pattern recognition and computer vision, astronomy, structural geology and many more. In literature ellipse fitting is broadly categorized in two techniques: (1) Algebraic fitting and (2) Geometric or Iterative fitting [46-54]. Algebraic technique uses least square fitting that minimizes some measured distance between data points and ellipse. Thus it becomes linear, simple and efficient. On the other hand geometric method uses nonlinear optimization technique to fit the ellipse which is computationally less expensive. Algebraic method of fitting is implemented for analysis of fringe signals generated in displacement mode configuration.

3.3 Phase Unwrapping

As discussed earlier phase expressed in equation (3.19) and (3.23) are wrapped and proper phase unwrapping algorithm needs to be developed to get the continuous phase distribution. First this mod π is converted to mod 2π phase by using four quadrant *arctan* functions described in equation (3.24) and then 2π phase jump is removed by using phase unwrapping algorithm described in equation (3.25) and (3.26).

$$\phi(t)=\begin{cases} \frac{\pi}{2} & I=0, I_1>0 \\ \frac{3\pi}{2} & I=0, I_1<0 \\ \arctan\left(\frac{I_1}{I}\right) & I>0, I_1\geq 0 \\ 2\pi+\arctan\left(\frac{I_1}{I}\right) & I>0, I_1<0 \\ \pi+\arctan\left(\frac{I_1}{I}\right) & I<0 \end{cases} \tag{3.24}$$

$$\phi_u(t)=w[\phi(t)] \tag{3.25}$$

$$\phi_u(t)=\phi(t)+2\pi k \tag{3.26}$$

where $\varphi_u(t)$ is the unwrapped phase and w is the unwrapping operator, k is an integer.

Various phase unwrapping algorithm are available which can be classified in two categories: time and frequency domain technique. In frequency domain approach

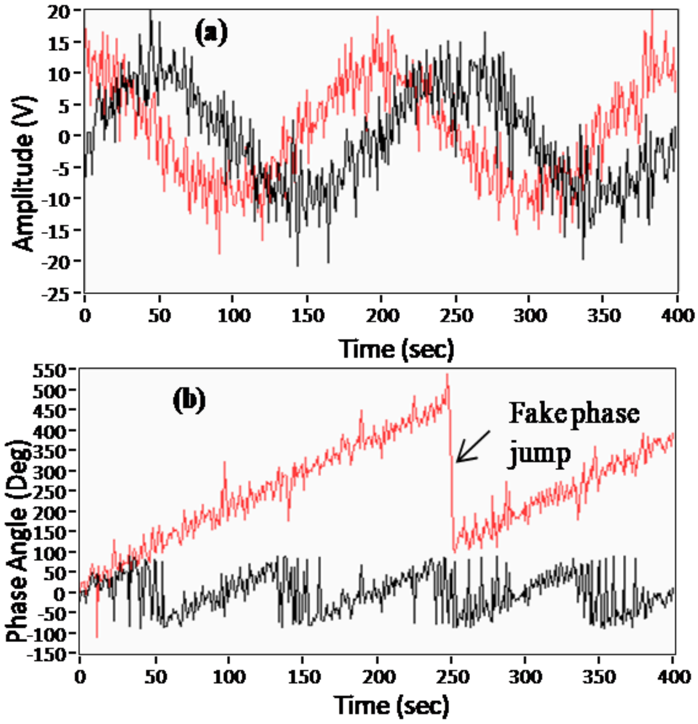

Fig. 3.1 (a) Simulated Sinusoidal noisy signal (b) Undesired phase jump in unwrapped signal

phase extraction depends upon the information of neighbouring points. Examples of this technique are Fourier fringe analysis, Wavelet fringe analysis and direct phase demodulation etc. In these techniques a single fringe is sufficient to extract the phase. In time domain approach phase extraction depends upon only the current amplitude of different fringes. It does not require the knowledge of surrounding point's amplitude values. Example of this technique is phase stepping algorithm. However, this technique requires more than one fringe to extract the phase information.

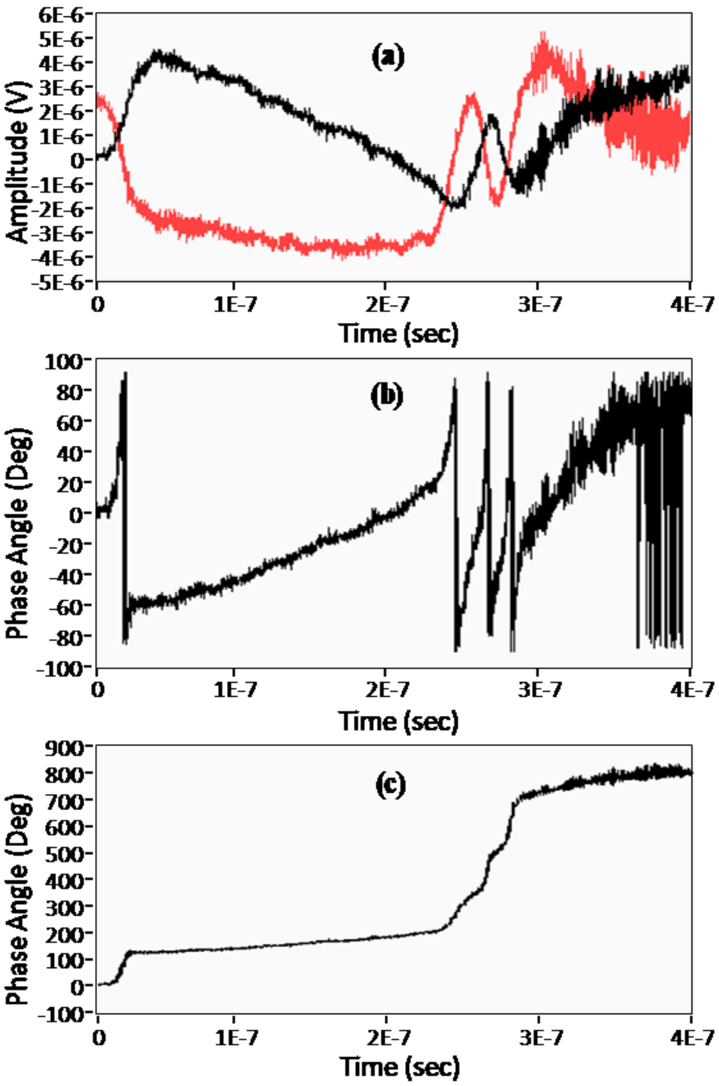

Fig. 3.2 (a) Experimentally recorded velocity interferometer fringe signal (b) Wrapped phase (c) Unwrapped Phase

Selection of particular technique depends on application i.e. dynamic, static, noise, computational complexity etc. Direct-recursive algorithm of phase stepping method is developed which is easy to implement, computationally simple, and relatively robust.

The basic principle of direct-recursive algorithm is that the absolute value of the phase difference between two adjacent points is smaller than π. If the phase sequence is considered as $\{\varphi_i\}_n$ then the calculation steps are as follows:

(i) Calculate the phase difference: $\Delta\varphi=\varphi_{i+1}-\varphi_i$;

(ii) Adjust the difference to $[0,2\pi)$:

$$\Delta\phi = \begin{cases} \Delta\phi - 2\pi & \Delta\phi \geq \pi \\ \Delta\phi + 2\pi & \Delta\phi < -\pi \\ \Delta\phi & \text{others} \end{cases}$$

(iii) Calculate the unwrapped phase: $\varphi_{i+1}=\varphi_i+\Delta\varphi$;

The algorithm is validated with simulated sinusoidal profiles with linear phase signal shown in Fig. 3.1 (a). Additive White Gaussian Noise (AWGN) is also added to simulated profiles and phase unwrapping is performed to test the robustness of the algorithm described in Fig 3.1(a). In Fig.3.1 (b) the undesired phase jump occurs for the value of SNR 5.9(dB). Above this value the algorithm is proved to be robust. Further to show the efficacy of the proposed phase unwrapping algorithm, experiments are conducted using Michelson interferometer in velocity mode configuration in Light Gas Gun facility for highly non linear phase signal. Prototype description of interferometer is shown in Fig. 1.2. Here, a flyer plate moving in very high velocity hits the target material and outer surface of target material starts moving. As the laser light focuses on the outer surface of the target material, the interference fringes are generated between two Doppler shifted signals at two different instant of time and velocity of target material is proportional to phase of the fringe signals. The recorded quadrature fringe signals are shown in Fig. 3.2(a). Further, proposed phase unwrapping algorithm is applied on this fringe signals and resultant wrapped (-90 to +90 degree) and unwrapped phase (in the rage of 0 to 800 degree) signals are plotted in Fig. 3.2(b) and Fig. 3.2(c) respectively.

3.4 Experimental Program

Optical fringe signal is generated by using basic displacement Michelson interferometer by periodic movement of one of the mirrors while keeping other mirror stationary. The PZT transducer is used to generate periodic displacement. Two fringe shift based configuration is shown in Fig.3.3. Measured quadrature fringe signals along with applied PZT voltage are shown in Fig.3.4. This optical fringe signal is converted to electrical signal by using PMT and stored in digital storage oscilloscope (DSO). FFT analysis of one of the recorded fringe signals is also carried out for better understanding the non-stationary nature of frequency component and is shown in Fig.

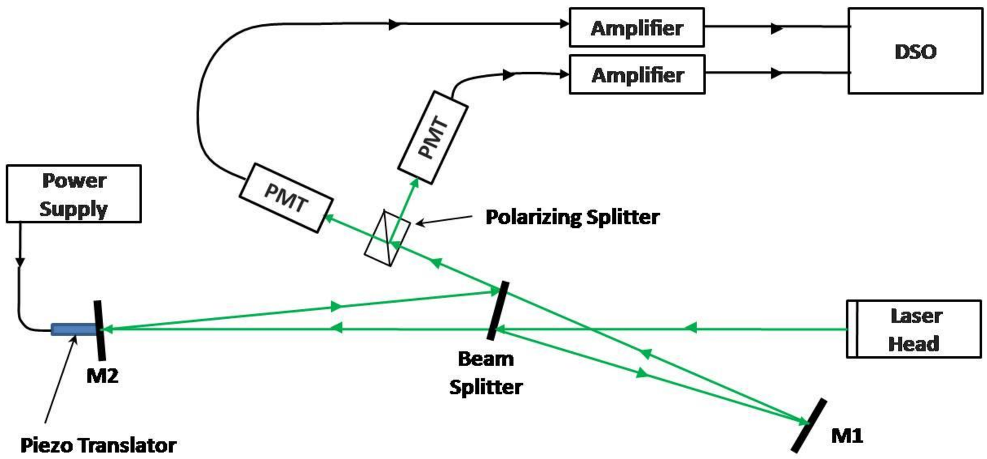

Fig. 3.3 Michelson interferometer in displacement mode configuration

3.5. The required phase can be obtained using equation (3.23). However, equation (3.23) needs calculation of ellipse parameters. The extracted ellipse parameters in one of the complete fringes of Fig. 3.4 are a_1=0.018, a_2=0.015,b_1=0,b_2=0.002 and ε=0.48, and lissajeous plot of fringe signals and fitted ellipse are shown in Fig. 3.6. Using this ellipse parameters phase is calculated using equation (3.23). However, this phase is wrapped and phase unwrapping algorithm is applied to get the unwrapped phase. After calculating the unwrapped phase, number of fringe shifts is determined using equation (3.27) and finally displacement is calculated using equation (3.28) and shown in Fig.3.7. Measured peak displacement is 2.06μm. It is also observed that extracted displacement profile is closely equivalent to PZT supply voltage shown in Fig. 3.4, as displacement of PZT is proportional to supply voltage.

$$F(t) = \frac{\phi(t) - \phi(t_i)}{2\pi} \tag{3.27}$$

$$s(t) = \frac{\lambda}{2} F(t) \tag{3.28}$$

Here, $s(t)$ is the displacement of the mirror, Laser wavelength λ=532nm, $F(t)$ is total fringe shift, $\varphi(t_i)$ is the initial phase.

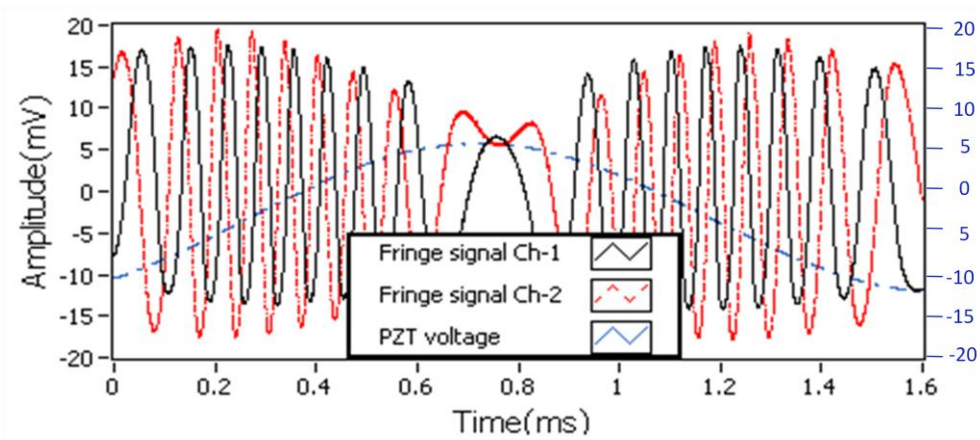

Fig. 3.4 Measured fringe signal of two fringe shift method

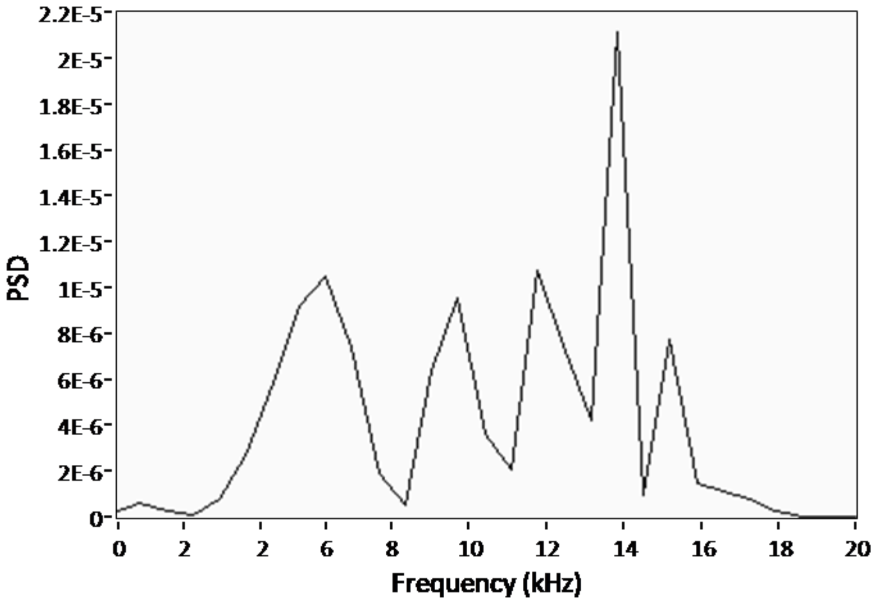

Fig. 3.5 FFT analysis of fringe signal of Ch-1

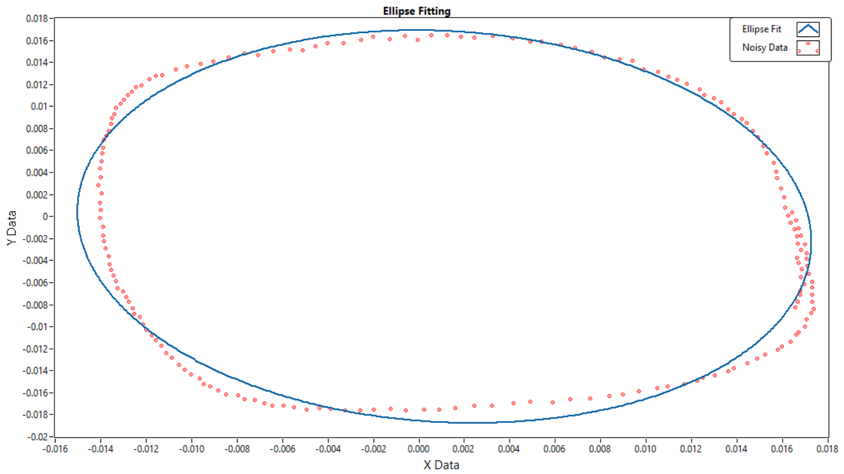

Fig. 3.6 Ellipse fitting of measured fringe signal

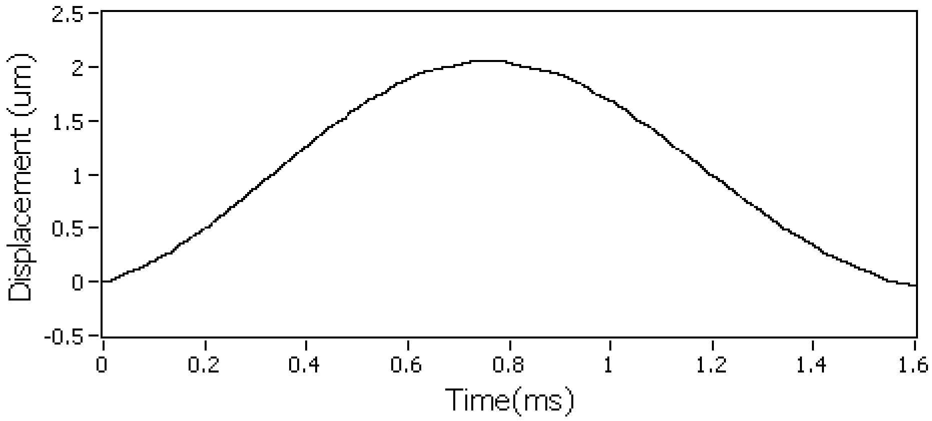

Fig. 3.7 Extracted displacement profile

3.5 Conclusion

Optical phase extraction algorithm based on two fringe shift technique is demonstrated. Measurement imperfections are modelled and corrective action is proposed by introducing ellipse fitting method. Phase unwrapping technique is developed based on direct recursive phase stepping algorithm. Robustness of the phase unwrapping algorithm is tested with additive Gaussian noise and found to be robust above SNR 6dB. Further, phase unwrapping is applied to experimentally recorded fringe signal in velocity mode configuration and found to be effective. Finally, experiment is conducted in displacement interferometer and fringes are generated by moving one of the mirrors with applied PZT voltage. Phase unwrapping algorithm works properly. Although amplitude and phase angle are corrected by ellipse fitting technique, relative non-linear error presents in displacement profile.

CHAPTER 4 Phase Extraction by Reassigned Continuous Wavelet Transform Method

4.1 Introduction

In the previous chapter phase extraction based on quadrature phase shifting method is introduced. It is found that relative non-linear error between fringes presents in the extracted displacement profile. Therefore single fringe based analysis is always demanding. To address this problem Continuous Wavelet Transform based technique is introduced in this chapter.

4.2 Background

4.2.1Ridge of Continuous Wavelet Transform

A wavelet is an oscillatory function $\psi(t) \in L_2(R)$ with limited number of oscillation, zero mean and centred at $t=0$.The function $\psi(t)$ is called "mother wavelet". A wavelet $\psi_{a,b}(t)$ at any time and scale obtained by dilating and translating the mother wavelet with a, b respectively can be expressed as:

$$\psi_{a,b}(t) = \frac{1}{\sqrt{a}}\psi\left(\frac{t-b}{a}\right), a \ \varepsilon \ R^{+}, b \ \varepsilon \ R) \tag{4.1}$$

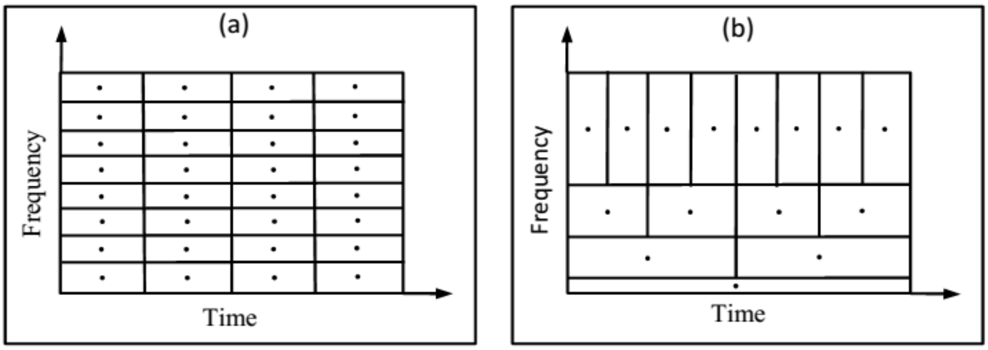

Fig. 4.1 Time frequency tiling (a) STFT (b) CWT

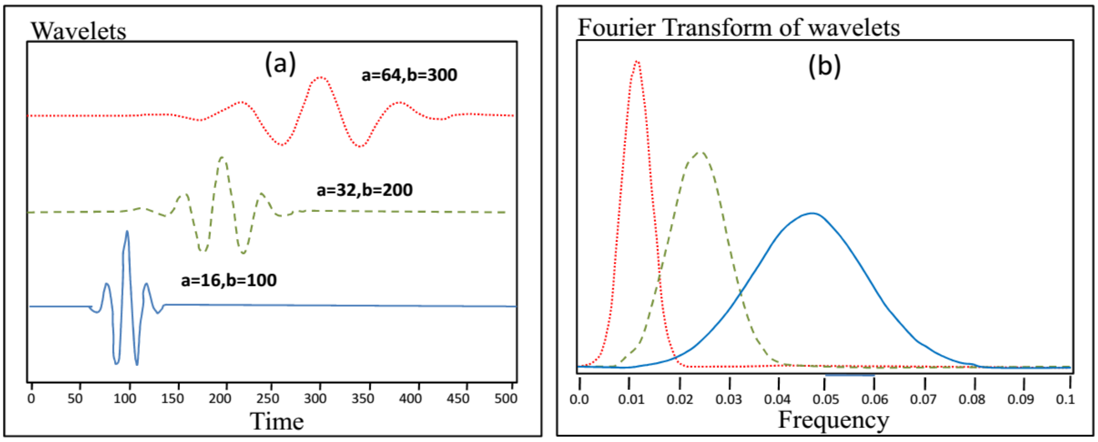

Fig. 4.2 (a) Dilated and Translated Morlet wavelet (b) Fourier transform of Morlet wavelet

The Continuous Wavelet Transform (CWT) of a function $f(t) \in L^2(R)$ is the inner product of $f(t)$ and $\psi_{a,b}(t)$

$$W_f(a,b;\psi) = \langle f, \psi_{a,b} \rangle = \int_{-\infty}^{\infty} f(t)\psi^*\left(\frac{t-b}{a}\right)dt \tag{4.2}$$

The function $f(t)$ can be reconstructed from wavelet coefficient $W_f(a,b;\psi)$ by using following relation

$$f = \frac{1}{C_\psi} \int_{-\infty}^{\infty} \int_{-\infty}^{\infty} W_f(a,b) \frac{1}{\sqrt{a}} \psi\left(\frac{t-b}{a}\right) db \frac{da}{a^2} \tag{4.3}$$

where constant C_ψ is defined as

$$C_\psi = \int_{-\infty}^{\infty} \frac{|\hat{\psi}(\omega)|^2}{\omega} d\omega < \infty \tag{4.4}$$

Equation (4.4) is called admissibility condition which ensures that inverse wavelet transform exists for a given problem. It may be noted that for C_ψ to be finite, wavelet should have no zero-frequency component-

$$\hat{\psi}(0) = 0 \tag{4.5}$$

This also implies that:

$$\int_{-\infty}^{\infty} \psi(t)dt = 0 \tag{4.6}$$

These two conditions also ensure that wavelet is localised in both time and frequency domain and behaves like a band pass filter.

As mentioned earlier the optical fringe signal is basically a frequency modulated signal expressed as:

$$f(t) = A(t)\cos\phi(t) \tag{4.7}$$

The analytic version of the above signal $f_a(t)$ may be obtained by using Hilbert Transform ($Hf(t)$) and is given as -

$$f_a(t) = f(t) + iHf(t) \tag{4.8}$$

If the fringe signal $f(t)$ is asymptotic, which is a reasonable approximation of many optical fringe signal, then $f_a(t)$ is closely equal to exponential model-

$$f_a(t) \approx A(t)e^{i\phi(t)} \tag{4.9}$$

This representation is useful to properly define the instantaneous frequency of the fringe signal as derivative of phase [37].

Consider Morlet as mother wavelet which is a plane wave modulated by a Gaussian function and is defined as-

$$\psi(t) = \frac{1}{\sqrt[4]{\sigma^2\pi}} \exp\left(-\frac{t^2}{2\sigma^2} + j\omega_0 t\right) \tag{4.10}$$

where σ^2 is the variance of the Gaussian envelope and ω_0 is central frequency of the mother wavelet. Dilated and translated version of Morlet wavelet in temporal and Fourier space are shown in Fig.4.2 (a) and (b) respectively. It is found that in Fourier space it is peaked near $\omega=\omega_0$.

By applying stationary phase principle, the Morlet wavelet transform for asymptotic and locally monochromatic analytic signal $f_a(t)$ can be described as [55]-

$$W_f(a,b;\psi) \approx \frac{1}{2} A(b) \exp\{i\phi(b)\} \hat{\psi}^*(a\phi'(b)) + O\left(\left|A'\right| / \left|A\right|, \left|\phi\phi''\right| / \left|\phi'\right|^2\right) \tag{4.11}$$

where $O(.)$ is an infinitesimal. If we ignore the infinitesimal part of the above expression it can be $\left|W_f(a,b;\psi)\right|$ ascertained that reaches maximum when:

$$a\phi'(b) = \omega_0 \tag{4.12}$$

$$a = a_r(b) = \frac{\omega_0}{\phi'(b)} \tag{4.13}$$

$$\omega_i(b) = \phi'(b) = \frac{\omega_0}{a_r(b)} \tag{4.14}$$

Equation (4.14) justifies that phase derivative in analytic representation of signal is simply an instantaneous frequency. The set of points $\{b, a_r(b)\}$ form a curve known as ridge of the wavelet transforms and related to instantaneous frequency (ω_i) of the signal at different scale. Thus, $\left|W_f(a,b;\psi)\right|$ forms a local time-scale energy density of the signal called scalogram. Further using equation (4.14) scalogram can be converted to time-frequency spectrogram. Ideally ridge can be extracted from the time-frequency (T-F) energy density using the maximum modulus of complex array. However, due to various imperfections maxima search algorithm fails to detect the exact ridge points. To address this problem, in 1997 R. A. Carmona et al [28] proposed various algorithms of ridge detection like cost function minimization, snake penalisation, phase map algorithm, simulated annealing and later in 1999 proposed crazy climber algorithm [29]. All these algorithms use complex dynamic optimization techniques. Later cost function minimization and phase map algorithm have only been applied for optical phase extraction application [21,31].

Once the instantaneous frequency ω is computed by using (4.14), the phase distribution can be extracted by integrating the instantaneous frequencies and no phase unwrapping algorithm is required. This method is known as frequency estimation technique.

It is to be noted that phase can also be extracted from wavelet coefficients known as phase estimation technique. In this method, complex Morlet wavelet is applied to the fringe signal and two dimensional complex arrays are generated. Hence, the modulus and the phase arrays can be calculated by using (4.15) and (4.16) respectively.

$$abs(a,b) = \left| W_f(a,b;\psi) \right| \tag{4.15}$$

$$\varphi(a,b) = \tan^{-1}\left(\frac{\Im\{W_f(a,b;\psi)\}}{\Re\{W_f(a,b;\psi)\}} \right) \tag{4.16}$$

To compute the phase of the signal, first ridge points are determined and then its corresponding phase values are found from the phase array using equation (4.16). A wrapped phase map from $-\pi$ to $+\pi$ is resulted and unwrapping algorithm is required to unwrap it. In this technique simultaneous IF estimation is difficult as noise sensitive numerical differentiation of phase signal may be required.

4.2.2 Time-frequency resolution

The time frequency resolution of CWT depends on spread of $\psi(a,b)$ in time-frequency domain. As $\psi(t)$ is centred at $t=0$ the $\psi_{a,b}(t)$ is centred at $t=b$. The spread or variance in time domain is calculated from

$$\int_{-\infty}^{\infty}(t-b)^2\left|\psi_{a,b}(t)\right|^2 dt = a^2\sigma_t^2 \tag{4.17}$$

where

$$\sigma_t^2 = \int_{-\infty}^{\infty} t^2\left|\psi(t)\right|^2 \tag{4.18}$$

In frequency domain, the centre frequency $\boldsymbol{\omega_0}$ of $\hat{\psi}(\omega)$ is expressed as

$$\omega_0 = \frac{1}{2\pi}\int_0^{\infty}\omega\left|\hat{\psi}(w)\right|^2 d\omega \tag{4.19}$$

The centre frequency of $\hat{\psi}_{a,b}(\omega)$ is

$$\omega = \frac{\omega_0}{a} \tag{4.20}$$

The spread in frequency domain around ω_0/a is

$$\sigma_\omega^2 = \frac{1}{2\pi}\int_0^{\infty}(\omega-\omega_0)^2\left|\hat{\psi}(\omega)\right|^2 d\omega \tag{4.21}$$

4.2.3 Time-frequency reassignment

Time-frequency reassignment technique is predominantly applied to bi-linear transformation like pseudo Wigner-Ville distribution [37,38] for sharpening the T-F energy density where smoothing kernel is used to reduce interference effect but at the same time it smears T-F energy density. Being a post processing method this technique can also be applied to T-F energy density of linear transform like CWT or

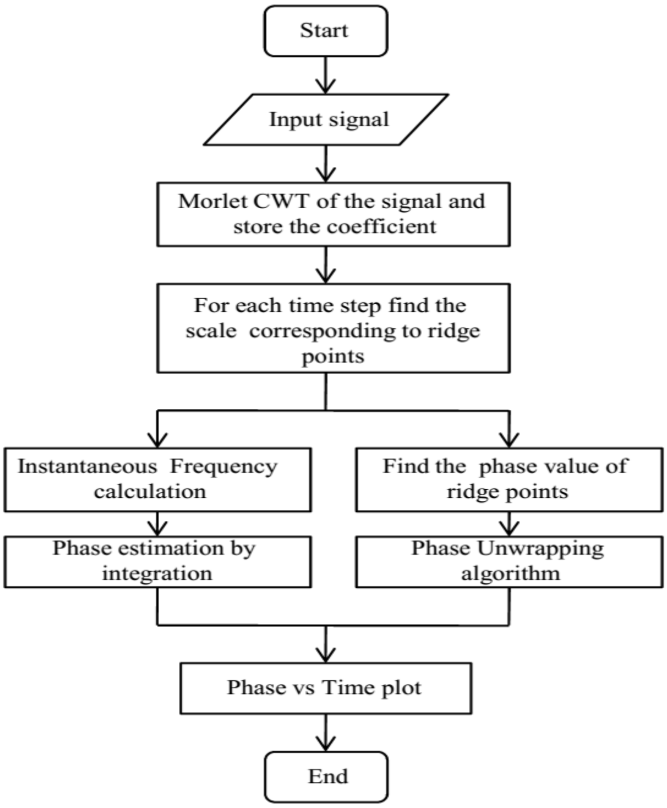

Fig. 4.3 Flowchart of proposed algorithm

Gabor. This technique was first developed by Kodera et al [56] for STFT signal in 1978 and after 15 years it was generalized to use in any bi-linear time-frequency or time-scale representation by F. Auger and P. Flandrin [38]. Applicability of this technique in CWT is justified as CWT also suffers from resolution problem limited by uncertainty principle. But instead of fixed resolution in Gabor it has adaptive resolution related to scale at ridge points and resolution of mother wavelet. Though reassignment technique does not improve the resolution problem directly but it can able to improve the signal concentration particularly low energy components, which in turn lead to improvement in readability of spectrogram. Moreover, due to this improved readability, the direct maxima search algorithm performs better and overall measurement accuracy improved significantly. In reassignment technique of CWT, time-scale gravity centre of resolution window is calculated and shifted by its neighboring geometrical center. It can be described as-

$$RMSG_f\left(\hat{a},\hat{b};\psi\right)=\iint\left(\frac{\hat{a}}{a}\right)^2 MSG_f\left(\hat{a},\hat{b};\psi\right)\delta\left[\hat{b}-b^{'}(a,b)\right]\delta\left[\hat{a}-a^{'}(a,b)\right]dadb \qquad (4.22)$$

where

$$b^{'}(a,b)=b-\mathrm{Re}\left[a\frac{W_f\left(a,b;\psi^{'}\right)W_f^{*}(a,b;\psi)}{\left|W_f\left(a,b;\psi^{'}\right)\right|^2}\right] \qquad (4.23)$$

$$\frac{\omega_0}{a^{'}(a,b)}=\frac{\omega_0}{a}+\mathrm{Im}\left[\frac{W_f\left(a,b;\hat{\psi}\right)W_f^{*}(a,b;\psi)}{2\pi a\left|W_f(a,b;\psi)\right|^2}\right] \qquad (4.24)$$

$$\psi^{'}(t)=t\psi(t),\hat{\psi}(t)=\frac{d\psi}{dt}(t) \qquad (4.25)$$

Here, $RMSG_f$ denotes reassigned and modified scalogram.

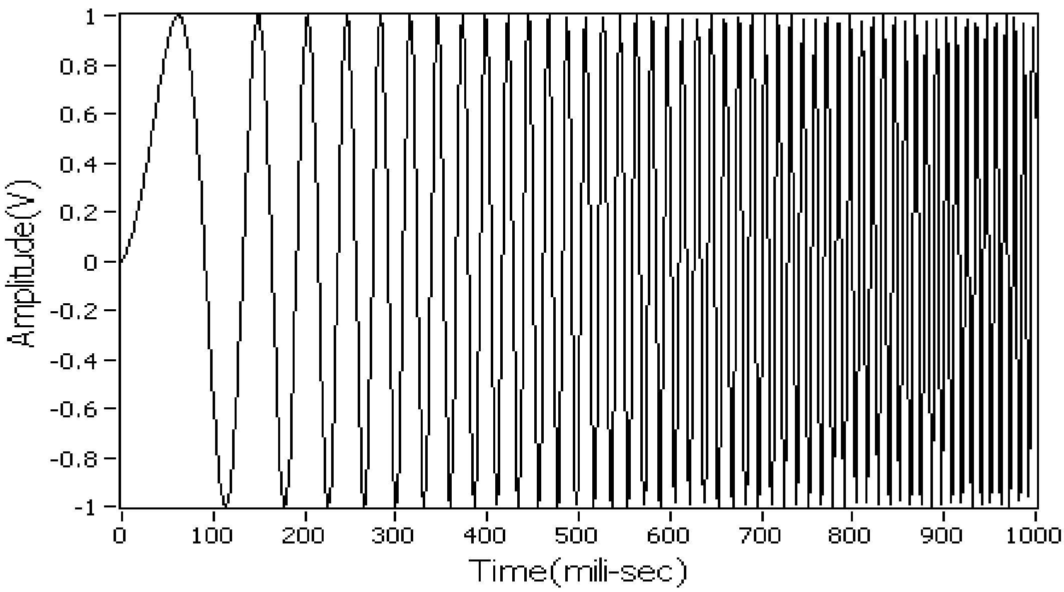

Fig. 4.4 Simulated linear chirp signal

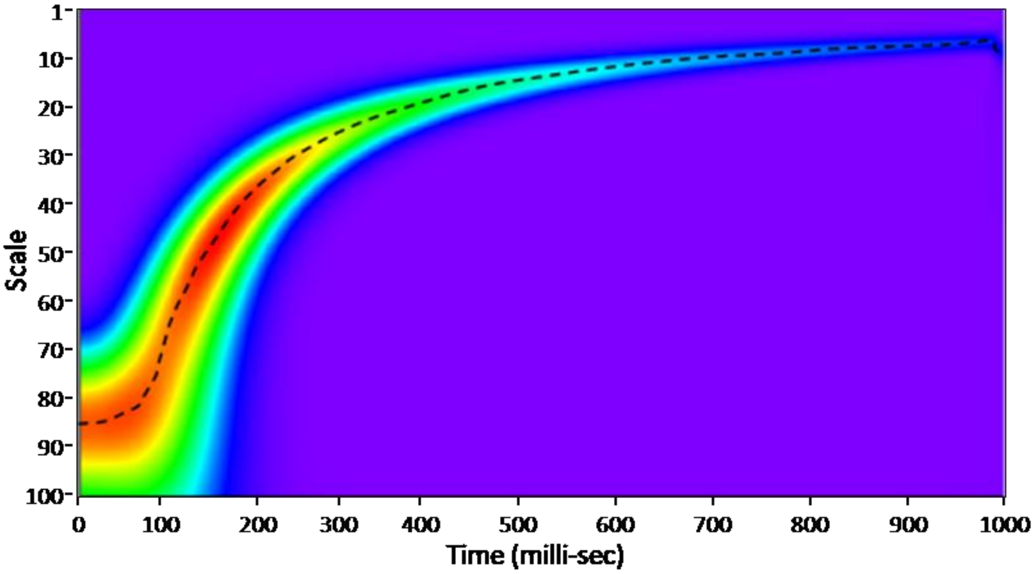

Fig. 4.5 Scalogram of linear chirp signal

4.2.4 Phase Extraction of Linear Chirp signal

The developed algorithms are first validated by generating known non-stationary linear chirp signal of quadratic phase and linearly increasing frequency. It is described as-

$$Y_i = A\sin((0.5ai + b)i) \tag{4.26}$$

$$a = \frac{2\pi(f_2 - f_1)}{n} \tag{4.27}$$

$$b = 2\pi f_1 \tag{4.28}$$

where,

i=0,1,..n-1,A=Amplitude, f_1=Starting frequency(samples/cycle), f_2=Ending frequency(samples/cycle), n=Number of samples [23]. The quadratic phase and instantaneous frequency can be written as

$$\varphi_i = (0.5ai + b)i \tag{4.29}$$

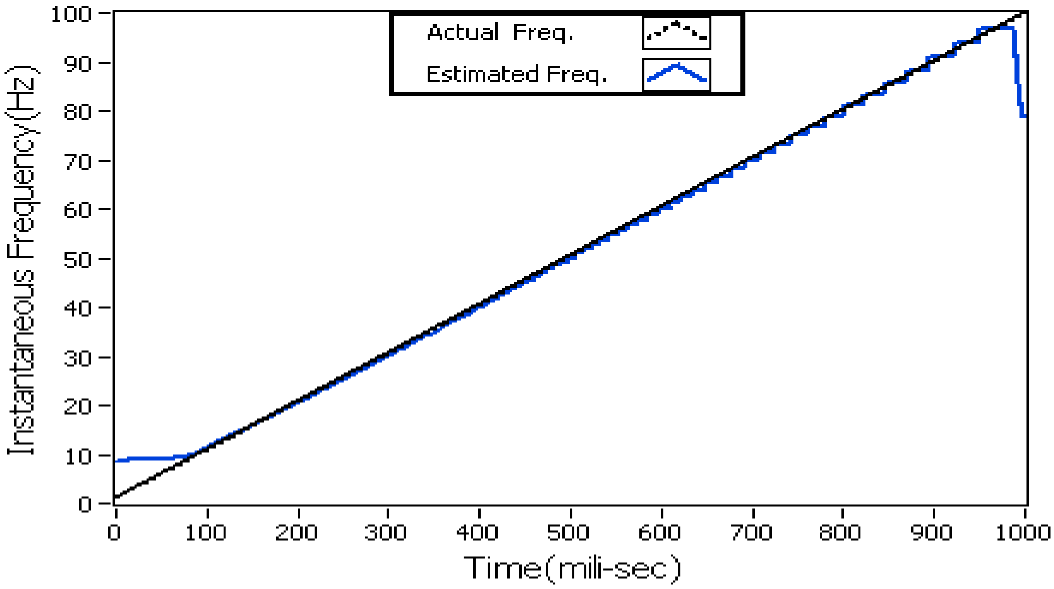

Fig. 4.6 Comparison of recovered and exact frequency of linear chirp signal

$$f_i = \frac{1}{2\pi}\left(\frac{d\varphi_i}{di}\right) = \frac{1}{2\pi}(ai + b) \tag{4.30}$$

In this work we set i=1000, f_1=1Hz, f_2=100Hz and sampling frequency (f_s)=1000Hz. The chirp signal is plotted in Fig 4.4. Figure 4.5 shows the modulus of CWT of this signal using Morlet wavelet. The ridge points are determined by using maxima search algorithm and it is plotted and superimposed on the modulus of CWT signal by black dotted line. It is clearly seen that increase in frequency the optimal value of scaling factor decreases. Here scales (a) are discretized as 0.25,0.5,0.75,1....100. The instantaneous frequency is calculated from the values of scaling factor (a) on the ridge using equation (4.20) and actual frequencies are determined from equation (4.30). Both are plotted in the same graph shown in Fig.4.6. The recovered fringe frequency contains error at the left and right hand edges due to abrupt truncation of data. In left side edge close to 1 Hz the low frequency identification problem also exists. Finally,

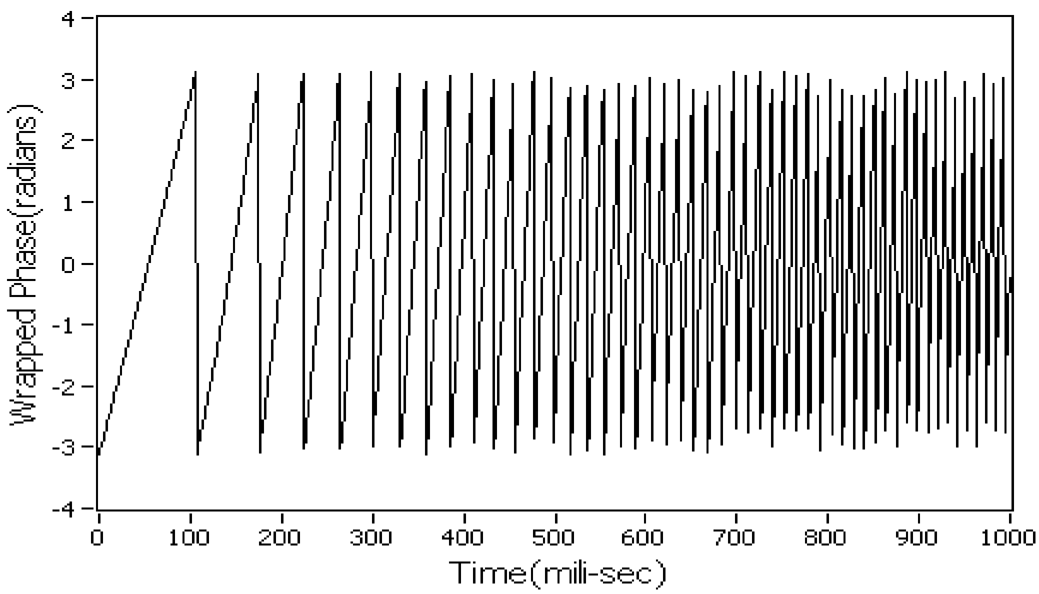

Fig. 4.7 Wrapped phase

the recovered phase by both the techniques and actual phase are plotted in Fig.4.8. It is observed that root mean square errors (RMSE) calculated between actual phase and estimated phase using phase technique and frequency technique are 1.96 and 1.44 respectively. Again same work is carried out with scale settings as 1,2,3...100 and

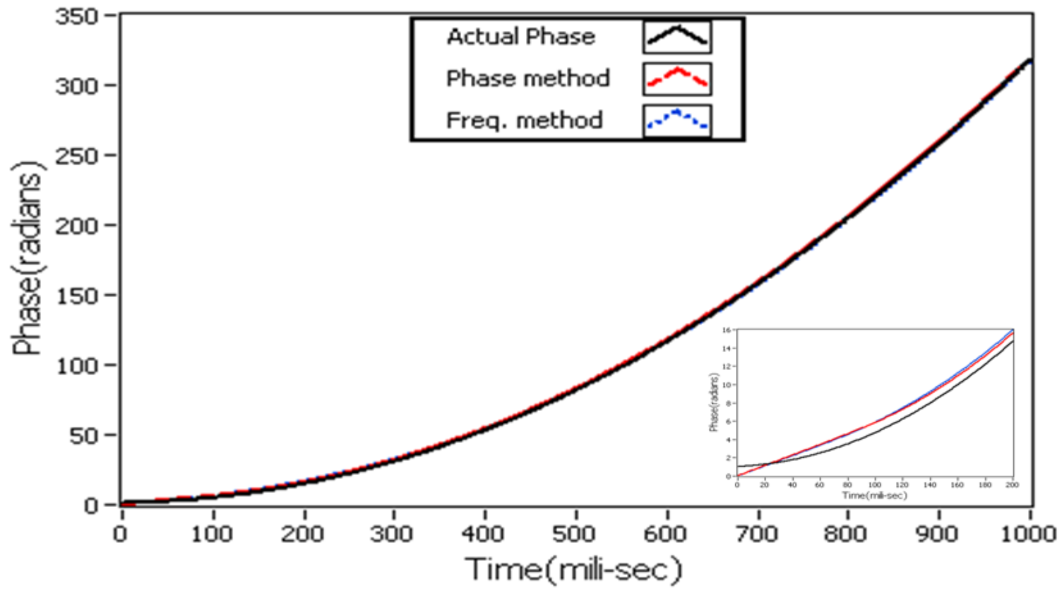

Fig. 4.8 Comparison of recovered phase and actual phase

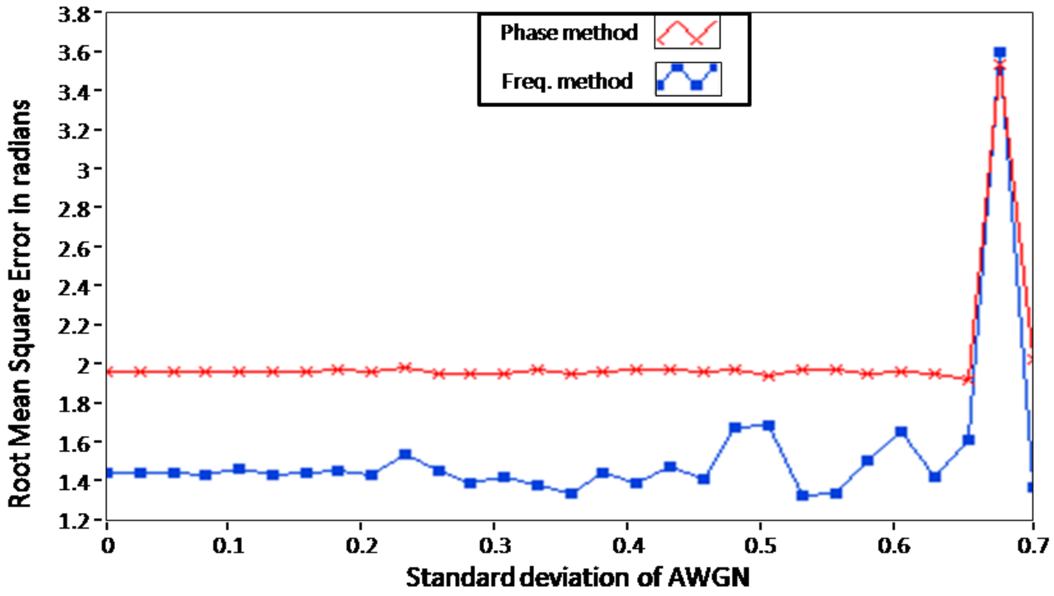

Fig. 4.9 Noise performance of phase extraction techniques

RMSE in phase technique and frequency technique are found as 1.96 and 2.54 respectively. Therefore results suggest that performing the phase technique more or less insensitive to scale discretization whereas that of the frequency technique yields better results for finer scale of discretization. However, due to finer scale discretization the computation time has also increased. Therefore in some applications where speed and computer resource are limited then phase estimation technique gives better result for using relatively less fine scale. To check the robustness of the proposed algorithm Additive White Gaussian Noise (AWGN) with zero mean and

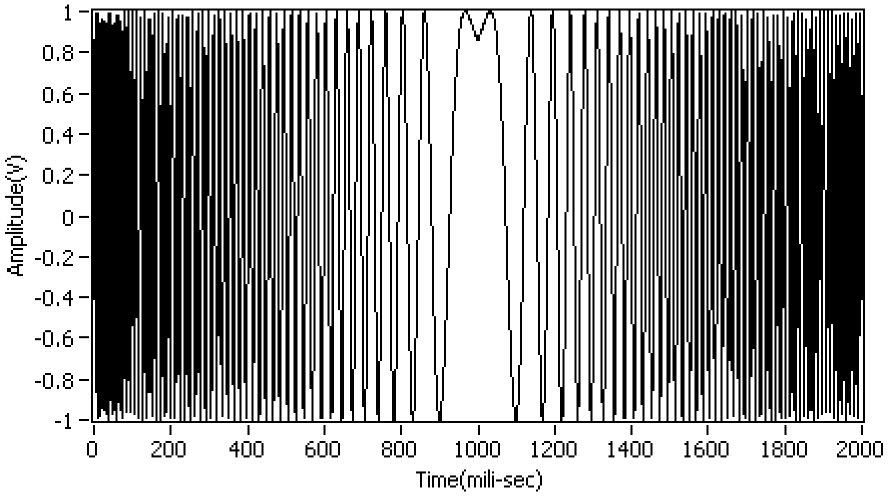

Fig. 4.10 Linear chirp signal with decreasing and increasing IF

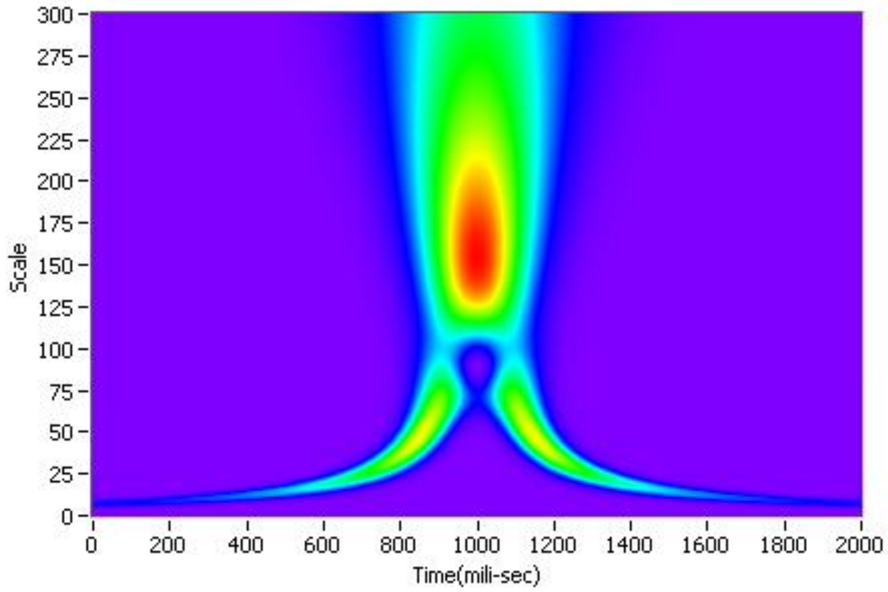

Fig. 4.11 Scalogram of linear chirp signal with decreasing and increasing IF

standard deviation σ is added to the simulated profile and noisy signal is then analysed using both the techniques with scale discritization as 0.25,0.5,0.75,1....100. Finally RMSE of phase is found with respect to standard deviation of AWGN and it is shown in Fig.4.9.

Simulation study is also carried out to cross linear chirp signals one decreasing and one increasing shown in Fig.4.10. Scalogram of this signal is described in Fig.4.11. It

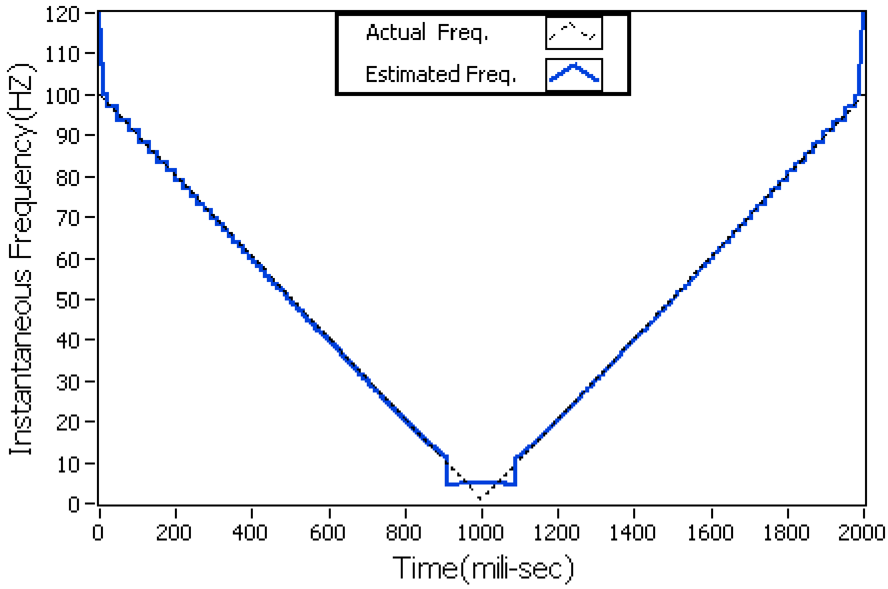

Fig. 4.12 Frequency of linear chirp signal with decreasing and increasing IF

is found that, significant error occurs at low frequency point demonstrated in Fig.4.12 in extracted IF apart from distortion at edge points.

4.3 Analysis of simulated interferometric signal

4.3.1 Frequency modulated sinusoidal signal

In the last section it is shown that RMSE of frequency estimation technique is more accurate than phase estimation technique. Moreover, frequency estimation technique does not require complex phase unwrapping and velocity and displacement both can be simultaneously extracted. Therefore, interferometric signal analysis is focused only with frequency estimation technique.

To show the applicability of CWT technique, a simulated fringe with a predetermined sinusoidal frequency variation (0.05 Hz to 0.45 Hz) and initial phase is generated. Figure 4.13 depicts the simulated instantaneous frequency and modulated fringe signals. Considering only the conventional Morlet wavelet with f_0t=1, the modulus of

CWT for this signal appears as shown in Fig. 4.13(a). The ridge points are determined using maxima search algorithm and plotted as black dotted line superimposed on the modulus of CWT signal. Recovered fringe frequency contains an error at low frequency zone due to spreading of mother wavelet to its adjacent points.

Therefore, altering f_0t in mother wavelet is considered and the mean square errors (MSEs), calculated from extracted frequency together with actual frequency, are obtained as shown in Table 4.1. It is to be noted that for MSE calculation a few points at edges are discarded since numerical discontinuities occur due to abrupt truncation of data, commonly referred to as cone of influence (COI). As seen in Table 4.1, MSE is lowest at f_0t=0.6 for which CWT is computed again as shown in Fig. 4.13(b). However, even with some signature of improvements, discontinuity and error in low frequency zone still exist. To further reduce these distortions, reassignment technique with f_0t=1 is applied to scalogram and the result is shown in Fig. 4.13(c). Discontinuity has reduced but error in low frequency zone still persists. Finally, reassignment technique with f_0t=0.6 is applied as shown in Fig. 4.13(d), increasing overall measurement accuracy. Optimal selection of mother wavelet and then applying reassignment technique [Fig. 4.13(d)] has improved MSE percentages for IF from 0.0085 Hz to 0.0031 Hz. Finally, phase is calculated by performing numerical integration of extracted IF in Fig. 4.13(d).

The improved performance of reassigned and modified CWT method in low frequency regime is due to reduction in energy of adjacent bins. This can be better understood by plotting modulus of CWT coefficients with respect to frequency at a

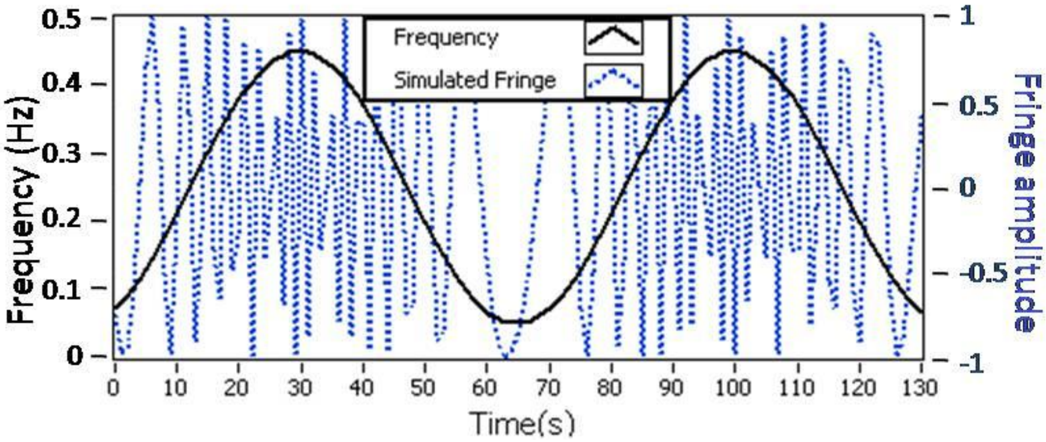

Fig. 4.13 A sinusoidal frequency variation and corresponding simulated fringe signal.

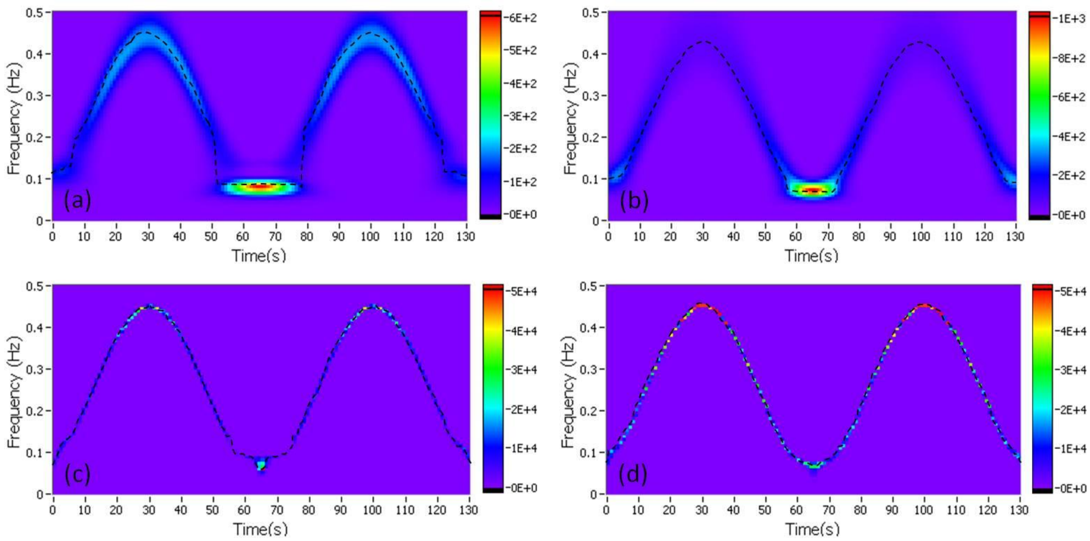

Fig. 4.14 Morlet spectrogram with (a) f_0t=1 and (b) f_0t=0.6. Reassigned Morlet spectrogram with (c) f_0t=1 and (d) f_0t=0.6.

given time instant. Fig.4.14 describes the absolute value of CWT coefficients of Morlet spectrogram with f_0t=1, f_0t=0.6, and reassigned spectrogram with f_0t=0.6 at different instants of time. Each peak of these distributions represents the estimated frequencies at corresponding time instants. In Fig. 4.14 (a) using Morlet spectrogram with f_0t=1, at time instant 51 s the peak frequency occurs at 0.1928 Hz. However, a dominant second peak also present at 0.06 Hz. At next immediate data point of 52 s,

[Fig. 4.14(b)] the magnitude of CWT coefficient at low frequency is more than expected value of 0.1785 Hz and incorrectly identified as frequency of 0.0714 Hz due to numerical discontinuity in extracted frequency [Fig. 4.13(a)]. Extracted frequency nearby high frequency zone is more accurate whereas at low frequency zone at 62 s it is worse shown in Fig. 4.14(c). Dominance of this low frequency component is due to continuous spread of mother wavelets to their adjacent bins. Therefore, relatively low frequency mother wavelet is considered which has less oscillation in fixed Gaussian window. Using Morlet spectrogram with f0t=0.6 [Fig. 4.14(d), (e) and (f)], this low frequency effect is significantly reduced. Further, reassignment operation (by shifting geometrical centre to gravity centre) on these modified spectrograms sharpens the

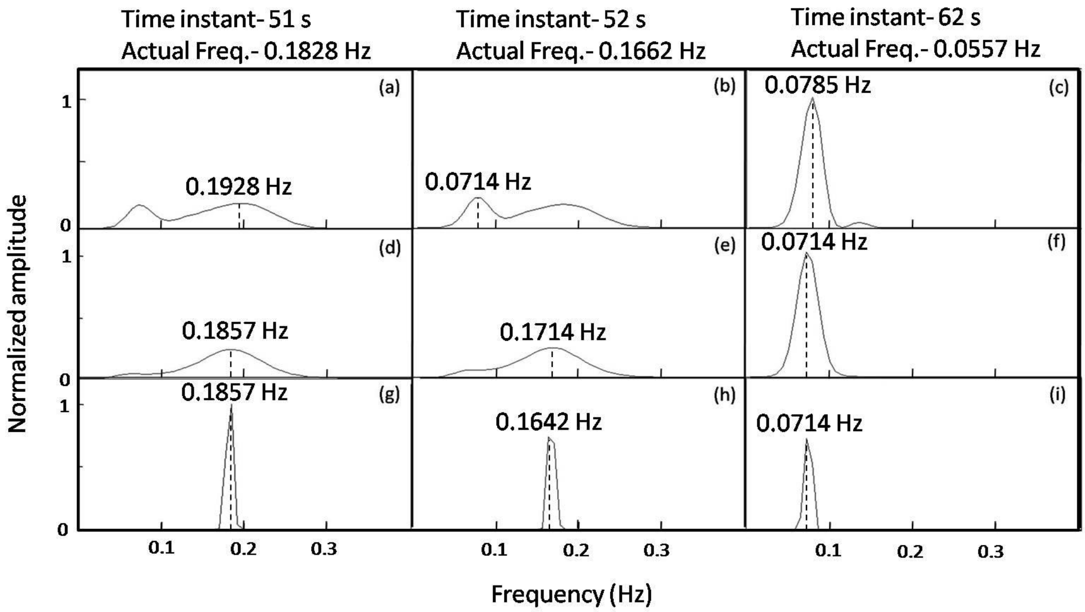

Fig. 4.15 Modulus of CWT coefficients at different instant of time- (a), (b), (c) Morlet spectrogram with $f_0t=1$; (d), (e), (f) Morlet spectrogram with $f_0t=0.6$ and (g), (h), (i) Reassigned Morlet spectrogram with $f_0t=0.6$. Vertical dashed lines indicate the extracted frequencies.

signal concentration and improves the accuracy as shown in Fig. 4.14(g), (h) and (i) i.e. at time instant 52 s, error of extracted frequency is 57.03% for Morlet spectrogram with $f_0t=1$ whereas it is 3.12% and 1.20% respectively for Morlet spectrogram with $f_0t=0.6$ and Reassigned Morlet spectrogram with $f_0t=0.6$. Absolute errors in IF are also plotted in Fig.4.16 where it can be seen that numerical discontinuity almost vanishes for reassigned CWT.

The advantage of reassigned and modified CWT technique is also justified by comparing the percentage in mean square error (considered as merit criterion) for IF. Additive white Gaussian noises (AWGN) with different SNR (signal to noise ratio) are added to simulated fringe signal for which mean square error of estimated frequency are calculated using reassigned and modified CWT and CWT with $f_0t=0.6$. The results are shown in Tab. 4.2.

The phase stepping method as described in Chapter 3 is also used to extract phase from simulated fringe signal. Quadrature counterpart of the fringe signal (Fig. 4.13) is obtained using Hilbert transform shown in Fig. 4.17. Robustness of the proposed algorithm is also tested with simulated fringe signal by applying AWGN with different SNR. Table 4.3 displays the true and fitted values of ellipse parameters of quadrature fringe signals for one of the noise realizations (SNR 10 dB) along with RMS misfit. Phases are extracted with equation (3.23) and unwrapped phase is plotted

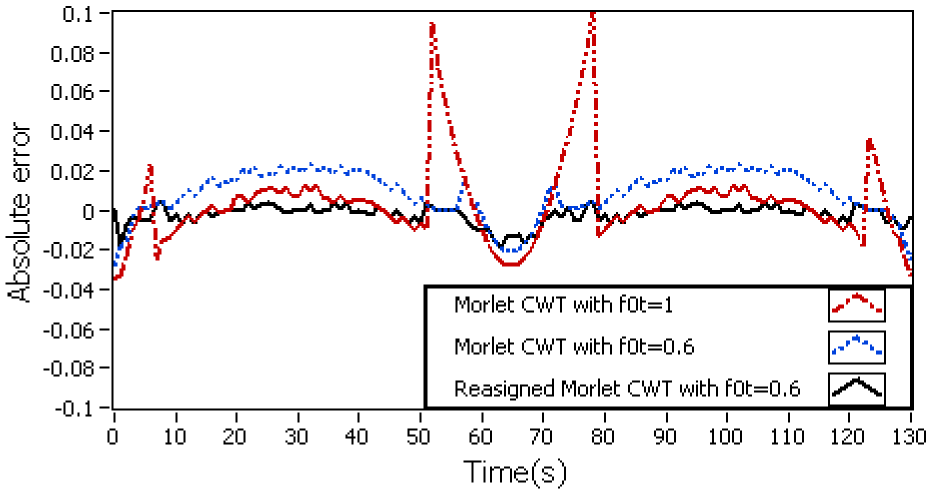

Fig. 4.16 Absolute error in IF

Table 4.1 MSE percentage in Instantaneous frequency

f_0t	CWT
0.1	2.22
0.2	0.3340
0.3	0.1081
0.4	0.0418
0.5	0.0221
0.6	0.0165
0.7	0.0186
0.8	0.0269
0.9	0.0362
1	0.0507
1.1	0.0585
1.2	0.081

in Fig. 4.18 along with phases extracted by CWT technique. Error in phase stepping method occurs mainly due to noise-induced jump in phase unwrapping algorithm. Performance comparison in extracted phase of proposed technique using phase stepping method with different noise realization is also carried out and summarized in Tab. 4.4. It is observed that for low noise case both the algorithms perform equally well but at higher noise level reassigned and modified CWT is more robust.

With simulated signal, the additional computational burden with current technique is also evaluated. It is found that MSE percentages in normalized IF have decreased significantly from 0.0507 Hz to 0.0032 Hz with marginal increase in computational time (0.932 s for reassigned and modified CWT against 0.909 s for CWT).

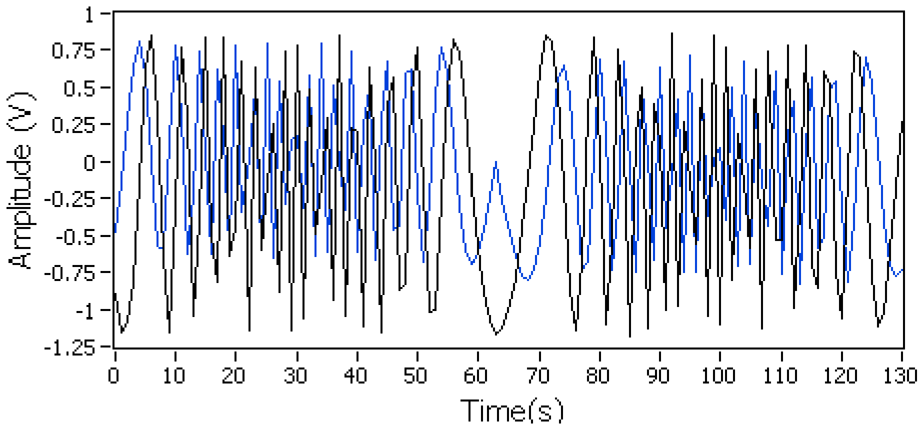

Fig. 4.17 Simulated quadrature fringe Signal obtained using Hilbert Transform

Table 4.2. MSE percentage in instantaneous frequency using CWT (f_0t=0.6) with AWGN added to fringe

SNR(dB)	CWT	Reassigned CWT
30	0.0218	0.0031
25	0.0238	0.0036
20	0.0240	0.0038
15	0.0242	0.0060
10	0.0265	0.0081
5	0.0373	0.0281

Table 4.3 Fitted ellipse parameters

Ellipse parameters	True value	Simulation with SNR(10dB)	Experimental
$a(t)$	0.15	0.13	0.015
$a_1(t)$	-0.05	-0.03	0.018
$b(t)$	1	1.005	0.002
$b_1(t)$	0.75	0.78	0
ε	0	0.001	0.48
RMS		0.13	0.19

4.4 Analysis of Experimental Signals

Sinusoidal frequency-modulated fringe signal is generated by moving mirror attached to one of the legs of the Michelson interferometer where reference light combines with a Doppler shifted light. The phase of this fringe signal is proportional to surface displacement whereas instantaneous frequency or beat frequency is proportional to surface velocity. Here, we have applied sinusoidal type voltage signal to PZT (Piezo-electric translator) attached to one of the mirrors to produce a moving surface. Generated optical fringe signals are converted to electrical signal using PMT (Photomultiplier tube) and stored in digital storage oscilloscope (DSO). Schematic of the setup is shown in Fig. 3.3.

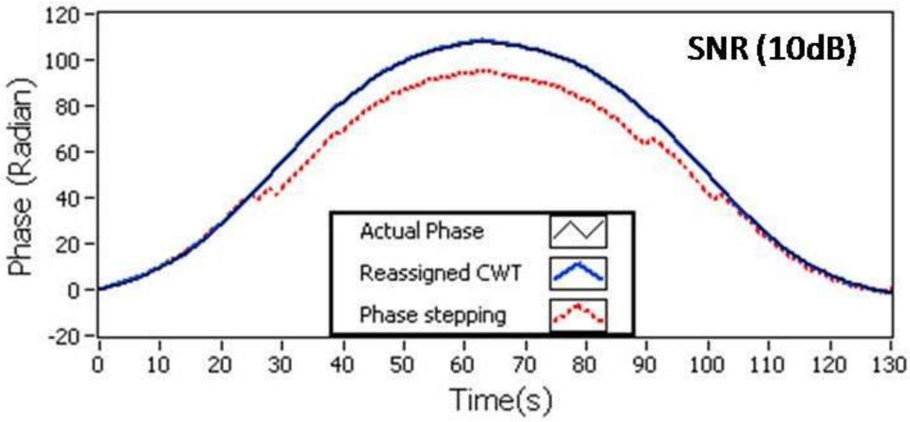

Fig. 4.18 Phase of simulated fringe signal with AWGN

Table 4.4 MSE in phase with AWGN

SNR(dB)	Reassigned CWT	Phase stepping
30	0.0705	1.3792
25	0.1797	1.3821
20	0.2259	6.0316
15	0.3995	29.36
10	0.4623	50.47
5	7.10	331.05

The measured signal intensity by Michelson Interferometer can be expressed as [4]:

$$I(t) = I_0(t) + I_d(t) + 2\sqrt{I_0(t) I_d(t)}\cos(\phi(t)) \tag{4.31}$$

where $I_0(t)$ and $I_d(t)$ are the intensity of light of the two legs of the interferometer, one from reference mirror and other from PZT driven mirror, and $\varphi(t)$ is the phase shift of fringe signal at a given time.

The phase can be expressed as

$$\phi(t) = 2\pi \int_0^t (f_d(t) - f_0(t))dt + \phi_0 = 2\pi \int_0^t (f_i(t))dt + \phi_0 \tag{4.32}$$

where $f_0(t)$ and $f_d(t)$ are the frequency of reference light and Doppler shifted light respectively.

Equation (4.31) can be re-written as -

(4.33)

$$I(t) = a(t) + b(t)\cos(\phi(t))$$

where,

$$a(t) = I_0(t) + I_d(t) \tag{4.34}$$

$$b(t) = 2\sqrt{I_0(t)I_d(t)} \tag{4.35}$$

Equation (4.33) describes the recorded time averaged output intensity $I(t)$, background intensity $a(t)$, fringe amplitude $b(t)$. Background intensity $a(t)$ is removed by filtering method, manual technique or fitting method. The background corrected fringe signal and its analytic form may be expressed as-

$$I(t) = b(t)\cos(\phi(t)) \tag{4.36}$$

$$I(t) \approx b(t)e^{i\phi(t)} \tag{4.37}$$

CWT is applied on this analytic representation of the fringe signal and IF is extracted by determining ridge points of the CWT coefficients. Phase is then deduced by integrating the extracted IF. Finally the velocity and displacement as a function of

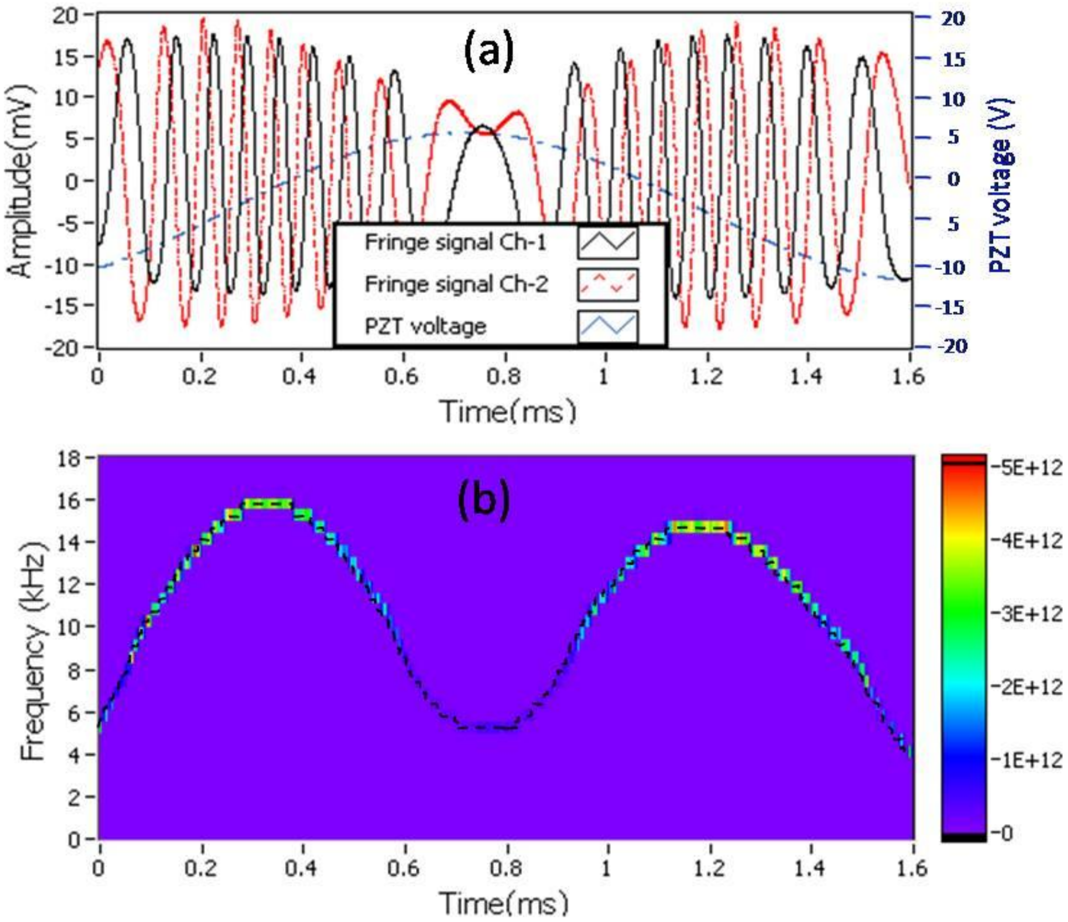

Fig. 4.19 (a) Measured quadrature fringe signal with PZT supply voltage (b) Reassigned spectrogram (f_0t=0.6) obtained from Ch-1 fringe signal.

time are obtained using following equations:-

$$v(t) = \frac{\lambda}{2} f_i(t) \tag{4.38}$$

$$s(t) = \frac{\lambda}{2} \frac{\phi(t) - \phi_0}{2\pi} \tag{4.39}$$

Here, $v(t)$ is the velocity, $s(t)$ is the displacement of the mirror and λ(532nm) is laser wavelength.

Experimentally recorded typical quadrature fringe signal as shown in Fig. 3.4 with applied PZT voltage again is shown in Fig. 4.19(a) for the sake of continuity. The recorded fringe signal Ch-1 is analyzed by reassigned and modified CWT with Morlet wavelet parameter f_0t=0.6. The modulus of coefficients or spectrogram so obtained is plotted in Fig. 4.19(b). Ridge points extracted by using maxima search algorithm are shown in the same plot (dotted line). Analysis is also carried out with conventional Morlet mother wavelet and modified one with f_0t=0.6 resulting in discontinuity in neighbouring low frequency zone, similar to those seen for simulated signal, shown in Fig. 4.20. Phase is then deduced by integrating extracted IF from Fig. 4.19(b). For direction control of phase variation, quadrature based fringe signal is used from which inflection point is identified (at 0.756 ms) and phase reversal algorithm is applied to produce continuous phase, described in Fig 4.21.

Finally, displacement profile is calculated using equation (3.28) for reassigned and

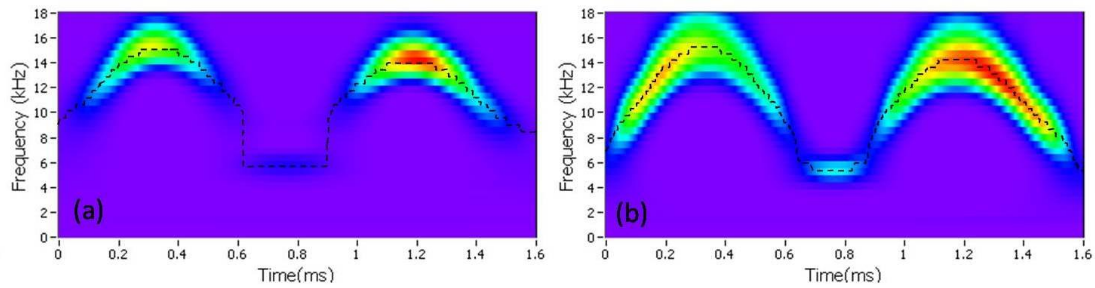

Fig. 4.20 Morlet spectrogram (a) with with f_0t=1 (b) with f_0t=0.6

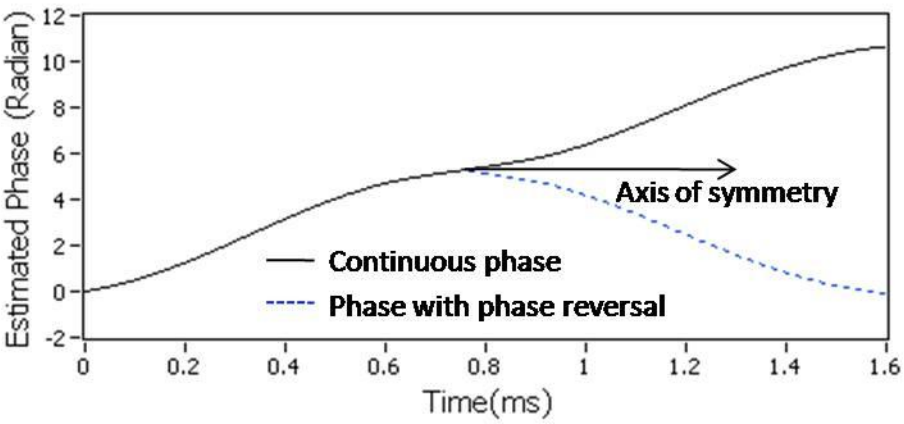

Fig. 4.21 Phase variation

modified CWT. Results of phase stepping technique as described in Fig. 3.6 and CWT technique are both simultaneously plotted shown in Fig. 4.22. It can be observed that apart from smaller peak value, the displacement profile derived from phase stepping suffers from artificial acceleration and deceleration as well. This may be due to relative nonlinear error in the fringe profile. The peak displacement using reassigned and modified CWT is estimated as 2.23 µm. This may be compared with 2.06 µm obtained by phase stepping technique and also 2.20 µm obtained by well established peak-picking technique. Velocity profile is deduced using equation (3.29) shown in Fig. 4.23 and maximum velocity of 4137 µm/s is observed.

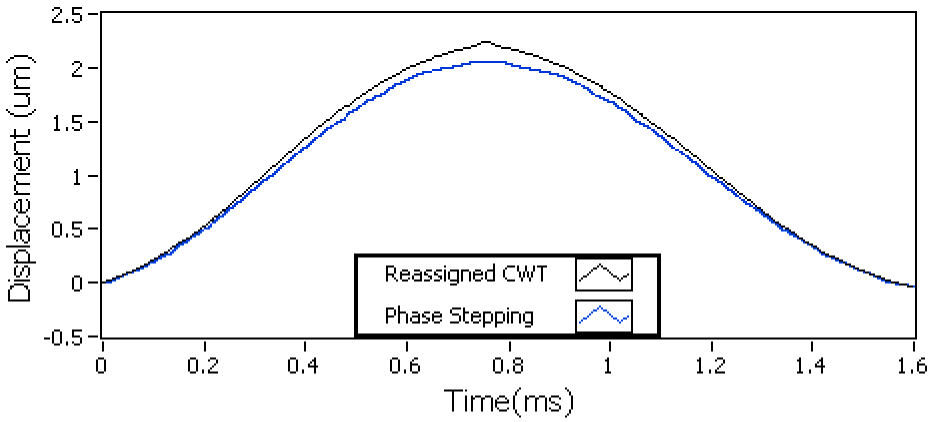

Fig. 4.22 Displacement profile

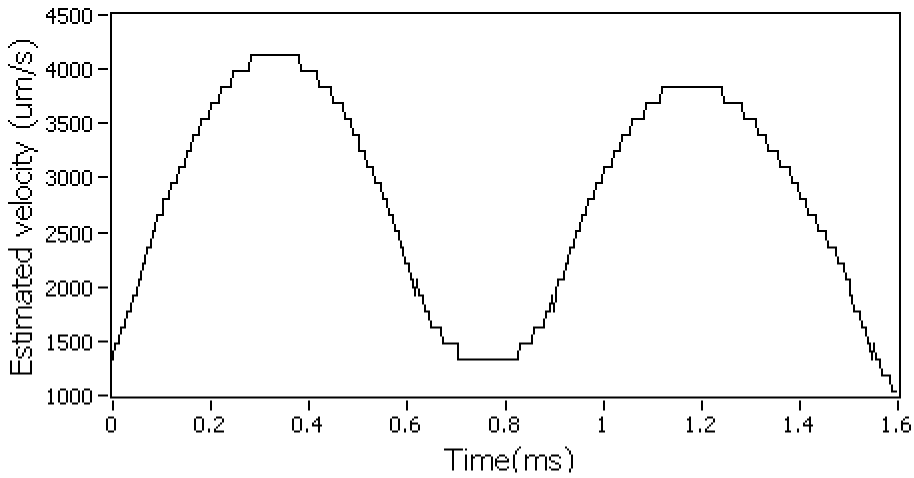

Fig. 4.23 Velocity profile

4.5 Summary and Conclusion

CWT with mother wavelet as Morlet is used to extract the phase of highly non-stationary sinusoidal frequency-modulated optical fringe signal. To obtain the optimum time and frequency resolution, mother wavelet parameter combination $f_0 t$ is modified. MSE percentage in instantaneous frequency in actual and extracted frequency is considered as merit criterion and $f_0 t$ as 0.6 found to be optimal. However, this optimal value does not ensure desired measurement accuracy in extracted frequency. A new approach of using reassigned and modified CWT technique is proposed to simultaneously adopt mother wavelet and reassignment. A combination of these provides better concentration of low energy components of the spectrogram compared to conventional CWT technique that uses $f_0 t$ as 1. This leads to an improvement in readability and increase in accuracy of mean square error percentage in normalized instantaneous frequency from 0.0507 Hz to 0.0032 Hz, with marginal increase in computational time from 0.909 s to 0.932 s. Optimal selection of mother wavelet helps to reduce wavelet energy to its adjacent bins and then reassignment technique sharpens the spectrogram effectively. Thus, simple ridge detection technique performs well and can be utilized for many practical applications. Proposed technique is also compared with existing two fringe-based phase stepping techniques and found to be more robust for sinusoidal fringe signals contaminated by additive Gaussian noise. At SNR 10 dB, the MSE in phase by the proposed technique is 0.4623, whereas, the same for phase stepping technique is 50.47. This large MSE in case of later is due to noise-induced phase jump in phase stepping technique.

Further, the performance of the proposed technique is validated using fringe signal generated by a Michelson interferometer. The peak displacements in the fringe signal determined by the current and the phase stepping techniques are 2.23 µm and 2.06 µm, respectively. The former is more close to the 2.20 µm determined using popular peak-picking technique. Additionally, the displacement profile derived using proposed technique is free from ripples and distortions as compared to that obtained through phase stepping technique. Though, the experimental fringe signal so generated does not have much noise, still the inferior performance of phase stepping technique is due to relative non-linear error between quadrature fringe signals.

CHAPTER 5 Phase Extraction of Cubic Phase Signal by Pseudo Wigner Ville Distribution Method

5.1 Introduction

In the last chapter CWT based technique is explored for better extraction of IF in sinusoidal frequency modulated signal. In this chapter Wigner Ville Distribution method is described for the IF extraction in polynomial phase signal. In this method also complex phase unwrapping can be avoided. Many interesting mathematical properties like energy conservation, marginality etc. are preserved in WVD.

5.2 Theory

5.2.1 Background

WVD of signal $I(t)$ is defined as the Fourier transform of time-dependent instantaneous auto-correlation function and represented as

$$WVD\,(t,\omega) = \frac{1}{2\pi}\int_{-\infty}^{+\infty} I(t+\frac{\tau}{2})I^{*}(t-\frac{\tau}{2})e^{-j\omega\tau}d\tau \qquad (5.1)$$

where t, ω and τ represent the time, angular frequency and lag variable respectively and $(*)$ denotes the complex conjugate. The above expression is also called quadratic due to presence of product of two signal terms. Peak of WVD is the estimator of IF. This estimator is optimal when the signal phase is quadratic function or linear IF [41]. For polynomial phase signal of order greater than two, this optimality is lost and polynomial Wigner Ville Distribution is proposed to handle such class of signals [40]. It is defined by

$$WVD_I^{(q)}(t,\omega) = \frac{1}{2\pi}\int_{-\infty}^{+\infty}\left[\prod_{l=1}^{q/2} I(t+d_l\tau)I^*(t+d_{-l}\tau)\right]e^{-j\omega\tau}d\tau \tag{5.2}$$

where q is an even integer, denoting the order of nonlinearity of WVD, d_l is the real coefficients. Proper selection of coefficient d_l for obtaining 4th and 6th order Poly-WVD is explained in literature [57]. In fact WVD is a special case of Poly-WVD when $q=2$ and $d_l=d_{-l}=0.5$.

Though WVD has many good properties like marginality, preserving total energy, real valued distribution and possibly best resolution among all of the time-frequency (TF) techniques, undesirable cross-term or interference effect due to presence of signal product terms, is its main drawback. For Poly-WVD this interference effect is more dominating than traditional WVD due to its multi-linear nature for hyperbolic type signal.

WVD is also highly non local and to convert it into local, windowing operation is introduced popularly known as Pseudo Wigner-Ville Distribution (PWVD)[37]

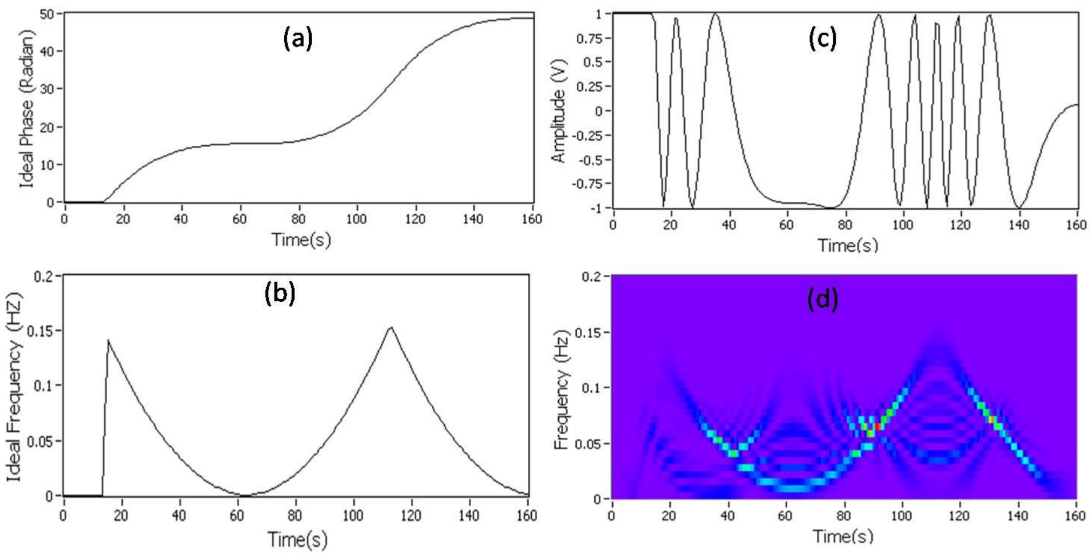

Fig. 5.1. (a) Cubic phase signal (b) Instantaneous Frequency of cubic phase signal (c) Simulated cubic phase based fringe signal (d) WVD of simulated fringe signal

which mathematically can be described as

$$PWVD(t,\omega) = \frac{1}{2\pi}\int_{-\infty}^{+\infty} h(\tau) I(t+\frac{\tau}{2}) I^*(t-\frac{\tau}{2}) e^{-j\omega\tau} d\tau \tag{5.3}$$

where window function $h(\tau)$, is an even function and peaked around $\tau = 0$. Multiplication with $h(\tau)$ is an equivalent to frequency filtering, thus an immediate consequence is reduction of cross-terms to some extent for multi-component signal particularly in frequency direction. However, these benefits lead to the smearing of the auto-terms of the signal and a loss of many desirable theoretical properties. Cohen [37] proposed general approach and introduced 2-D kernel function defined as

$$C(t,\omega) = \frac{1}{4\pi^2}\int_{-\infty}^{+\infty}\int_{-\infty}^{+\infty}\int_{-\infty}^{+\infty} I(u+\frac{\tau}{2}) I^*(u-\frac{\tau}{2}) g(\tau,\theta) e^{-j[\theta(t-u)+\omega\tau]} du\, d\theta\, d\tau \tag{5.4}$$

where $g(\tau,\theta)$ is the kernel function. Different kernel will lead to different time frequency representation (TFR) and by examining a particular kernel function various properties of bilinear TF distribution can be ascertained. Therefore, kernel function allows both the suppression of the cross-terms and the preservation of the auto-ambiguity terms of the analyzed signal.

In Fourier space kernel function $g(\tau,\theta)$ can be represented as-

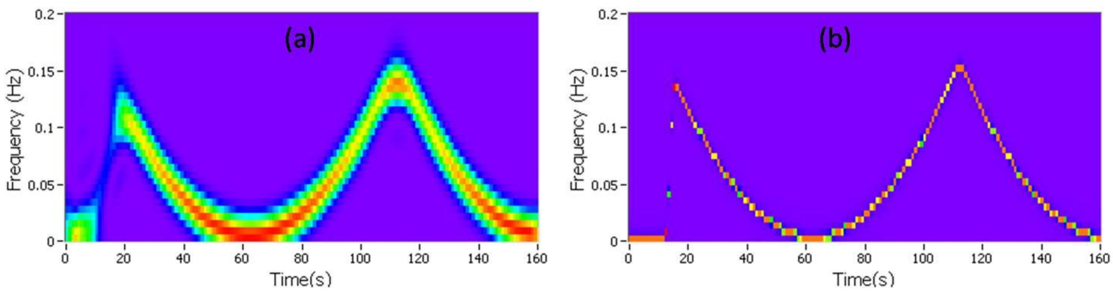

Fig. 5.2. (a) SPWVD of fringe signal (b) Reassigned SPWVD with modified kernel of fringe signal

$$\Pi(t,\omega) = \int_{-\infty}^{+\infty}\int_{-\infty}^{+\infty} g(\tau,\theta) e^{-j(\omega\tau+\theta t)} d\tau d\theta \tag{5.5}$$

If a separable kernel function is considered, it can be defined as the product of window function in both time and frequency direction i.e.

$$\Pi(t,\omega) = g(t)H(-\omega) \tag{5.6}$$

where $H(\omega)$ the Fourier transform of window function $h(t)$ performs smoothing in parallel to frequency axis and $g(t)$ performs smoothing in parallel to time axis. Therefore, Smoothed Pseudo Wigner-Ville Distribution (SPWVD) [37] can be expressed as -

$$SPWVD\,(t,\omega;g,h) = \int_{-\infty}^{+\infty} h(\tau) \int_{-\infty}^{+\infty} g(u-t) I(u+\frac{\tau}{2}) I^*(u-\frac{\tau}{2}) e^{-j\omega\tau} du d\tau \tag{5.7}$$

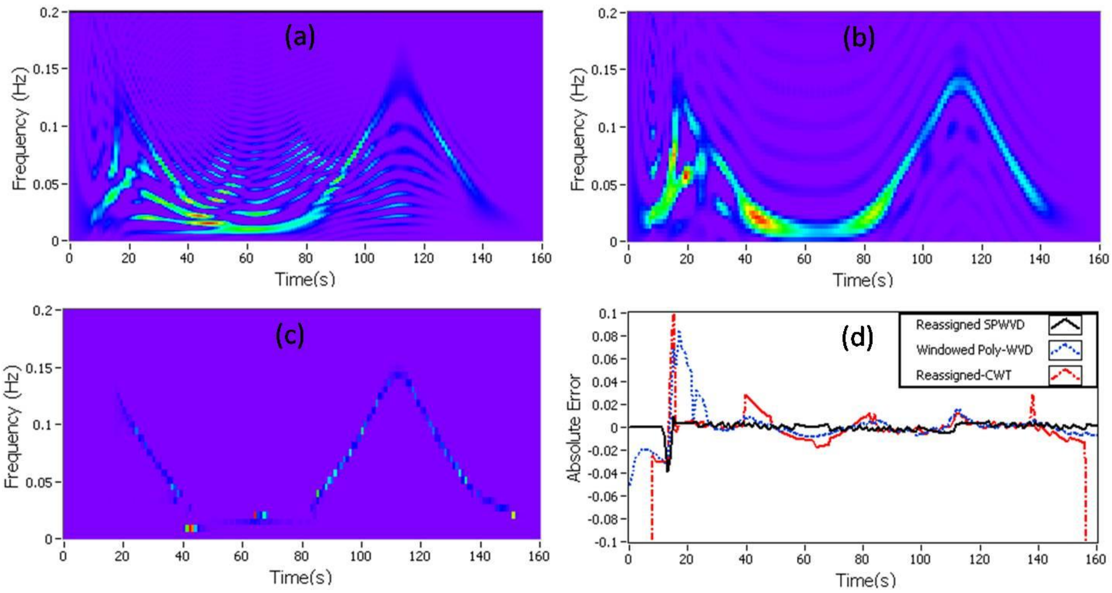

Fig. 5.3. (a) Poly-WVD of fringe signal (b) Poly-WVD of fringe signal with lag window length 35 (c) Reassigned CWT of fringe signal (d) Absolute error in IF of various methods

In the present work, Gaussian kernel is used

$$g(\tau,\theta) = \exp(-\tau^2/\eta_\tau)\exp(-\theta^2/\eta_\theta) \tag{5.8}$$

where η_τ and η_θ decide the spread of the kernel. It is to be noted that more spread of kernel will lead to more reduction of interference but at the cost of blurring of signal concentration and loss of localisation property. In order to improve the signal concentration from blurred TFR, simultaneously reassignment technique is applied, explained in last chapter in the context of CWT. Same technique can be adopted in SPWVD that relocates any point (t,ω) of SPWVD(t, ω) to its centre of gravity $(\hat{t}, \hat{\omega})$ and improves the signal readability significantly.

5.2.2 Method of Phase Extraction

As mentioned earlier the measured signal from Michelson Interferometer can be expressed as

$$I(t) = a(t) + b(t)\cos(\phi(t)) \tag{5.9}$$

where $I(t)$ is time averaged output intensity, $a(t)$ is background intensity, $b(t)$ is fringe amplitude, and $\varphi(t)$ is the phase shift of fringe signal at a given time. The fringe signal represented by equation (5.9) can be expressed in analytic form as follows

$$I(t) \approx b(t)e^{i\phi(t)} \tag{5.10}$$

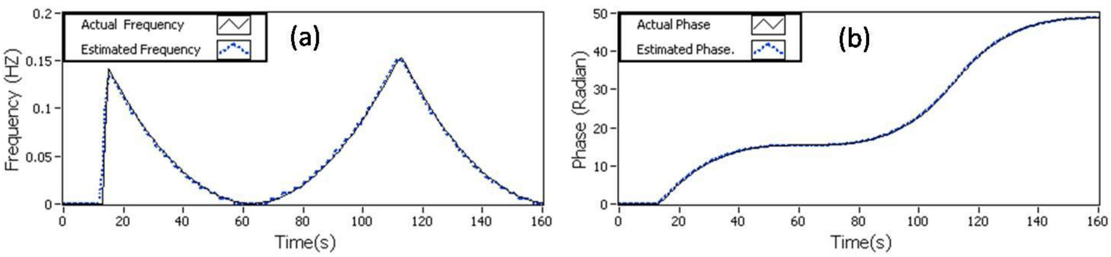

Fig. 5.4. Estimated (a) IF and (b) Phase by reassigned SPWVD

Representation of the signal in above analytic form is useful for properly defining IF and beneficial to reduce the interference effect presents in WVD [37,38]. If phase is considered to be a polynomial function of order p, then equation (2) can be expressed as

$$I(t) = b(t)\exp\left\{ j \sum_{i=0}^{p} a_i t^i \right\} \tag{5.11}$$

where a_i are real coefficients of polynomial phase signal. The IF can be defined as:

$$f_i(t) = \frac{1}{2\pi}\frac{d\phi(t)}{dt} = \frac{1}{2\pi}\sum_{i=1}^{p} i a_i t^{i-1} \tag{5.12}$$

The phase from derived IF can be expressed using following equation

$$\phi(t) = 2\pi \int_0^t \left(f_i(t)\right) dt + \phi_0 \tag{5.13}$$

Reassigned SPWVD expressed in equation (5.7) with Gaussian kernel is applied on analytic representation of the fringe signal given in equation (5.10) and IF is extracted by determining ridge points of the SPWVD coefficients. Phase is then deduced by integrating the extracted IF. Finally, the velocity and displacement as a function of time are obtained using equations:-

$$v(t) = \frac{\lambda}{2} f_i(t) \tag{5.14}$$

$$s(t) = \frac{\lambda}{2}\frac{\phi(t) - \phi_0}{2\pi} \tag{5.15}$$

Here, $v(t)$ is the velocity, $s(t)$ is the displacement of the mirror and λ(532nm) is laser wavelength.

Table 5.1. Mean Square Error (MSE) in IF

Type	MSE percentage in IF
WVD	0.1957
SPWVD with spread factor 2.5	0.3340
Reassigned SPWVD with spread factor 20	0.0020
Windowed Poly-WVD with window length 35	0.0293
Reassigned CWT with central frequency 0.6	8.0899

5.3 Numerical Simulation

The proposed IF extraction algorithm based on Reassigned SPWVD has been validated by known IF and phase of a simulated fringe signal. For this purpose, a cubic phase signal is first generated using piece-wise polynomial functions of order three shown in Fig. 5.1(a) and IF of the signal deduced using equation (5.12) is shown in Fig. 5.1(b). Optical fringe corresponding to this IF signal [Fig.5.1(b)] is generated in such a way that integral of IF is approximated as cumulative summation function given by:

$$\begin{aligned} &I = \exp(j * 2 * pi * cumsum(IF)) \\ &and \\ &I = I * conj(I(t_0)) \end{aligned} \tag{5.16}$$

Generated fringe signal is shown in Fig. 5.1(c). Wigner Ville Distribution (WVD) is first applied and as expected many undesirable interference are seen to be present in the TFR, shown in Fig. 5.1(d). SPWVD is then applied with 2-D kernel where $g(t)$ and $h(t)$ are Gaussian window with odd(N/10) and odd(N/4) data points respectively with

Table 5.2. MSE in Phase with respect to Signal to Noise Ratio (SNR)

SNR (dB)	MSE percentage in IF	MSE in phase
50	0.0020	0.0259
40	0.0021	0.0385
30	0.0022	0.0537
20	1.4273	347.57

spread factor of 2.5, N being the number of frequency bins in FFT [38]. It is to be noted that spread factor denotes the reciprocal of standard deviation of Gaussian window and is a measure of width of its Fourier transform. Larger the value of spread factor, implies narrow in temporal space, suitable for analyzing strong nonlinear signal in time direction but poor resolution in frequency direction. Resultant SPWVD is shown in Fig.5.2(a) and as compared to Fig.5.1(d) interference is reduced significantly at the cost of smeared signal concentration. Then we further increase the spread factor of Gaussian kernel to 20 and apply reassigned SPWVD, as shown in Fig. 5.2(b). Narrow Gaussian kernel in temporal space can be seen to improve measurement accuracy particularly at strong nonlinear region and further simultaneous application of reassignment technique increases signal concentration significantly in frequency direction.

Comparative study of IF extraction by Poly-WVD method as well as reassigned CWT [18] based technique are also carried out. In Poly-WVD method polynomial nonlinearity of order 4 is considered as it is sufficient to analyze cubic phase signal. In fact 6^{th} order Poly-WVD will produce more interference term than 4^{th} order one. Figure 5.3(a) and 5.3(b) represent Poly-WVD and windowed Poly-WVD with

Gaussian window length of 35 respectively. Effect of window length of Poly-WVD on IF extraction can be found in literature [41]. Even though, poly-WVD is theoretically appealing for such class of signal, interference effect severely distorts the TFR. In CWT method, Morlet as mother wavelet with central frequency (*f*) and time bandwidth (*t*) product is considered to be 0.6 and reassigned CWT is applied on simulated fringe signal, shown in Fig. 5.3(c). Consideration of Morlet mother wavelet parameters (central frequency and time bandwidth) is discussed in details in last chapter. Finally, absolute error in IF using reassigned SPWVD, Windowed Poly-WVD and reassigned CWT are plotted in Fig.5.3(d). It may clearly be observed that reassigned SPWVD technique is more accurate than windowed Poly-WVD as well as reassigned CWT technique. Finally, IF is extracted by reassigned SPWVD method and phase is estimated using equation (5.13). Figure 5.4 (a) and (b) describe extracted IF and phase respectively along with actual value. To evaluate the performance and accuracy of proposed method, mean square error (MSE) in IF is considered as figure of merit. Table 5.1 depicts the MSE percentage of IF with respect to different approaches and it is observed that reassigned SPWVD with spread factor of 20, the MSE is least.

Robustness of the proposed algorithm is also checked with additive white Gaussian noise (AWGN). Table 5.2 describes the MSE percentage in IF and MSE in phase with respect to different signal to noise ratio (SNR). It is seen that for SNR of 20 dB or less the algorithm is not robust. Since, narrow window is chosen as a Gaussian kernel that is quite effective for sharp change in IF but susceptible to noise due to fewer numbers of captured samples.

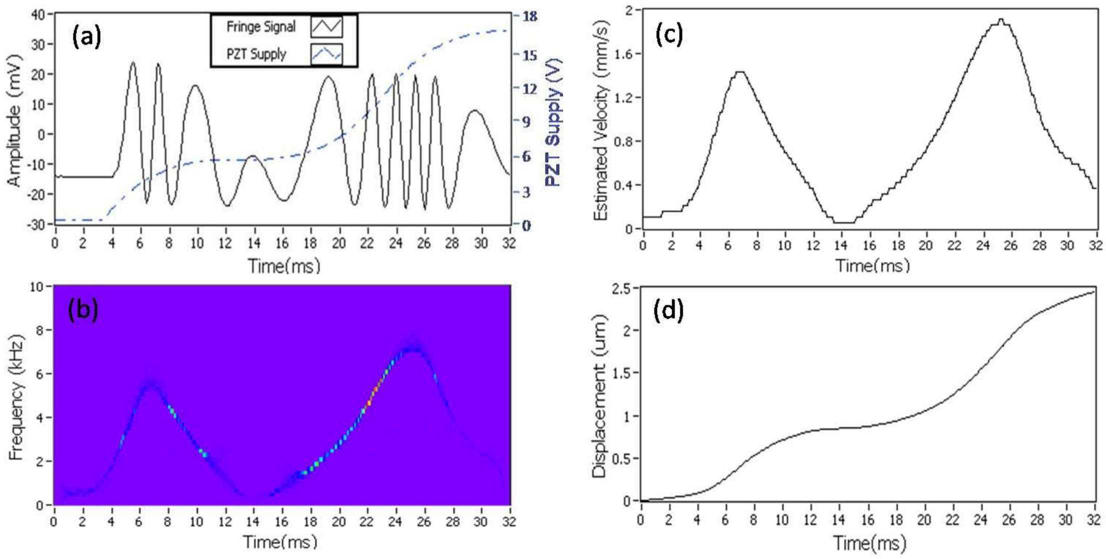

Fig. 5.5. (a) Experimentally observed fringe signal with PZT supply voltage (b) Reassigned SPWVD with modified kernel of experimental signal (c) Velocity profile of experimental signal (d) Displacement profile of experimental signal

5.4 Experimental Program

Simulated cubic phase signal shown in Fig. 5.1(a) is used to drive PZT attached to mirror (M-2) in one of the legs of the Michelson Interferometer given in Fig. 3.3. First this simulated signal is scaled to 0-10V range and then DAQ (Data Acquisition) system is developed using PXI based analog input/output card to drive the PZT. Analog output update rate is considered as 10kS/s so that it suits dynamic range of the PZT. Further amplifier is used to increase the voltage range that helps to get more number of fringes. A single mode continuous wave (CW) 532nm laser with variable power up to 2W is used along with PMT having 0.57ns rise time, 230-950nm spectral response and adjustable control voltage from 0.5 to 1.1V. Laser power, aperture opening, PMT control voltage and gain are adjusted in such a way that overall signal recording system operates in linear region [58]. The measured peak PZT supply voltage is 16.11V. Optical fringe signal corresponding to PZT supplied voltage, is converted to voltage signal using PMT (Photomultiplier tube) and stored in DAQ using analog input channel. Analog input sampling frequency (100kS/s) is considered relatively high to properly record the fringe signal in strong nonlinear region. Both PZT supply voltage and background corrected fringe signals are simultaneously recorded, as shown in Fig. 5.5(a). Here background intensity $a(t)$ is 0.068V, fringe amplitude $b(t)$ is 0.024V, and hence fringe visibility (ratio of fringe amplitude to background intensity) is 0.35. Hilbert transform is used to convert the real signal to its analytic form. Figure 5.5(b) describes instantaneous frequency in spectrogram based on proposed reassigned SPWVD of analytic form for experimentally recorded fringe signal. The velocity is calculated using equation (5.14) and shown in Fig. 5.5(c). Finally, phase is calculated by integrating the extracted instantaneous frequency and then displacement is derived using equations (5.15). As expected displacement profile shown in Fig.5.5(d) is quite similar to that of simulated phase signal shown in Fig. 5.1(a). In experimental signal relatively less strong nonlinearity is observed, possibly due to response problem in PZT. We have also performed stability check of the proposed algorithm of experimental signal by executing the program 10 times, but could not find any variation in mean square error. The measured peak velocity and displacement are 1.86±0.06 mm/s and 2.54±0.04 μm respectively.

5.5 Conclusion

Instantaneous frequency extraction based on reassigned smooth pseudo Wigner Ville Distribution (SPWVD) is proposed. Cubic phase signal along with strong nonlinear IF law based fringe signal is considered to show the efficacy of the proposed method. Spread in Gaussian separable kernels are independently optimised for smoothing both time and frequency direction of SPWVD and reduction of interference as well as improvement in accuracy is achieved significantly with simultaneous application of reassignment technique. Proposed method is also compared with polynomial Wigner Ville Distribution as well as Continuous Wavelet Transform method and found to be more accurate. Though, poly-WVD is theoretically appealing for such class of signal, interference effect severely distorts the TFR. In case of CWT, in spite of using modified Morlet wavelet, IF extraction could not be improved significantly. Simulation and experimental results justify the use of this new technique in precision displacement and velocity measurement using optical interferometric method for highly non-stationary fringe signal.

CHAPTER 6 Applications to Free Surface Velocity Measurement in High Strain Rate Experiments

6.1 Introduction

Free surface velocity measurement of the target material subjected to transient compressions in shock wave experiments is an important problem. Many interesting material properties like Hugonoit Elastic Limit (HEL), dynamic yield strength, spall strength etc can be inferred from the free surface velocity history of target material [4,7,8]. These material properties find immense applications in the area of defense, geophysics, aerospace, automobile etc. Michelson interferometer in two different configuration-(1) Velocity mode and (2) Displacement mode are widely used for free surface velocity measurement of target material under shock compression. This chapter describes these two types interferometer configuration with emphasis on signal analysis.

6.2 Velocity Interferometer

In velocity mode VISAR (Velocity Interferometer System for Any Reflector) is widely used instrument in shock compression experiments. VISAR is basically a modified version of wide angle Michelson interferometer where two Doppler shifted lights (with one of them delayed by placing an etalon in one of the legs of the interferometer) from target free surface interfere each other to form fringe pattern. Therefore it works in the velocity mode or differential displacement mode configuration. Quadrature coded interference fringes are utilized for differentiating between the acceleration and deceleration of target free surface.

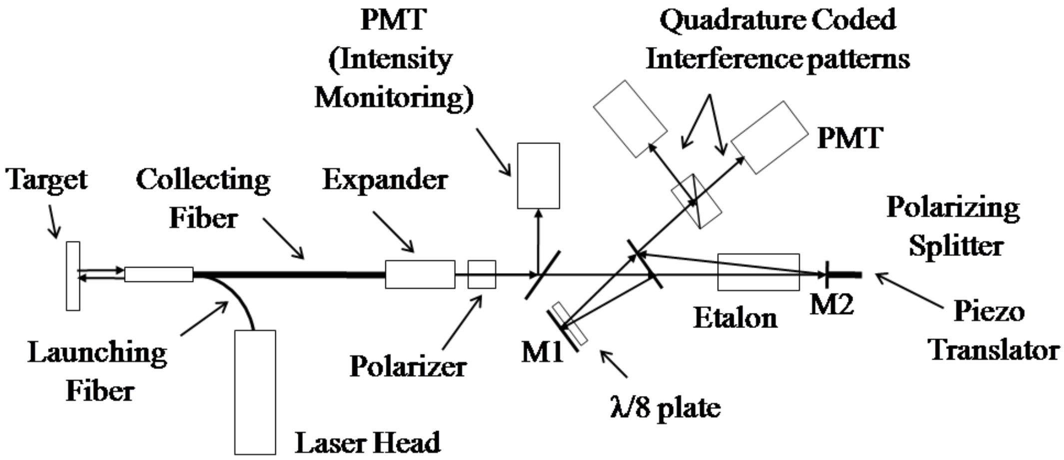

Fig.6.1Schematic of VISAR system

6.2.1 Method of VISAR Signal Analysis

Figure 6.1 depicts the schematic of VISAR system developed in our laboratory where three detector signals two from quadrature coded fringe patterns and one from beam intensity monitor are simultaneously recorded. The normalized quadrature signal measured by VISAR system can be expressed as

$$I_\alpha(t) = \alpha_0 + \alpha_1(t)\cos(\phi(t)) \tag{6.1}$$

$$I_\beta(t) = \beta_0 + \beta_1(t)\sin(\phi(t) - \varepsilon) \tag{6.2}$$

where $I_\alpha(t)$ and $I_\beta(t)$ are the two Doppler shifted lights from the two legs of the interferometer, α_0, β_0 are the offset, $\alpha_1(t)$,$\beta_1(t)$ are time varying amplitude of sinusoid and ε is quadrature error angle, $\varphi(t)$ is the phase of the signal which carries the information of interest. As described in Chapter 3, equations (6.1) and (6.2) $\varphi(t)$ can be expressed as-

$$\phi(t) = \arctan\left\{ \frac{I_\beta(t) - \beta_0\alpha_1}{I_\alpha(t) - \alpha_0\beta_1} \sec\varepsilon + \tan\varepsilon \right\} \tag{6.3}$$

Here, $I_{\alpha}(t)$ and $I_{\beta}(t)$ are the known measured quantity and α_0, β_0, $\alpha_1(t)$, $\beta_1(t)$, ε are unknown parameters those can be estimated by ellipse fitting. It may be noted that equations (6.1) and (6.2) form a family of ellipse where α_0, β_0 are the centre, $\alpha_1(t)$,$\beta_1(t)$ are axes and ε is the rotational angle of ellipse. The phase shift $\varphi(t)$ is then derived using equation (6.3) with fitted ellipse data. However, the phase described in equation (6.3), is wrapped between –π/2 to π/2 or 0 to 2π due to inherent property of mathematical arctangent function. The 2π phase jump is removed by using phase unwrapping algorithm. Details of phase unwrapping is explained in section 3.2. Phase stepping technique of phase unwrapping algorithm is implemented as it is simple, easy to implement and works satisfactorily for VISAR signals. Once the phase is unwrapped the fringe shift is calculated using equation (6.4) and finally free surface velocity is derived using equation (6.5)-

$$F(T) = \frac{\phi(t) - \phi(t_i)}{2\pi} \tag{6.4}$$

$$U_{fs}(t) = kF(t) \tag{6.5}$$

Here, $F(t)$ is the fringe shift, U_{fs} is the free surface velocity and k is the known fringe constant related to laser wavelength and etalon delay time.

6.2.2 Ellipse Fitting

As discussed in Chapter 3 that effect of amplitude and phase angle error in final velocity profile could be solved by proper ellipse fitting technique. A detail description of ellipse fitting technique with an emphasis on VISAR signal analysis is provided in this Chapter. As mentioned earlier ellipse fitting is broadly categorised as (1) Algebraic method and (2) Geometric method is explained bellow.

6.2.2.1 *Algebraic Method*

In algebraic method ellipse is fitted using general conic equation given as

$$f(\mathrm{X},\lambda) = ax^2 + bxy + cy^2 + dx + ey + f = 0 \tag{6.6}$$

with the condition

$$b^2 - 4ac \leq 0 \tag{6.7}$$

where $\boldsymbol{\lambda}$=[a b c d e f]^t and **X**=[x^2 xy y^2 x y 1]^t. Now if we have k number of measurement points which are not lying exactly on equation (6.6), then right hand side of equation. (6.6) will be non zero. Therefore, we can rewrite the equation (6.6) in the following simultaneous equations form with residual r_i.

$$\begin{pmatrix} x_1^2 & x_1 y_1 & y_1^2 & x_1 & y_1 & 1 \\ \vdots & \vdots & \vdots & \vdots & \vdots & \vdots \\ x_i^2 & x_i y_i & y_i^2 & x_i & y_i & 1 \\ \vdots & \vdots & \vdots & \vdots & \vdots & \vdots \\ x_k^2 & x_k y_k & y_k^2 & x_k & y_k & 1 \end{pmatrix} \begin{pmatrix} a \\ b \\ c \\ d \\ e \\ f \end{pmatrix} = \begin{pmatrix} r_1 \\ \vdots \\ r_i \\ \vdots \\ r_k \end{pmatrix} \tag{6.8}$$

Algebraic distance is then defined as distance of a point (x,y) to the conic f(X, λ). The fitting can be carried out by minimising the squared algebraic distances $S(\lambda)$

$$S(\lambda) = \sum_{i=1}^{k} r_i^{\,2} \tag{6.9}$$

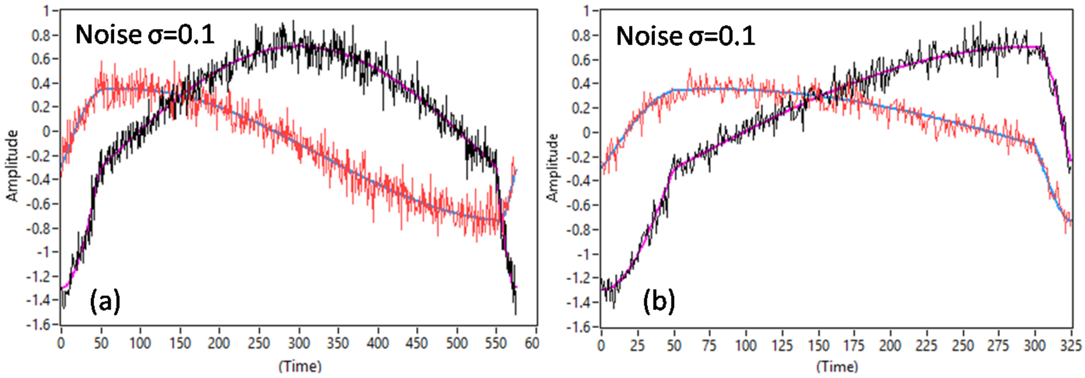

Fig.6.2 Simulated fringe signal (a) complete ellipse (b) 0.75 fractional ellipse

Thus, the problem becomes to find out λ such that $S(\lambda)$ is minimum. In general λ is normalised to avoid trivial solution of kind a = b = c = d = e = f = 0. In literature majority of the work is carried out in that direction by varying different normalisations [46,47]. Most popular choice is $\|\lambda\| = 1$, but Gander and Rosin suggested a + c = 1 [46,47]. Later Rosin [47] studied comparison between a + c = 1 and f = 1 and suggested f=1 was more accurate as it was less sensitive to curvature bias effect. In 1979 Bookstein [48] proposed ellipses fitting with Euclidian invariant constraint $a^2 + \frac{1}{2}b^2 + c^2 = -1$ and later Sampson [49] modified it. All these fittings were based on generalised conic fitting and it was not guaranteed that solution will always provide an ellipse. In 1999 Fitzgibbon [50] first time proposed an ellipse specific efficient fitting by making b^2-4ac = -1. Later R Halir et al [51] presented numerically robust version of Fitzgibbon algorithm. Ray et al [52] also explored the possibility of genetic algorithm in ellipse fitting.

In order to look for best suited method for analysis of VISAR signals, in this work, a comparative study of the most cited work on algebraic ellipse fitting techniques-(a) Bookstein fitting (b) Trace fitting by Gander et al and (c) Fitzgibbon fitting are carried out. After completing fitting from each of these methods, the VISAR ellipse parameters are calculated with fitted conic parameters (*a, b, c, d, e, f*) using ellipse parametric conversion equations, described below [59]-

$$\alpha_0 = \frac{bc - 2cd}{4ac - b^2} \tag{6.10}$$

$$\beta_0 = \frac{bd - 2ac}{4ac - b^2} \tag{6.11}$$

$$\alpha_1(t) = \sqrt{\frac{2(ae^2 + cd^2 + fb^2 - bde - 4acf)}{(b^2 - 4ac)(\sqrt{(a-c)^2 + b^2} - (a+c))}} \tag{6.12}$$

$$\beta_1(t) = \sqrt{\frac{2(ae^2 + cd^2 + fb^2 - bde - 4acf)}{(b^2 - 4ac)(-\sqrt{(a-c)^2 + b^2} - (a+c))}} \tag{6.13}$$

$$\varepsilon = \begin{cases} 0 & \text{for } b = 0 \text{ and } a < c \\ \dfrac{\pi}{2} & \text{for } b = 0 \text{ and } a > c \\ \dfrac{1}{2}\cot^{-1}\left(\dfrac{a-c}{b}\right) & \text{for } b \neq 0 \text{ and } a < c \\ \dfrac{\pi}{2} + \dfrac{1}{2}\cot^{-1}\left(\dfrac{a-c}{b}\right) & \text{for } b \neq 0 \text{ and } a > c \end{cases} \tag{6.14}$$

The main advantage of algebraic fitting is the computational efficiency by solving linear least square problem. However, in general results are not always satisfactory and it is unclear what is being minimised. In 1997 Zhang [48] pointed out the problem of high curvature bias effect for the same Euclidian misfit of algebraic fitting. It implies that this method performs better conic fitting at low curvature sections than to those at high curvature sections for the same noise level of the measurement data.

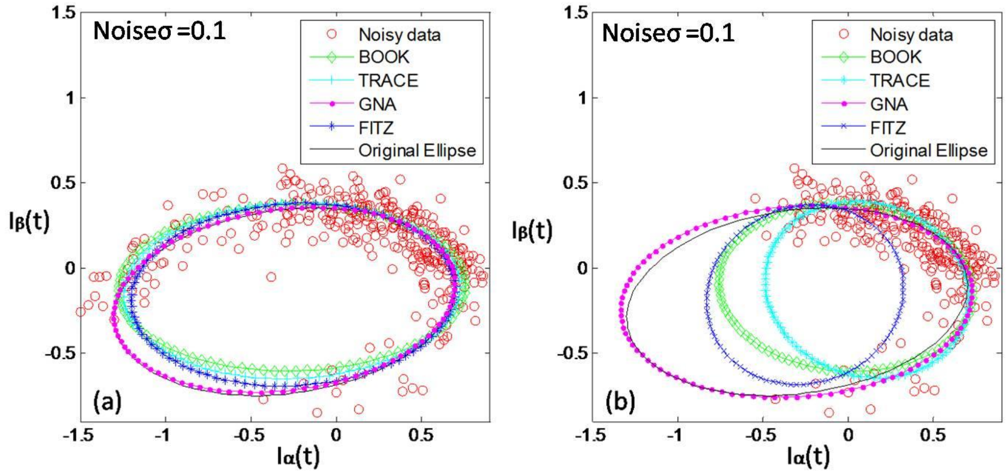

Fig.6.3 Ellipse fitting with simulated fractional fringe (a) 0.75 fraction (b) 0.5 fraction

Finally, Gander et al [46] also mentioned the problem of producing quite different ellipse for different normalisations of algebraic fitting.

6.2.2.2 Geometric Method

Geometric method is applied to overcome the problems mentioned in the algebraic method by replacing algebraic distances to orthogonal distances which are Euclidean invariant to space transformation. If d_i is the orthogonal distance from the measured k number of data points (x, y) to the estimated curve $f(x,\lambda)$ then we can optimize the model parameters λ by minimizing the following function-

$$S(\lambda) = \sum_{i=1}^{k} {d_i}^2 \tag{6.15}$$

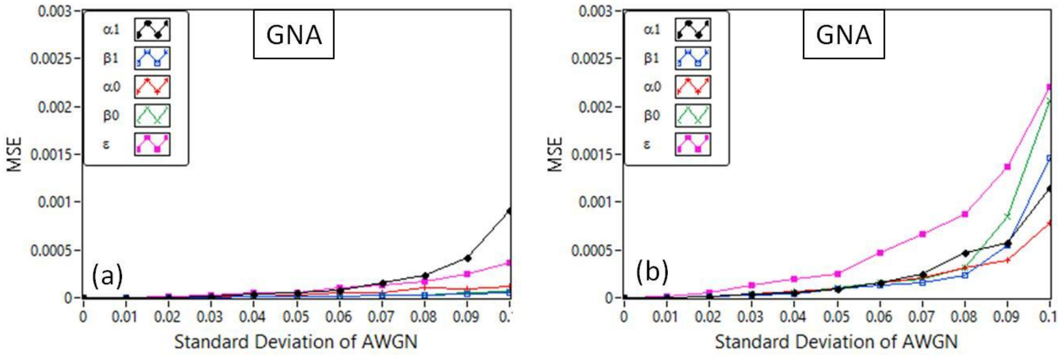

Fig.6.4 Error percentage of ellipse parameters for fractional fringe signal with different noise σ

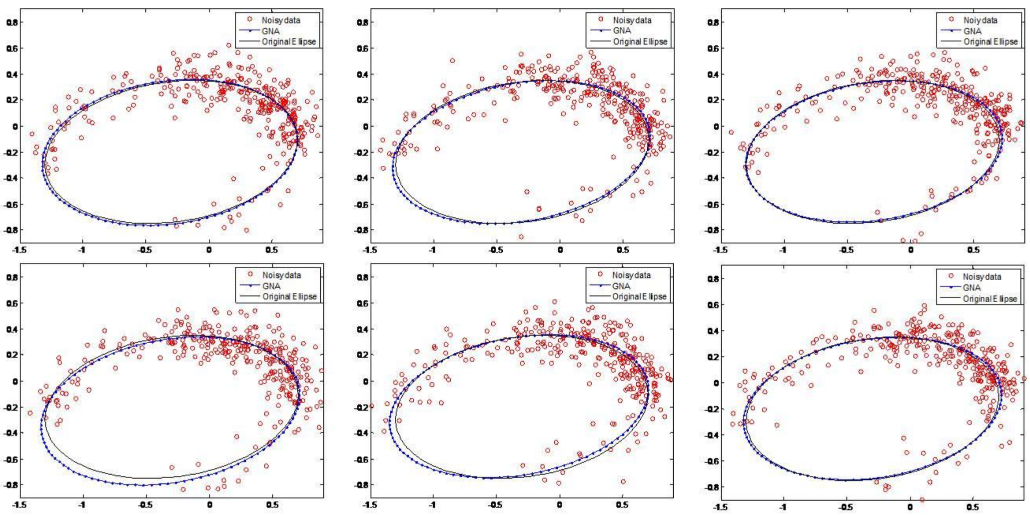

Fig 6.5 Ellipse Stability Check

As the expression of d_i is complicated an iterative optimization technique is usually applied to obtain the parameters vector λ. The equation (6.15) can be generalised as

$$S(\lambda) = \sum_{i=1}^{k} \left[y_i - f(x_i, \lambda) \right]^2 \qquad (6.16)$$

Here y_i is the measured data points and $f(x_i, \lambda)$ is the model function. For minimisation process some initial parameters of λ are guessed and value of $S(\lambda)$ is evaluated. In each iteration step vector λ is updated by a new estimate, $\lambda+\delta$ such that values of $S(\lambda)$

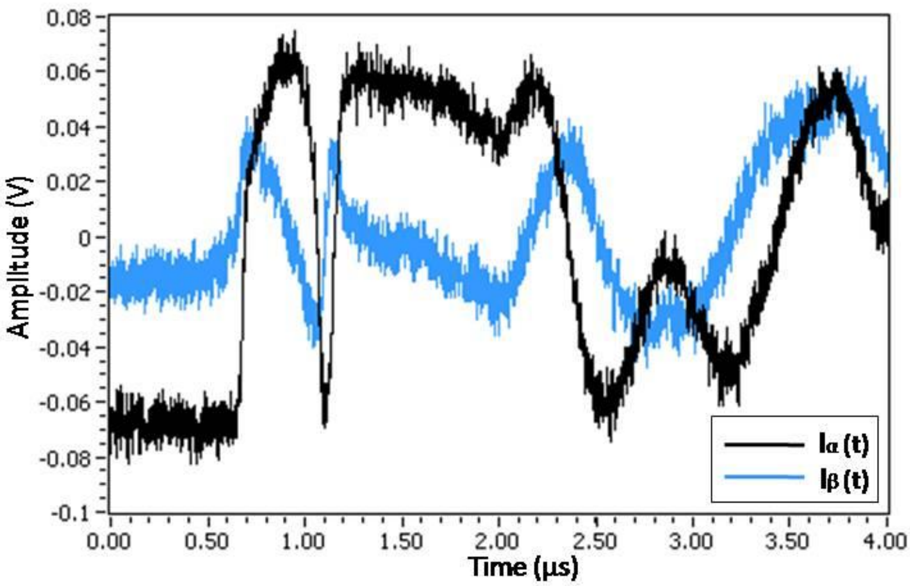

Fig.6.6 Offset corrected recorded fringe signal of Al-2024T4 material for Exp-1

become smaller than the earlier one. These steps are continued until some convergence criteria are satisfied. In literature many optimization techniques are available for application to conic fitting like Steepest Gradient Descent method, Gauss-Newton Algorithm (GNA), Lavenberg-Marquardt Algorithm (LMA) etc [53,54].

In Steepest Gradient Descent method update parameter δ_{GD} moves the parameters in negative of the gradient direction and it is expressed as-

$$\delta_{GD} = \alpha J^T \left[y - f(\lambda) \right] \tag{6.17}$$

where α is a positive scalar parameter. The advantage of this method is that it converges fast when the solutions are away from the minima. However, it converges very slowly close to the local minima with a required accuracy.

In Gauss-Newton Algorithm update parameter δ_{GN} is defined as-

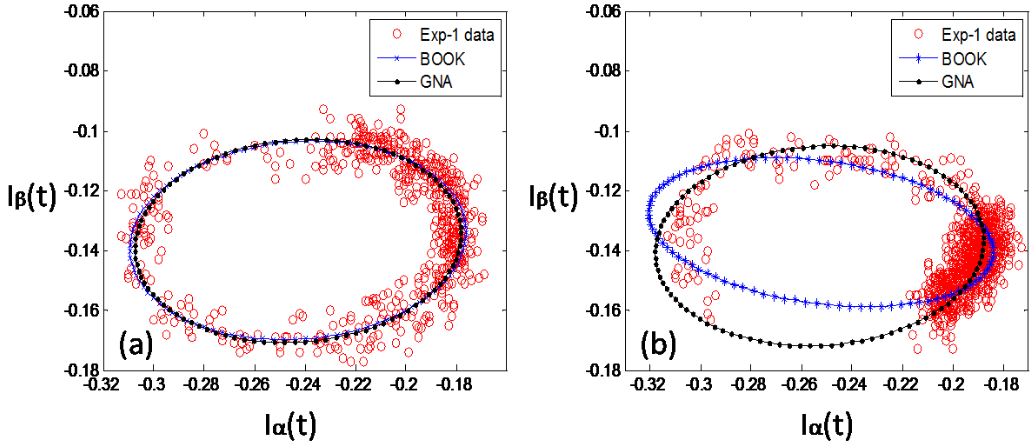

Fig. 6.7 Ellipse fitting on the VISAR signals recorded in experiment-1 (a) complete fringe (b) fractional fringe

$$(J^T J)\delta_{GN} = J^T[y - f(\lambda)] \tag{6.18}$$

where J is the Jacobian expressed as

$$J = \frac{\partial f(x,\lambda)}{\partial \lambda} \tag{6.19}$$

GNA converges quickly when solutions are close to minima value. But if the initial guess is chosen far from the minimum, GNA may converge slowly or may not at all converge. Another problem is that if the ellipse is a circle the Jacobian becomes singular and GNA will not work. This problem can be solved by using LMA update parameter.

Lavenberg-Marquardt Algorithm judicially utilises the advantages of both the algorithms by adaptively varying update parameters between Gradient Descent update and Gauss-Newton update. It is described as

$$(J^T J + \mu diag(J^T J))\delta_{LMA} = J^T[y - f(\lambda)] \tag{6.20}$$

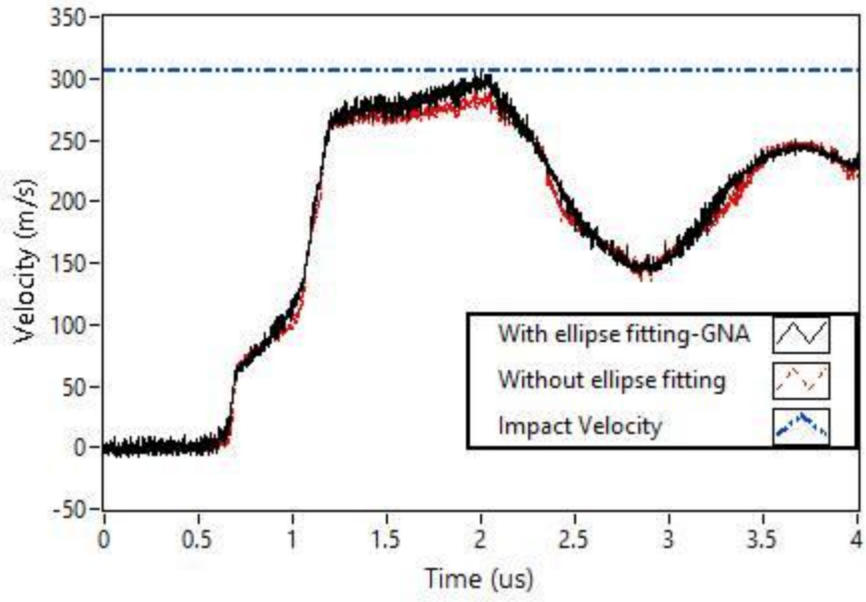

Fig.6.8 Free surface velocity profile derived using fitted results for Exp-1

where I is the identity matrix and μ is the algorithmic parameter.

It should also be noted that LMA algorithm is no way optimal but it is heuristic. Its performance cannot be guaranteed but in many practical scenarios it works better.

In present work, a comparative study of different ellipse fitting techniques is provided and GNA fitting technique of geometric method is proposed, especially when the ellipse is fractional. The convergence problem of GNA could be improved by utilising the Bookstein algebraic fitting data as its initial guess parameters.

For geometric fitting technique the model function $f(x,\lambda)$ is implemented in parametric representation of ellipse as it requires less number of parameters to estimate than general conic equations given as-

$$\begin{pmatrix} x \\ y \end{pmatrix} = \begin{pmatrix} x_0 \\ y_0 \end{pmatrix} + \begin{pmatrix} \cos\alpha & -\sin\alpha \\ \sin\alpha & \cos\alpha \end{pmatrix} \begin{pmatrix} a\cos\varphi \\ b\sin\varphi \end{pmatrix} \tag{6.21}$$

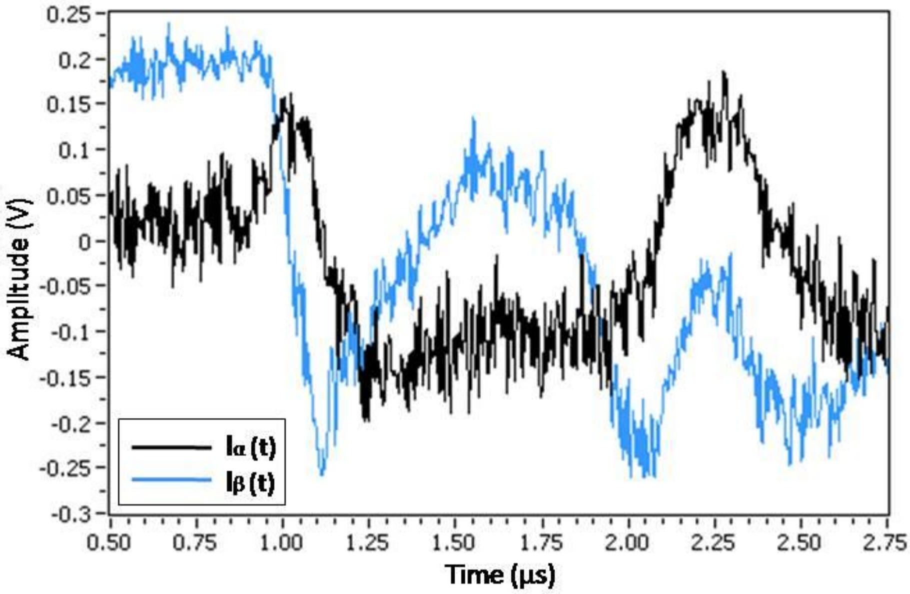

Fig. 6.9 Offset corrected recorded fringe signal of Al-2024T4 material for Exp-2

where x_0 and y_0 are the centre of the ellipse, a, b are the semi axes, α is the angle of inclination of a from x axis and φ is the parameter runs anticlockwise from 0 to 2π. Thus model vector $\boldsymbol{\lambda}=(x_0\ y_0\ a\ b\ \alpha)^t$ can completely characterize the ellipse. Therefore geometric fitting directly provides the parameters of our interest α_0, β_0, α_1, β_1, ε which are equivalent to x_0, y_0, a, b, α respectively.

Table 6.1. Ellipse parameters with different fitting algorithm for complete fringe signal with added noise σ=0.1

Ellipse parameters	True Value	BOOK	TRACE	FITZ	GNA
α_0	-0.3	-0.2911	-0.2739	-0.2552	-0.3027
β_0	-0.2	-0.1945	-0.1916	-0.1944	-0.2061
α_1	1.0064	1.0462	1.0062	0.9603	1.0332
β_1	0.5382	0.5432	0.5549	0.5827	0.5424
ε	0.1336	0.1240	0.1222	0.1263	0.1444
RMS	0	0.2061	0.2135	0.2181	0.2001

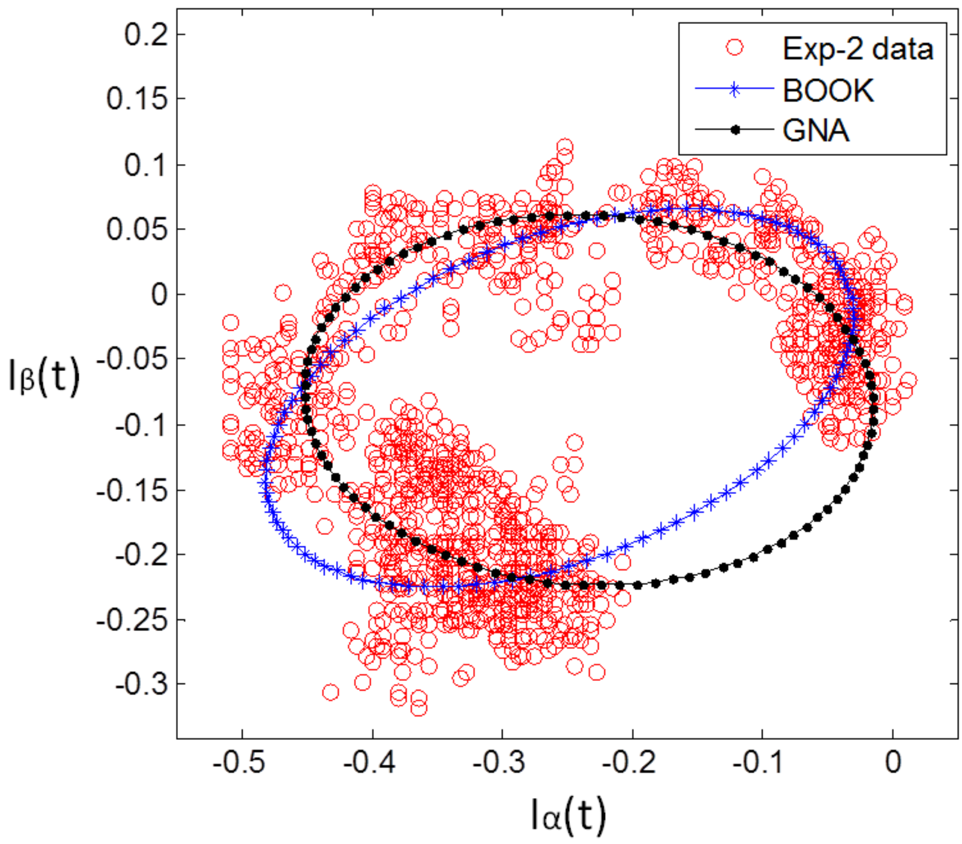

Fig.6.10 Ellipse fitting on the VISAR signals recorded in Exp-2

6.2.3 Numerical Simulation

In order to compare the performance of different ellipse fitting techniques for VISAR like signals, two tests, one with complete ellipse data and the other with fractional ellipse are conducted. The fringe signals are created using piece-wise sinusoid with variable frequency signal as VISAR signal is also non-stationary in nature. Additive White Gaussian Noise (AWGN) with different noise standard deviation (σ) is added to the simulated fringe signal to check the robustness of the algorithms. Figure 6.2(a) and 6.2(b) represent the two different fringe signals representing complete ellipse and fractional ellipse (0.75 fraction), respectively with added noise σ=0.1. The convergence criterion for geometric fitting is set as maximum number of iterations 400 and tolerance 1e-5. Various ellipse fitting techniques compared are as follows:

I. BOOK= Bookstein method;

II. TRACE= Gander method;

III. FITZ= Fitzgibbon method;

IV. GNA= Gauss-Newton method;

Table 6.2. Ellipse parameters with different fitting algorithm for fractional fringe signal with added noise σ=0.1

Ellipse parameters	True Value	BOOK	TRACE	FITZ	GNA
α_0	-0.3	-0.2613	-0.2599	-0.2542	-0.3073
β_0	-0.2	-0.1179	-0.1352	-0.1582	-0.1873
α_1	1.0064	1.0183	0.9857	0.9493	1.0059
β_1	0.5382	0.4878	0.5147	0.5337	0.5326
ε	0.1336	0.0188	0.0037	0.0534	0.1289
RMS	0	0.2254	0.2343	0.2233	0.1660

Table 6.3. Experimental configuration.

Name	Target Thickness (mm)	Impactor Thickness(mm)	Impact Velocity (m/s)	Fringe Constant (m/s)
Exp-1	15.03	4.97	306±4.1	175
Exp-2	7.98	4.96	198.4±1.8	250

Table-6.1 depicts the different ellipse parameters (true and fitted) corresponding to complete fringe signal obtained from different fitting algorithms. RMS deviation from true value for each algorithm is also calculated. As clear from Table-6.1 all the algorithms perform reasonably well for complete fringe signal even in the presence of 10% noise level. However, as listed in Table 6.2 and shown in Fig. 6.3(a), for fractional fringe signal of 0.75 fraction of ellipse, the results from different ellipse fitting techniques differ significantly and GNA technique appears to perform better than the other techniques. Furthermore, as displayed in Fig. 6.3(b), in case of 0.5 fraction of the ellipse (*i.e.* 0.5 fraction of fringe data shown in Fig. 6.2(b) the only viable option remains GNA technique and all the other algorithms fail to provide reasonable fitting. We also found that in noise free cases all the algorithms perform equally good leading to perfect ellipse reconstruction. The stability testing of estimated ellipse parameters with increasing noise level for GNA method is also performed. The ellipse corrupted with noise (from 0 to 0.1) for 100 iterations and Mean Square Error (MSE) of all the ellipse parameters were recorded for both complete and fractional fringe signal depicted in Fig 6.4. In both the cases the ellipse parameters degrade gracefully with increase in noise level an indication of good fitting. As expected for fractional fringe signal MSE is more than that for complete fringe signal.

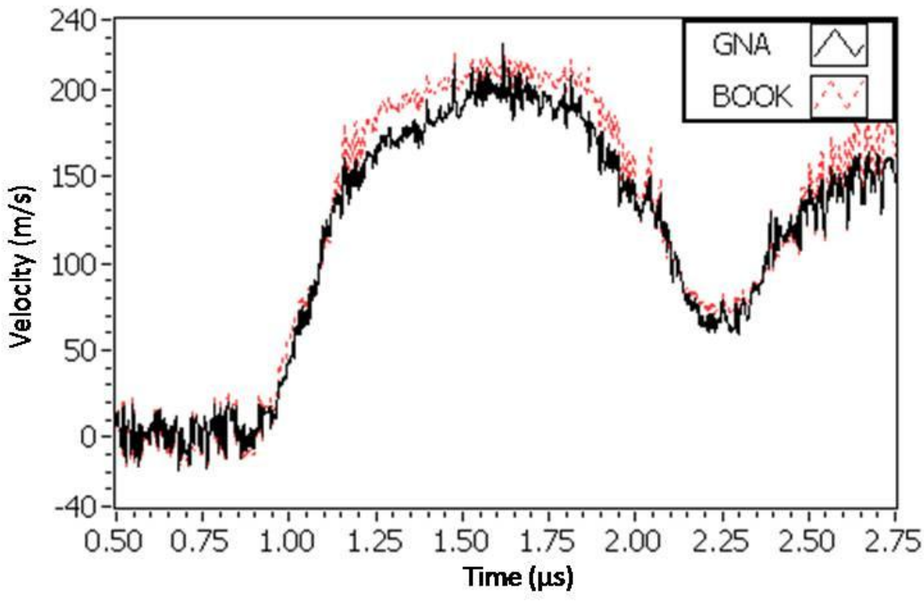

Fig.6.11 Free surface velocity profile derived using fitted results for Exp-2

Table 6.4. Ellipse parameters with different fitting algorithm for Exp-1.

Ellipse parameters	BOOK	TRACE	FITZ	GNA
α_0	-0.2429	-0.2425	-0.2419	-0.2430
β_0	-0.1366	-0.1365	-0.1364	-0.1367
α_1	0.0667	0.0653	0.0639	0.0646
β_1	0.0330	0.0337	0.0352	0.0338
ε	0.0568	0.0526	0.0452	0.0560
RMS	0.1265	0.1287	0.1322	0.1201

Table 6.5. Ellipse parameters with different fitting algorithm Exp-2.

Ellipse parameters	BOOK	TRACE	FITZ	GNA
α_0	-0.2561	-0.2479	-0.2435	-0.2342
β_0	-0.0794	-0.0790	-0.0788	-0.0807
α_1	0.2378	0.2156	0.2044	0.2186
β_1	0.1246	0.1363	0.1458	0.1422
ε	0.3792	0.3192	0.0452	-0.0538
RMS	0.2695	0.2761	0.3348	0.2222

6.2.4 Experimental Program

To validate the proposed algorithm two plate impact experiments on Al2024-T4 target material are conducted in single stage gas gun. The VISAR instrument is used to record the time resolved fringe shift arising due to motion of free surface of the target. Table-6.3 displays the target and impactor details used in the experiments. Details of VISAR system is described elsewhere [8]. Impact velocities are measured by time of flight technique. Figure 6. 5 displays that more than one complete fringe shift occurred due to movement of free surface in first experiment. The lissajaeous plot for one complete portion of fringe signal and corresponding fitted ellipse are shown in Fig. 6.6(a). As is clear from Table 6.4 and Fig. 6.6(a), just like that for the simulated signals, for experimental signals also, the performance of different fitting techniques is equally good. For sake of clarity the fitting from only two techniques namely BOOK and GNA are shown in the Fig. 6.6(a). However, if the remaining fractional part of the fringe signal is considered, the GNA accurately constructs the complete ellipse from the information available only on fractional fringe data, whereas the BOOK and other methods deviate significantly. Here also, in Fig. 6.6(b), for sake of clarity, results are shown for only two fitting algorithms BOOK and GNA. The peak free surface velocity (u_f) of 298.3±3.4m/s obtained using the GNA fitted data is more close (within ~ 2%) to the impact velocity of 306±4.1m/s measured using time of flight method, as compared to 283.8±2.1m/s that obtained employing simple arc-tangent function without ellipse fitting algorithm. Further, unlike that for the simple arc-tangent method (without ellipse fitting data), the free velocity profile derived employing GNA method does not contain numerical artifacts (Fig.6.7) like artificial acceleration and deceleration etc. It may be noted that the target and impactor used for these plate impact experiments were made of same material. Hence the impact velocity is expected to be equal to the peak free surface velocity. Different dynamic mechanical properties such as spall strength (σ_S=1.1±0.013GPa), Hugoniot elastic limit (σ_{HEL}=0.73±0.008GPa) and dynamic yield strength (Y=0.37±0.005GPa) of Al2024-T4 target material derived from free surface velocity profiles are also calculated. The details of methodology employed for deriving these parameters are mentioned in Appendix 1.1.

Figure 6. 8 depicts the fringe shift occurred due to free surface motion of target in the second plate impact experiment. Analysis of this signal poses more challenge as only fractional part of the ellipse exists in this case and high level of noise is present. Table-6.5 provides various ellipse parameters obtained using different fitting algorithms. The Lissajeous plot along with the fitted ellipses using two algorithms *i.e.* BOOK and GNA are also displayed in Fig.6.9. As evident from the figure, the complete ellipse derived from the GNA technique fits better with experimental data as that obtained from BOOK algorithm. The measured peak free surface velocity obtained from free surface velocity profiles (Fig.6.10) determined employing GNA and BOOK algorithms are 200.8±6.07m/s and 211.1±7.43m/s, respectively. In this figure, it is not shown the free surface velocity profile derived without using ellipse fitting as its demerits are already displayed in Fig. 6.7. Again like in first experiment, the free surface velocity derived by using GNA method is more close to the measured impact velocity of 198.4±2.3 m/s as compared to that obtained from BOOK algorithm.

6.3 Displacement Interferometer

Basic configuration of displacement mode Michelson interferometer is described in Chapter 1. However, due to implementation difficulty of Fig. 1.1, heterodyne method is widely used in shock compression experiments. This technique is commonly used in telecommunication for generating new frequency by mixing two frequencies based on trigonometric identity that is multiplying two sine functions $sin(2\pi f_1 t)$ and $sin(2\pi f_2 t)$ at two different frequency f_1 and f_2 results summation of two sine function one at (f_1-f_2) and other at (f_1+f_2).

Similar technique is implemented in heterodyne laser interferometry by mixing (using a circulator) a reference laser frequency (f_0) and its Doppler shifted frequency (f_d) from a moving target, generating heterodyne beat signals. Fig.6.12 briefly describes the schematic of the system, where laser light enters to the circulator through port 1 and comes out of port 2 and focuses to the target plate. When flyer with velocity $v(t)$ hits the target plate, free surface of the target plate starts moving causing Doppler effect. Then Doppler shifted light with frequency (f_d) enters to the circulator through port 2 and heterodyne beat signal comes out through port 3, converted to electrical signal by photodiode and stored to high speed oscilloscope.

6.3.1 Analysis Technique

Measured heterodyne beat signal can be expressed as

$$I(t) = I_0(t) + I_d(t) + 2\sqrt{I_0(t) I_d(t)} \cos\left(2\pi \int_0^t f_b(t)dt + \phi_0\right) \tag{6.22}$$

where$I_0(t)$ and $I_d(t)$ are the reference laser light intensity and Doppler shifted light intensity respectively, $f_b(t)$ is the heterodyne beat frequency expressed as

$$f_b(t) = f_d(t) - f_o(t) \tag{6.23}$$

and ϕ_0 is the initial phase difference. According to the Doppler effects, the beat frequency can be written as

$$f_b(t) = f_d(t) - f_o(t) = \frac{2U_{fs}(t)}{\lambda_0} \quad . \tag{6.24}$$

Therefore, free surface velocity $\{U_{fs}(t)\}$ can be related to instantaneous frequency of recorded heterodyne beat signal as per following equation-

$$U_{fs}(t) = \frac{\lambda_0}{2} f_b(t) \quad (6.25)$$

6.3.2 Simulation

VISAR velocity profile is used for generating simulated heterodyne type fringe signals. Free surface velocity profile (Fig.6.8) measured by VISAR (Velocity Interferometer System for Any Reflector) in AL-2024T4 material under shock compression is considered as an instantaneous frequency or beat frequency of heterodyne fringe signals. The velocity profile of 0-300 m/s is normalized to a corresponding instantaneous frequency range of 0 to 0.3 Hz as shown in Fig. Fig.6.13(a). Next integral of IF signal is approximated as cumulative summation function for producing simulated heterodyne fringe signal shown in Fig. 6.13(b). The frequency components in the spectrum induced by the amplitude modulation are much smaller than that of direct frequency modulation and majority of bandwidth contribution comes from frequency modulation only.

For extracting instantaneous frequency from recorded highly non-stationary fringe signal reassigned CWT method is applied as explained in Chapter 4. Figure 6.13(c) and 6.13(d) display the Morlet spectrogram and reassigned and modified Morlet spectrogram of the simulated fringe signal respectively. IF is extracted by ridge detection method using reassigned and modified CWT as well as CWT and plotted in the same original signal [Fig.6.13(a)]. Extracted IF, using CWT, indicates an error (increased strain rate) at low frequency, particularly at slow rising part of free surface velocity corresponding to Hugoniot elastic limit whereas reassigned and modified CWT is in agreement with the original signal as shown in Fig.6.14.

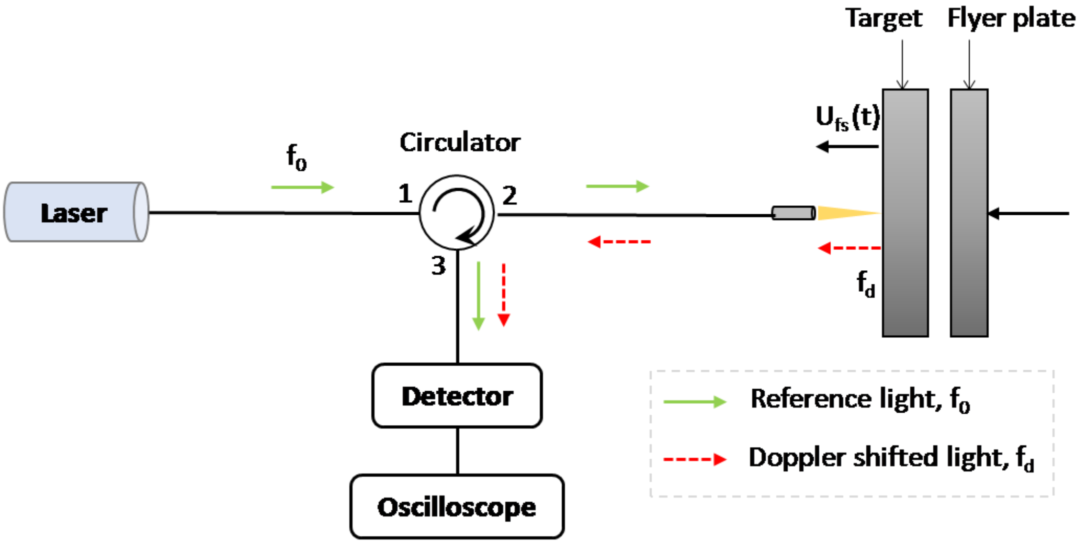

Fig.6.12 Schematic of Heterodyne laser interferometry system

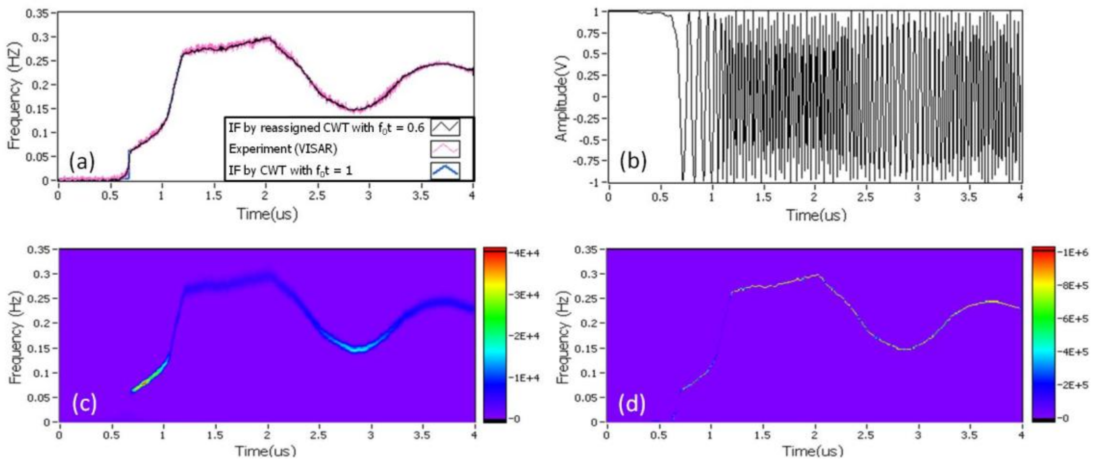

Fig.6.13 (a) Instantaneous frequencies obtained from VISAR velocity profile and two CWT techniques (b) Heterodyne type fringe signal deduced from the VISAR velocity profile. This signal is used by two CWT techniques to extract IF (c) Morlet spectrogram with f0t=1 (d) Reassigned and modified Morlet spectrogram with f0t=0.6.

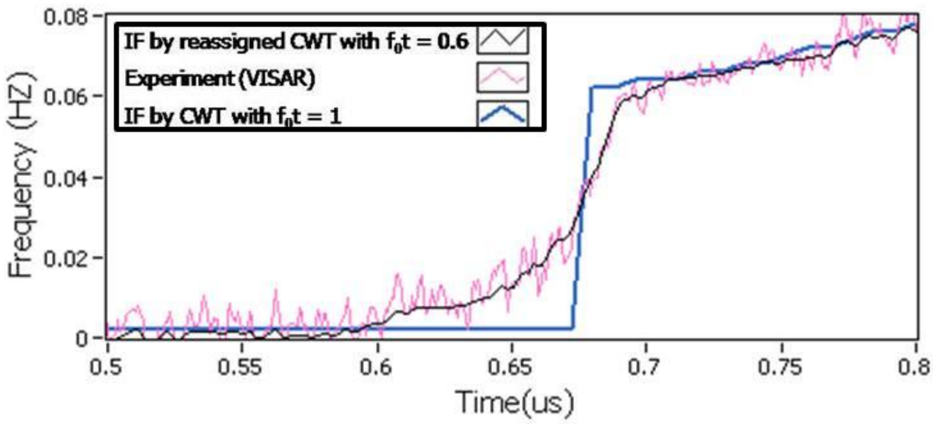

Fig.6.14 Slow rising part of extracted instantaneous frequencies of Fig. 6.13(a).

6.4 Conclusion

Phase extraction based on quadrature phase shifting method is successfully applied for free surface velocity measurement using VISAR of the target material under shock compression. The effects of amplitude and phase angle error on VISAR measurements are described and ellipse fitting technique is applied to overcome the problem in free surface velocity calculation. Comparative studies of various ellipse fitting techniques are carried out and geometric fitting technique of GNA with initial conditions from Bookstein method is proposed for better result. Two high strain rate experiments on Al2024T4 material are conducted to validate the proposed method and different fundamental mechanical properties are derived from extracted free surface velocity profiles. This method can be extended to any other applications including line imaging VISAR analysis, where quadrature error corrections are required. In conventional line imaging VISAR only one fringe signal based measurement is carried out and Fourier transform method is applied to extract the phase. However, quadrature or push pull based configuration is always desirable even for line VISAR. In that condition current investigation may be helpful for quadrature error correction.

Heterodyne laser interferometric technique is also explored in free surface velocity measurement in shock compression. As described in Chapter 4, reassigned CWT with Morlet as mother wavelet is proposed for analysing the heterodyne type fringe signals. Free surface velocity profile measured by VISAR under shock compression is considered as an arbitrary IF law and a corresponding heterodyne velocimetry type fringe signal is generated through simulation. The frequency profile corresponding to this simulated fringe signal extracted employing reassigned CWT technique and conventional CWT are compared with actual frequency profile. In low frequency region, corresponding to Hugoniot Elastic limit, the frequency profile extracted using reassigned and modified CWT is more close to the actual profile as compared to that obtained by conventional CWT. In high frequency regime, however, both the methods display similar performance. Further, the velocity profile obtained from reassignment technique is comparatively less distorted. Thus, this method finds an application for analyzing fringe signals obtained in heterodyne velocimetry for free surface velocity profile measurement under impact experiments.

In all the experiments have been carried out in light Gas Gun facility at BARC, Trombay, which has the maximum velocity range of 1000 m/s. However, in general it is possible to generate even higher velocities of several km/s with other kind of devices. The limitations in monitoring the higher velocities mainly arise due to bandwidth of signal recording system for heterodyne velocimetry technique and length of etalon or optical delay for VISAR system. In general, higher is the velocity of the object larger is the required bandwidth of the recording system.

Appendix 1.1

Method of Extraction of Fundamental Mechanical Properties from Free Surface Velocity Profile

In high strain rate plate impact experiment an impactor plate hits the stationary target plate that causes planner shock wave propagation in forward direction in target plate, and also in backward direction in impactor plate. The forward moving shock wave reflects from free surface of target plate as a backward moving release wave. In similar way, the backward moving shock wave reflects from the free surface of impactor plate as a forward moving release wave. When these release waves interact in the target plate, tensile stress is generated. If this tensile stress exceeds the strength of material, then it results in spall fracture. The free surface velocity (U_{fs}) history of the target plate represents this effect of spall fracture. The material undergoing elastic to plastic transformation followed by phase transition and spallation can be determined from an ideal free surface velocity profile shown in Fig. A1.1. The velocity profile is extracted from recorded fringe shift using VISAR in plate impact experiment.

The spall strength (σ_s) and strain rate ($\dot{\varepsilon}_t$) corresponding to σ_s, the Huogoniot elastic limit (σ_{HEL}), strain rate ($\dot{\varepsilon}_c$) corresponding to σ_{HEL} are determined from this profile as follows:

$$\sigma_s = \frac{1}{2}\Delta U_{fs}\rho_0 c_b \tag{A1.1}$$

$$\dot{\varepsilon}_t = \frac{\Delta U_{fs}}{2\Delta t_2}\frac{1}{c_b} \tag{A1.2}$$

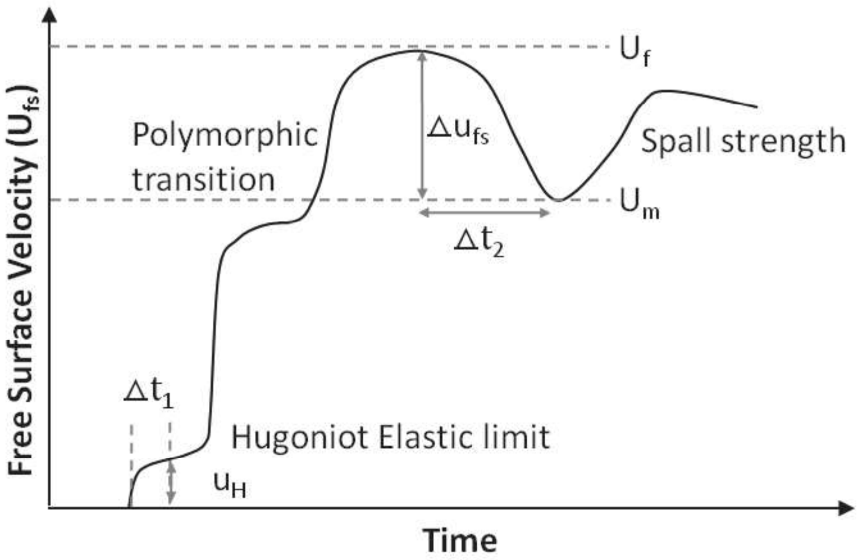

Fig. A1.1.1 Ideal free surface velocity profile of material showing features corresponding to various phenomenons

$$\sigma_{HEL} = \frac{1}{2}U_H \rho_0 c_l \tag{A1.3}$$

$$\dot{\varepsilon}_c = \frac{U_H}{2\Delta t_1}\frac{1}{c_l} \tag{A1.4}$$

The dynamic yield *Y* from the σ_{HEL} is deduced using following expression:

$$Y = \sigma_{HEL}\frac{(1-2\sigma)}{(1-\sigma)} \tag{A1.5}$$

Here, u_H is free surface velocity at σ_{HEL}. The Δt_1 is the time taken for free surface to reach a velocity of u_H. The $\Delta U_{fs}, c_b, c_l$ and σ correspond to pull back velocity of free surface, bulk sound speed, longitudinal sound speed and Poisson ratio, respectively. The pull back velocity is defined as $U_f - U_m$ where U_f is the peak free surface velocity and u_m is free surface velocity just ahead of spall pulse. The Δt_2 is the time taken by the free surface to retard from the peak velocity U_f to U_m.

Appendix 1.2

REVEAL: A Data Analysis Software for VISAR Measurements

Graphical User Interface based program (REVEAL) has been developed for analysis of VISAR signal by implementing the method proposed in chapter 6. Program has the features such as, reading '.csv' format data files, automatic error correction based on ellipse fitting, signal denoising, velocity plot, advanced analysis of different fundamental parameters, and finally report generation. Detailed program flowchart of REVEAL program is described below:-

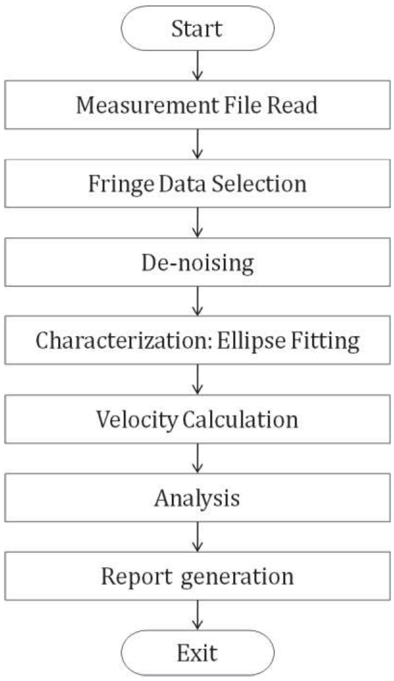

Fig. A1.2.1 Program Flowchart

REVEAL program offers a very easy and interactive graphical user interface for users. Various features and capabilities of the program are shown below.

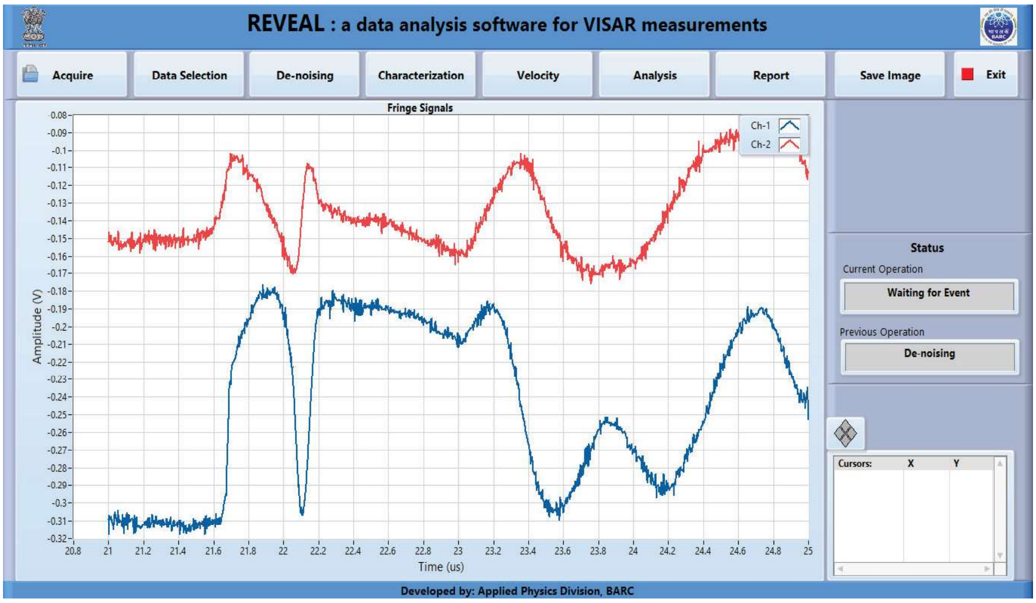

Fig. A1.2.2 Image of GUI after acquiring VISAR signal data for two channels.

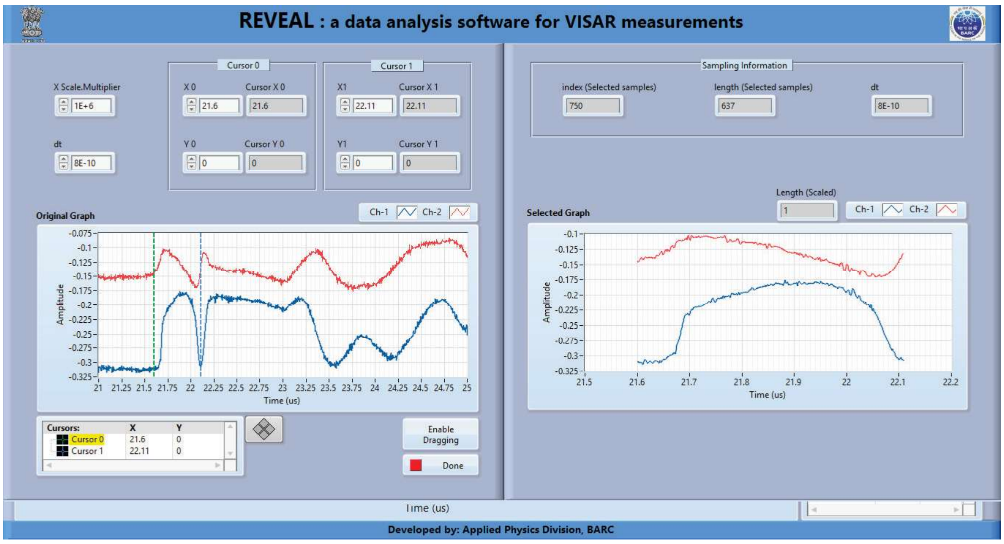

Fig. A1.2.3 Ellipse data selection

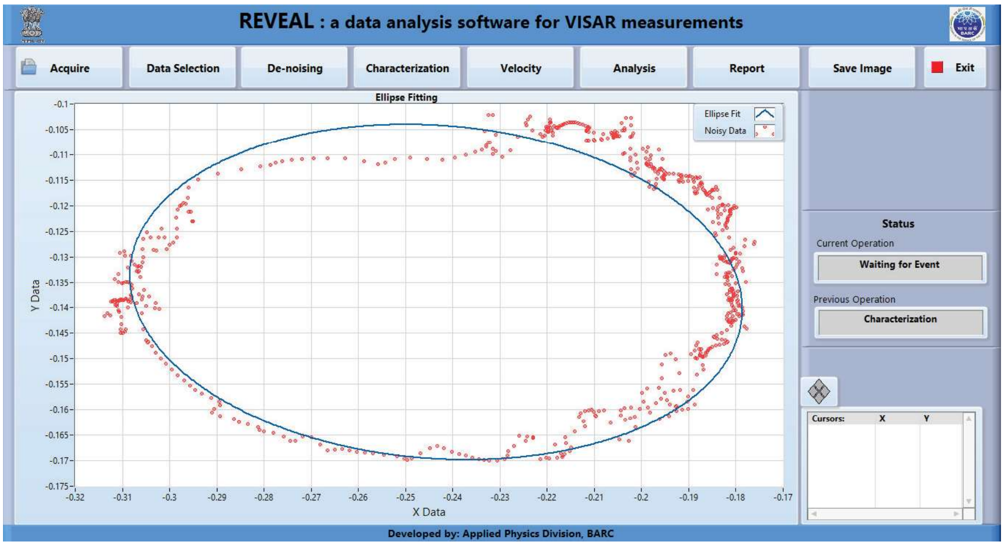

Fig. A1.2.4 Ellipse fitting

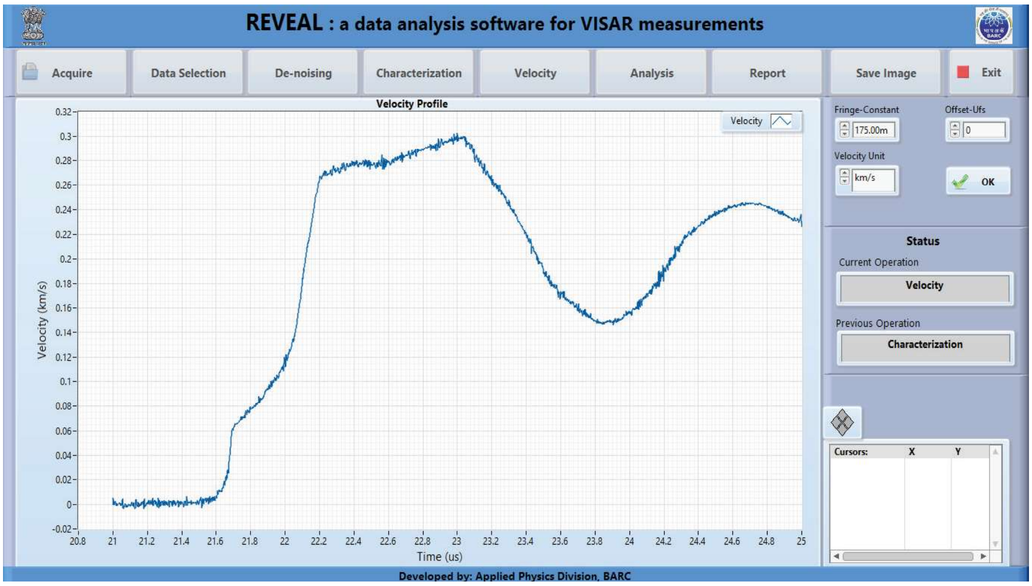

Fig. A1.2.5 Velocity profile

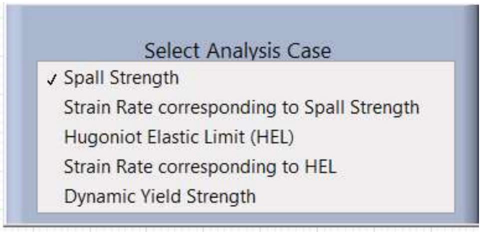

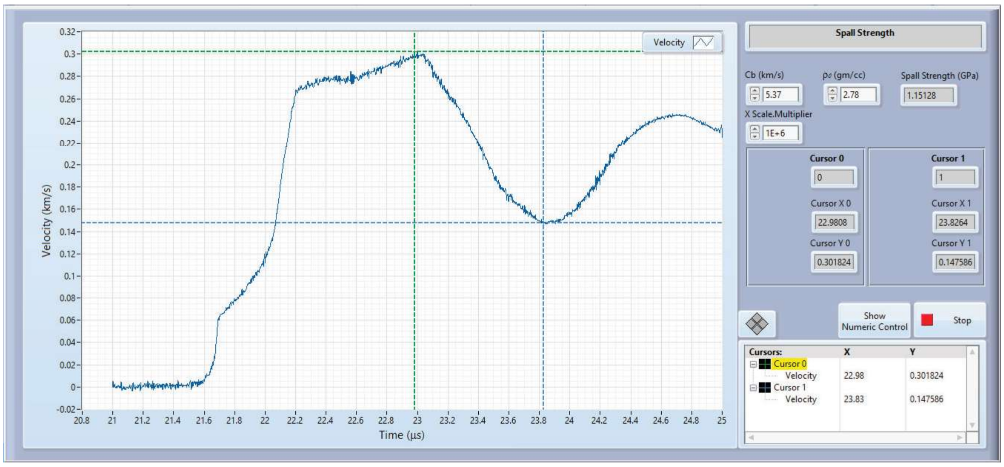

Fig. A1.2.1 Analysis for extracting different mechanical properties

References:

1. T. Kreis, Handbook of holographic interferometry: optical and digital methods, Wiley-VCH (2005).
2. P. Rastogi, Digital speckle pattern interferometry and related techniques, Chichester: John Wiley (2000).
3. G. Rajshekar, P rastogi, "Fringe analysis: Premise and perspectives," Opt. and lasers in Engg., 50, iii-x (2012).
4. L. M. Barker, and R.E. Hollenbach, "Laser interferometer for measuring high velocities of any reflecting surface" J. Appl. Phys. 43, 4669-4675 (1972).
5. W. Hemsing, "Velocity sensing interferometer (VISAR) modification" Rev. Sci. Instrum. 50, 73 (1979).
6. W. Hemising, "Coment on VISAR analysis in the presence of large intensity changes:Application to the expanding ring" Rev. Sci. Instrum., 60, 3832-3833 (1989).
7. K. D. Joshi, PhD Thesis, Mumbai University (2009).
8. K. D. Joshi, A. S. Rav, S. C. Gupta , "Development of Velocity Interferometer for Shock Wave Experiments" BARC Report , BARC/2011/E/002 (2011).
9. Q. Kemao, W. Xiaoping, A. Asundi, "Grating based real time polarization phase shifting interferometry:error analysis", Appl. Opt.;41(13):2448-2453 (2002).
10. J. Greivenkamp, J. H. Bruning, "Phase shifting interferometer", In:Malacara D, editor, Optical shop testing, New York:Wiley (1992).
11. C. J, Morgan, "Least-squaress estimation in phase measurement interferometry", Opt. Lett.;7(8):368-370 (1982).
12. P. Hariharan, B. F. Oreb, T. Eiju, "Digital phase shifting interferometry: a simple error compensating phase calculation algorithm", Appl. Opt.;26(13):2504-2506 (1987).
13. A. Patil, R. Langoju, P. Rastogi, "A state space approach in phase shifting interferometry", Opt. Commun.;263(2):281-288 (2006).
14. A. Patil, P. Rastogi, B. Raphael "A stochastic method for generalized data reduction in holographic moire", Opt. Commun.;248(4-6):395-405 (2005).
15. D. H. Dolan, "Foundation of VISAR analysis" Sandia National Laboratory, USA (2006).

16. A. D. White, G. B. McHale, D. A. Goerz, and R. D. Speer, “Faraday rotation data analysis with least-squares elliptical fitting”, Rev. Sci. Instrum., 81, 103108 (2010).
17. D. H. Dolan and S. C. Jones, “THRIVE: a data reduction program for three-phase PDV/PDI and VISAR measurement” Sandia National Laboratory, USA (2008).
18. M. Takeda, H. Ina, S. Kobayashi, “Fourier transform method of fringe pattern analysis for computer-based topography and interferometry”, J. Opt. Soc. Am.;72:156-160 (1982).
19. Q. Kemao, “Windowed Fourier transform for fringe pattern analysis”, Appl. Opt.;43(13):2695-2702 (2004).
20. L. R. Watkins, “Review of fringe pattern phase recovery using 1-D and 2-D continuous wavelet transform”, Opt. Lasers. Eng. 50(8), 1015-1022 (2012).
21. M. A. Gdeisat, A. Abid, D. R. Burton, M. J. Lalor, F. Lilley, C. Moore and M. Qudeisat, “Spatial and temporal carrier fringe pattern demodulation using one-dimensional wavelet transform: Recent progress,chllanges, and suggested developments”, Opt. Lasers Eng. 47, 1348-1361 (2009).
22. Z. Zhang, Z. Jing, Z. Wang and D. Kuang, “Comparison of Fourier transform, windowed Fourier transform and wavelet transform methods for phase calculation at discontinuities in fringe projection profilometry”, Opt. Lasers Eng. 50, 1152-1160 (2012).
23. C. J. Tay, C. Quan, W. Sun, X. Y. He, “Demodulation of a single interferogram based on continuous wavelet transform and phase derivative,” Opt. Commun. 280, 327-336 (2007).
24. J. M. Lilly and S. C. Olhede, “Generalised morse wavelets as a superfamily of analytic wavelets”, IEEE Trans. Sig. Proc., vol. 60, No. 11 (2012).
25. O. Kocahan, E. Tiryaki, E. Coskum and S. Ozder, “Determination of phase from the ridge of CWT using generalized Morse wavelet” Meas. Sci.Technol. 29, 035203 (2018).
26. A. Z. Abid, M. A. Gdeisat, D. R. Burton and M. J. Lalor, “ Fringe pattern analysis using a one-dimensional modified Morlet continuous wavelet transform” SPIE;7000:1-6 (2008).
27. J. L. Rueda, C. A. Juarez and I. Erlich, "Wavelet based analysis of power system low frequency electromechanical oscillations" IEEE Trans. Power Syst., vol.26, No.3 (2011).

28. R. A. Carmona, W. L. Hwang and B. Torresani, “Chaaracterization of Signals by the Ridges of Their Wavelet Transform”, IEEE Trans. Sig. Proc., vol. 45, No. 10 (1997).
29. R. A. Carmona, W. L. Hwang and B. Torresani, “Multiridge Detection and Time-Frequency Reconstruction”, IEEE Trans. Sig. Proc., vol. 47,No. 2 (1999).
30. H. Liu, A. N. Cartwright and C. Basaran, “Moire interferogram phase extraction: a ridge detection algorithm for continous wavelet transform” Appl. Opt., vol. 43, No. 4, (2004).
31. A Z Abid, M A Gdeisat, D R Burton and M J Lalor, “ Ridge extraction algorithms for one-dimensional continuous wavelet transform: a comparison” Journal of Physics:Conference Series, 76, 012045(2007).
32. K. Itoh, “Analysis of the phase unwrapping problem,” Appl. Opt., vol. 21, No. 14, p.2470, (1982).
33. D. Ghiglia and M. Pritt, Two-dimensional phase unwrapping theory, algorithm and applications, John Wiley & Sons (1998).
34. A. Fedrico, G. H. Kaufmann, “Phase retrieval in digital speckle pattern interferometry by use of a smoothed space-frequency distribution”, Appl. Opt.;42(35):7066-7071 (2003).
35. C. A. Sciammarella, T. Kim, “Determination of strains from fringe pattern using space-frequency representation”, Opt. Eng.;42(11):3182-3193 (2003).
36. G. Rajshekhar, S. S. Gorthi, P. Rastogi, “Strain, curvature and twist measurements in digital holographic interferometry using pseudo-Wigner-Ville distribution based method”, Rev. Sci. Instrum.;80(9):093107 (2009).
37. L. Cohen, “Time-Frequency Analysis” Prentice-Hall, New Jercy (1995).
38. F. Auger, P. Flandrin, P. Goncalves and O. Lemoine, “Tutorial on Time-Frequency Toolbox in MATLAB” CNRS-France and Rice University-USA, (1995-1996).
39. B. Boashash, “Time-Frequency Analysis” 1st Edition, ELSEVIER (2015).
40. B. Boashash and P. O’Shea, “Polynomial Wigner-Ville Distribution and Their Relationship to Time-Varying Higher Order Spectra”, IEEE Trans. Sig. Proc., vol. 42, No. 1 (1994).
41. G. Rajshekhar, S. S. Gorthi, P. Rastogi, “Polynomial Wigner-Ville distribution based method for direct phase derivative estimation from optical fringes”, J. Opt. A: Pure Appl. Opt.;11(12):125402 (2009).

42. D. H. Dolan, "Accuracy and precision in photonic Doppler velocimetry" Rev. Sci. Instrum. 81, 7053905 (2010).
43. W. H. Gourdin, "VISAR analysis in the presence of large intensity changes: Application to the expanding ring," Rev. Sci. Instrum., vol. 60, 754 (1989).
44. S. Liu, D. Wang, T. Li, G. Chen, Z. Li and Q. Peng, "Analysis of photonic Doppler velocimetry data based on the continous wavelet transform" Rev. Sci. Instrum.,82,023103 (2011).
45. H. Song, X. Wu, C. Huang, Y. Wei and X. Wang, "Measurement of fast-changing low velocities by photonic Doppler velocimetry" Rev. Sci. Instrum.,83,073301 (2012).
46. W. Gander, G.H. Golub, and R. Strebel, "Least-squares fitting of circles and ellipses", BIT, 34, 558-578 (1994).
47. P. L. Rosin, "A note on the least squares fitting of ellipses", Pattern Recognition Letters, 14, 799-808 (1993).
48. Z. Zhang, "Parameter Estimation Techniques: A Tutorial with Application to Conic Fitting", Image Vision Comput. Vol.15, No. 1, 59–76 (1997).
49. P. D. Sampson, "Fitting conic sections to 'very scattered' data: An iterative refinement of the bookstein Algorithm", Computer Graphics and Image Processing, 18,97-108 (1982).
50. A. Fitzgibbon, M. Pilu, and R. B. Fisher, "Direct least square fitting of ellipses", IEEE Transactions on Pattern Analysis and Machine Intelligence, 21(5):476 (1999).
51. R. Halir and J. Flusser, "Numerically stable direct least squares fitting of ellipses", Proceedings of the Sixth International Conference in Central Europe on Computer Graphics, Visualization, and Computer Vision, WSCG '98, 125-132 (1998).
52. A. Ray, D. C. Srivastava, "Non-linear least squares ellipse fitting using the genetic algorithm with applications to strain analysis", J. Structural Geology, 30,1593-1602 (2008).
53. H. P. Gavin, "The Levenberg-Marquardt method for nonlinear least squares curve-fitting problems", Duke University (2016).
54. S. Boyed and L. Vandenberghe, "Convex optimization", Cambridge University Press (2004).

55. N. Delpart, B. Escudie, P. Guillemain and R. Kronland-Martinet, "Asymptotic wavelet and Gabor analysis: extraction of instantaneous frequencies", IEEE Trans. Inf. Theory 38, 644 (1992).
56. K. Kodera, R. Gendrin and C. de Villedary, "Analysis of time-varying signals with small BT values", IEEE Trans. on Accoust., Speech, and Signal Proc. 34, 64 (1978).
57. B. Barkat and B. Boashash, "Design of Higher Order Polynomial Wigner-Ville Distributions", IEEE Trans. Sig. Proc., Vol. 47, No.9, September (1999).
58. Amit Rav, K. D. Joshi, Kulbhushan Singh and T. C. Kaushik, "Characterization of a signal recording system for accurate velocity estimation using a VISAR", Meas. Sci. Technol. 29 (2018).
59. E. W. Weisstein, MathWorld-A Wolfram Web Resource, http://www.wolfram.com .

Thesis Highlight

Name of the Student: **Amit Sur**

Name of the CI/OCC: Bhabha Atomic Research Centre **Enrolment No.: ENGG01201204004**

Thesis Title: Phase extraction of optical interferometric signals based on improved time-frequency method with application to high strain rate measurement.

Discipline: Electrical Engineering **Sub-Area of Discipline: Advanced Signal Processing**

Date of viva voce: 24-04-2021

Optical interferometry-based non-contact type measurements play a key role in determination of free surface velocity of target material under high strain rate experiments. Michelson interferometer in velocity as well as displacement mode configuration is widely used. As the information of velocity is hidden in phase or instantaneous frequency (IF), it is important to extract the phase or IF of the fringe signal. In time domain approach, multiple fringes are required to extract phase and noise sensitive numerical differentiation is necessary for getting the IF of the fringe signal. Although computationally less expensive, the accuracy of this method may get affected significantly by various measurement imperfections like, nonlinearity, amplitude and phase angle error. On the other hand, in frequency domain approach single fringe may be sufficient to extract IF and numerical differentiation could be avoided.

Here, phase extraction based on quadrature phase shifting method, reassigned Continuous Wavelet Transform (CWT) method and Smoothed Pseudo Wigner-Ville Distribution (SPWVD) method have been described and developed. In phase shifting method amplitude and phase angle error have been corrected by efficient ellipse fitting method by combining algebraic as well as geometric technique. In CWT, time-bandwidth product of Morlet wavelet is optimized as 0.6 and simultaneous reassignment technique is applied for accurate IF extraction. SPWVD method is proposed for extracting IF of highly non-stationary polynomial frequency modulated fringe signal. Cohen class signal representation is followed and time and frequency resolutions are independently optimized using Gaussian separable kernel. Reassignment technique is further applied for sharpening of the spectrogram with these optimized kernels that improves accuracy in IF significantly. Finally, some of these developed phase extraction algorithms are applied to free surface velocity measurement under high strain rate experiments and different dynamic mechanical properties such as Spall Strength, Hugonoit Elastic limit (HEL), Strain Rate at HEL etc. of AL2024T4 target material are derived from extracted velocity profile.

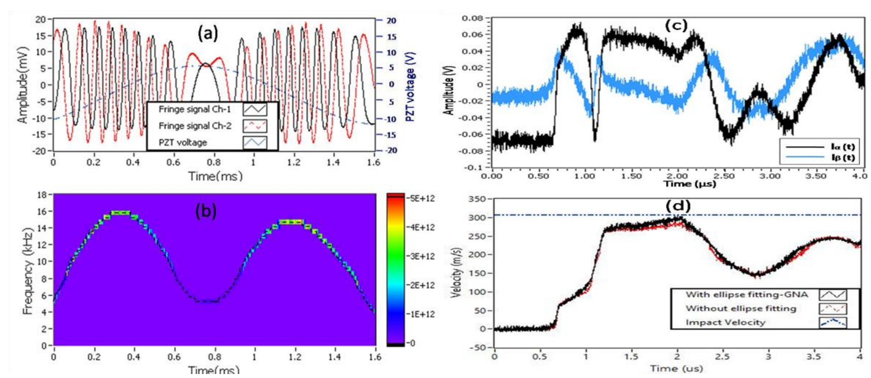

Figure 1. (a) Measured quadrature fringe signal with PZT supply voltage (b) Corresponding Reassigned CWT spectrogram (f_0t=0.6) obtained from Ch-1 fringe signal. (c) VISAR Fringe signals obtained in plate impact experiment using Gas Gun facility and (d) Corresponding free surface velocity profile by phase shifting method